SAPIENZA
UNIVERSITÀ DI ROMA

FACOLTÀ DI SCIENZE MATEMATICHE FISICHE E NATURALI

Dottorato in Matematica Applicata XXVII cicolo

High-order and coupled schemes for Hamilton-Jacobi-Bellman equations

Supervisor:
Prof. Maurizio Falcone

Candidate:
Smita Sahu
matricola 1512711

June 2015

Anno Accademico 2014-2015

Dipartimento di Matematica 'Guido Castelnuovo'

कर्मण्येवाधिकारस्ते मा फलेषु कदाचन।
मा कर्मफलहेतुर्भूर्मा ते सङ्गोऽस्त्वकर्मणि।

You should perform your best without having the desire of its resulting profit, you are not the one who decides the result and it doesn't mean that you should stop performing.

-Bhagavad Gita, Chapter II, Verse 47.

Dedicated to my parents

Shri. Jugul Kishore Sahu and Smt. Seema Sahu

Acknowledgements

A very special thank to my advisor Prof. Maurizio Falcone, who always supported, motivated and helped me with his patience, enthusiasm, and immense knowledge. His guidance helped me in all through the time of research and writing of this thesis. The topics, he has introduced to me, were always very interesting, exciting and challenging.

I would like to thank Olivier Bokanowski for his kind hospitality at Université Paris-Diderot (Paris 7) during my secondment (six-months). I also want to thank Emiliano Cristani to have the patience to work and believe in me. I would like to thank SADCO project and each member of the project. It was amazing experience of working and interacting with friends and professors from different nationality. I would like to thank the coordinator of SADCO project Prof. Hasnaa Zidani and Administrative Manager Estelle Bouzat for their constant support.
A special thanks to my parents without their support it was impossible for me to reach at this level . A special thanks to my siblings Asmita, Rishabh and Shubham. My uncle Shri Krishna Das Sahu his support was always with me since my childhood and many thanks to my cousin Harsh Vardhan.
A very big thanks to my friend Rajeev Gupta for his constant support. I would like to thanks Roberto Mecca and Ankit Kumar as they were always on my side in all the ups and down.
Very special thanks to Atoorva Sinha, her guidance and motivation always have given me a big support. Many thanks to Athena Picarelli for precious memories and her all time support. Thanks for the best guidance from Adriano Festa and Daniela Tonon. A very big thanks to Biagio Cassano, Giulia Fabrini, David Sarracco, Giuseppe Pipoli, Alessia Nota, Chiara Sorgentone and Claudia Ralo without them It was impossible task for me. Big thanks to Nishi Ratnam and Arti Singh who were always on my side in my whole journey. I would like to thank to Anupama Yadav, Ananya Chaturvedi, Anjali Sharma, Asha, Venugopal, Nishkam Tripathi, Shruti Malviya, Suraya Taranum and everyone who were the part of my journey.

I want to thank many more people but list is so long so I would like to end the list by saying thanks to everyone in the department of mathematics Guido Castelnuovo for their support and understanding.

Contents

List of Figures

List of Tables

Abbreviations

HJ	**H**amilton-**J**acobi
HJB	**H**amilton-**J**acobi-**B**ellman
DPP	**D**ynamic-**P**rogramming-**P**rinciple
ENO	**E**ssentially-**N**on-**O**sscilatory
WENO	**W**eighted-**E**ssentially-**N**on-**O**osscilatory
RK2	**R**unge-**K**utta-**S**econd order
TVB	**T**otal-**V**ariation-**B**ounded
TVD	**T**otal-**V**ariation-**D**iminishing
FTL	**F**ollow-**T**he-**L**eader
LWR	**L**ighthill-**W**hitham-**R**ichard
AD	**A**nti-**D**ifussive

Symbols

$\mathbb{R}^d$	the Euclidean d-dimensional space
$\mathbb{N}$	Natural numbers
$B(0,1)$	Unit open ball
$int(A)$	Interior of A
$\overline{A}$	Closure of A
A	Control spaces
$\mathcal{A}$	Set of measurable functions from $\mathbb{R}$ into A
$\mathcal{T}$	Target
$\mathcal{R}$	Reachable set
$y_x(t,\alpha)$	Trajectory of a control systems associated with the control α
∇f	Gradient of f

General Introduction

This PhD thesis deals with the development and the analysis of numerical methods for first order time dependent Hamilton-Jacobi-Bellman (HJB) equations. We consider the following form of the equation.

$$\partial_t v + H(x, \nabla v) = 0, \quad (t, x) \in [0, T] \times \mathbb{R}^d \tag{1}$$

$$v(0, x) = v_0(x), \quad x \in \mathbb{R}^d, \tag{2}$$

where $H : \mathbb{R}^d \times \mathbb{R}^d \to \mathbb{R}$ is the Hamiltonian and v_0 is the initial condition. This kind of equations, in general do not admit a classical solution even for regular initial data v_0. So the notion of viscosity solution (for precise definition, see Appendix B) has been introduced in the early 1980s by Pierre-Louis Lions and Michael G. Crandall [35] as a generalization of the classical concept of what is meant by a 'solution' to a partial differential equation (PDE). It has been found that the viscosity solution is the natural solution concept to use in many applications of PDE's, including for example first order equations arising in optimal control (the Bellman equation), differential games (the Isaacs equation) or front evolution problems.

The lack of smoothness of viscosity solutions makes it difficult to develop efficient approximations. Starting from the 80s, monotone finite difference methods have been proposed by Crandall and Lions [34] using the fact that in dimension one, viscosity solution of HJB equation is the integral of the entropy solution of hyperbolic conservation laws . On this basis, monotone finite difference methods conceived for conservation laws have been adapted to the approximation of the Hamilton-Jacobi (HJ) equation. In this thesis we develop numerical schemes for regular and discontinuous initial data v_0. First we focus on the high-order schemes for HJB equations when solution is regular. In this context there are some high-order schemes based on the relation between viscosity solution and entropy solution in dimension one. Several schemes developed for hyperbolic conservation law (see references [63], [64], [34], [59], [25]) and most of them extended to HJB equations. High-order essentially non-oscillatory (ENO) scheme have been introduced by A. Harten et al. in [65] for hyperbolic conservation laws, and then extended to HJB equation by Osher and Shu [71]. ENO schemes are of high-order and have been quite successful. However, till now and to the best of our knowledge, there is

no convergence proof of ENO schemes. However, in the general case although there is a numerical evidence that they converge to the viscosity solution of (1.6). Convergence results may hold for related schemes, see for instance Lions and Souganidis [81]. In [49], Fjordholm et. al. showed that ENO interpolation is stable but the stability result is not sufficient to conclude total variation boundedness (TVB) of the ENO reconstruction procedure. In [48], a conjecture related to weak total variation property for ENO schemes is given. Let us also mention, Semi-Lagrangian (SL), discontinuous Galerkin (DG) and the semi-discrete central schemes [75]. SL method developed by Falcone, Ferretti and Carlini [25, 41, 42]. In the SL setting the convergence proof for high-order scheme relies also on the work of Ferretti [26, 47] where higher than first order schemes are proposed. The finite difference schemes are used on structures grids where as SL schemes can be also applied to unstructured grids. DG finite element methods were originally devised for conservation laws later on extended to HJB equations. The DG spatial discretization was later combined with Runge-Kutta (RK) temporal discretization, giving birth to Runge-Kutta DG (RKDG) methods, introduced by Cockburn and Shu in [28] for hyperbolic conservation laws and later on extended for HJB equation. DG methods are flexible with complicated geometries, different boundary conditions, and various local approximations, they use compact stencils to achieve high order accuracy, and therefore are easy for parallel implementation but there is stability condition which is difficult to prove. Also there are several variation of DG methods for HJB equations [77, 79, 90]. In [26], where weighted essentially non-oscillatory (WENO) schemes have been applied to HJB equations.

We should also mention the work of Abgrall [1] where he proposed two different high-order schemes which are based on a particular decomposition of the initial data and decomposition of Hamiltonian. In [2] he also proposed hybrid schemes to solve steady HJ equation on conformal triangular type meshes and one can extend to solve time dependent HJB equation but proposed scheme is difficult to implement.

In the first part of the thesis in chapter 1 our focus is to develop high-order scheme for HJB equation when solution is regular. We introduce a new class of the"filtered scheme" for some time dependent first order HJB equations. The main idea of the filtered scheme comes from the recent work of Froese and Oberman [51, 86], that was presented for first and stationary second order HJ equations and based on the use of a "filter" function. Our focus on mainly evolutive HJB equations. In our setting we use the discontinuous

filter function from [86] for which the filtered scheme is still an ϵ-monotone scheme (see Eq.(1.14)), but that improves the numerical results. Filtered scheme behaves as a high order scheme when the solution is smooth and as a low order monotone scheme otherwise. Presentation of filtered scheme is simple and easy to implement. Rigorous error bounds hold, of the same order as the Crandall-Lions estimates in $\sqrt{\Delta x}$ where Δx is the mesh size. In the case the solution is smooth a high-order consistency error estimate also holds. Let us also mention the recent work [20] for steady equations where some ϵ-monotone semi-Lagrangian schemes are studied.

The theory of viscosity solutions has been tested on a variety of applications. One of the typical applications of HJ equation is the study and approximation of front propagation problems via the level set method. This technique has become very popular in the 90s due to its capability to follow front evolution after the onset of singularities and topological changes. There exist a number of physical situations which lead to models of these type, e.g., the description of industrial etching processes, bubbles moving in a fluid, crystal growth and so forth. More recently, these techniques have also been applied to image processing, which is one of the areas in which the introduction of nonlinear partial differential equations has had a strongest impact in the last decades. It is known since the work of Osher and Sethian [89] that front propagation problems can be solved by using level sets and HJ equations. For full introduction we refer the book [89, 100]. Several Numerical scheme has be developed for such a problems. For instance semi-Lagrangian method for the minimum time problem has been proposed by Bardi and Falcone in [7, 8], and its adaptation to the front propagation problem, as well as some a priori estimates of the error on the front propagation can be found in [40, 43]. We also mention a series of papers by Bokanowski et al. [17] where they used RKDG method. These methods have the advantage to be easily adapted to arbitrary unstructured meshes (see [14, 18]) but there is stability condition which is difficult to prove. We develop a specific application of the scheme proposed and analyzed in [19] to front propagation problems. The approach is based on the level-set method which leads in the isotropic case to a classical evolutive first order HJ equation. We use the idea of filtered scheme for the approximation of HJ equations in a general convergent setting. We consider in particular a simple coupling between a monotone first order scheme and a second order centered scheme, applied to front propagation problems. The effect of the filtering is to stabilize an otherwise unstable scheme, and also to switch to the high

order scheme whenever the solution is detected to be smooth.

Now we discuss numerical methods for HJB equation when solution is discontinuous. Monotone (first-order) schemes have been shown to be stable and convergent under mild regularity assumptions on the solution and to be first order accurate for the approximation of Lipschitz continuous solutions. However, in control and game problems, the value function can be discontinuous so these schemes have to be adapted in order to obtain accurate approximations which do not diffuse too much around the discontinuities of ∇v and/or don't introduce oscillations on the discontinuities of v. Now we give some details of some available work when v_0 is discontinues. We have also seen for continuous viscosity solution, there are several contribution dealing with numerical schemes. In [10] Barles and Souganidis give a general frame work for the convergence of approximated solution towards the viscosity solution under generic monotonicity stability and consistency assumptions. But when we deal with discontinuous initial data v_0, classical monotone schemes are no more adapted. In fact, if we attempt to use these schemes, we observe an increasing numerical diffusion around the discontinuities. This is happening due to the fact that monotone schemes used at some level finite difference or interpolation techniques. So that available schemes are typically diffusive. For the classical theory for discontinuous viscosity solution we refer the book by Barles [9].

Initially in 1985 Roe [96] developed scheme for conservation laws when the flow is discontinuous with the constant velocity. Later on the same scheme has been modified by Desprès and Lagoutière in [38] for capturing contact discontinuities for linear advection and compressible Euler system. In [38] it has been proved that the proposed scheme by Roe (which is called as Ultrabee scheme) has a property of exact advection for a large set of piecewise constant functions. Recently this scheme has been modified by Bokanowski and Zidani [13] for HJ equations with the convergence result [16] and an l^1 error estimate [15]. Whole Ultrabee scheme idea is present for dimension one only and by splitting one can extend to the higher dimensions. Proposed HJB-UltraBee scheme [13] is explicit and non-monotonous (neither ϵ-monotone). We know that, there are few non-monotone schemes that have been proved to converge for HJ equations (see [19] and [81]). In [81], Lions and Souganidis show the convergence of some MUSCL types non-monotone scheme which is TVD second order scheme, but implicit and difficult to implement.

We propose a new numerical approximation for linear advection and HJ equation which is based on the coupling of two schemes with different properties. The approach is general and can in principle be applied to couple many different schemes, for example one can couple an accurate method for the regions where the solution is smooth with another method which is more adapt to treat discontinuities and/or jumps in the gradients. Clearly one has to decide where to apply the first or the second method and this is done by means of an indicator parameter which has to be computed in every cell at every time step. Here we coupled an anti-dissipative scheme which has been proposed in order to deal with discontinuous solutions and a SL scheme which is more adapt to deal with Lipschitz continuous and can be more accurate for regular solutions provided a high-order local interpolation operator is used for the space reconstruction. We introduce the indicator parameter for this coupling, show how to couple the two schemes which typically use two different grids reconstructions and prove some properties of the resulting coupled scheme.

In the last part of the thesis we also deal another application: traffic models on networks. Traffic flow can be described at different scales, depending on the level of details one wants to observe. Typically, three scales of observation can be adopted: *microscopic*, *mesoscopic* and *macroscopic*. Connections between microscopic *follow-the-leader* and macroscopic fluid-dynamics traffic flow models are already well understood in the case of vehicles moving on a *single road*. Analogous connections in the case of *road networks* are instead lacking. This is probably due to the fact that macroscopic traffic models on networks are in general ill-posed, since the conservation of the mass is not sufficient alone to characterize a unique solution at junctions. This ambiguity makes more difficult to find the right limit of the microscopic model, which, in turn, can be defined in different ways near the junctions.

We propose a very natural extension of a first-order*follow-the-leader* on road networks and then we prove that its solution tends to the solution of the LWR-based multi-path model introduced in [22, 23] in the limit, i.e. as the number of vehicles tends to infinity while their total mass is kept constant. The limit is proved extending to networks the results already existing for a single road, and it is then confirmed by numerical experiments. Note that the multi-path method is able to select automatically an admissible solution at junction, thus resolving ill-posedness issues. However, the solution selected by the method does not match the one obtained by maximizing the

flux at junction. Therefore, the connection with the microscopic model promotes the solution computed by the multi-path method as "more natural", while the one based on the maximization of the flux should be seen as the "most desirable", to be achieved by means of *ad hoc* traffic regulations.

The literature about microscopic and macroscopic traffic flow models is huge and a detailed review is out of the scope of the chapter. For a quick introduction to the field we suggest the book [62] and the surveys [11, 66]. Regarding first-order models on a single unidirectional road, the micro-to-macro limit was already deeply investigated by means of different techniques: the papers [30, 50, 97]. Finally, the paper [32] attacks the problem exploiting the link between conservation laws and HJ equations.

Micro-to-macro limit for second-order models was instead investigated in [3, 60], where the Aw-Rascle model is derived as the limit of a second-order follow-the-leader model.

Macroscopic-only traffic models on networks were deeply investigated starting from [70]. A complete introduction can be found in the book [54], which discusses several methods to characterize a unique solution at junctions. Let us also mention the source-destination model introduced in [53] (see also [68]) and the buffer models [52, 55, 69]. Recently, a LWR-based multi-path model on networks was introduced in the paper [22], together with a Godunov-based numerical scheme to solve the associated system of conservation laws with discontinuous flux.

Outline of the thesis

The thesis is organized as follows.

In chapter 1 we give a very simple way to construct high-order schemes in a convergent framework. In present a high-order filtered scheme for time dependent first order HJ equations. In section 1.2 we present some basic properties and definitions and "filtered scheme". In Section 1.3, we present the schemes and give main convergence results. Section 1.4 tests is devoted to the numerical tests on several academic examples to illustrate our approach in one and two-dimensional cases. Also is included a test on nonlinear steady equations, as well an evolutive "obstacle" HJ equation in the form of $\min\left(u_t + H(x, u_x), u - g(x)\right) = 0$ for a given function g. Last section of the chapter contains concluding remarks.

In chapter 2 we present an application of HJ equation. We solve front propagation problems by the filtered scheme introduced in chapter 1. In section 2.2 we recall front propagation equation and introduce some notations and definitions for the model problem. Section 2.3 is devoted to new numerical examples for the front propagation problems up to three dimensions.

Chapter 3 deals with coupled numerical schemes for discontinuous initial data v_0. In section 3.2 we recall the basic facts about the semi-Lagrangian (SL) method [42] and the anti-dissipative (AD) [13] scheme which we use in the coupling. In section 3.3 we present the general form of the coupled scheme and we describe how it will be applied to solve the linear advection equation and how it has been extented of Hamilton-Jacobi equation. Section 3.4 we will prove some important properties of the coupled scheme. Finally, Section 3.5 will be devoted to the numerical tests fro hyperbolic conservation laws and HJ equations dimension one.

Chapter 4 is devoted to traffic problems. In the section 4.2 we give the details about existing macroscopic models on a single road and then the on road networks with numerical schemes. In section 4.3 we recall basic microscopic model on a single road and then we introduce the basic *follow-the-leader* model and the LWR model on a single road. Moreover, the existing results about the micro-to-macro limit on a single road are recalled. In section 4.4 we extend the model to networks, and in section 4.5, which is the core of the chapter, we show the relationship between the follow-the-leader model on networks and the LWR-based multi-path model. Finally, in section 4.6 we present fully discrete algorithms for the numerical solutions of the equations considered in the chapter and in section 4.7 we confirm our findings by means of some numerical tests and confirm our findings by means of some numerical tests.

Contribution: Let us briefly mention the original contributions which are behind this thesis.

- Chapter 1 is based on the submitted paper [BFS15].

  [BFS15] O. Bokanowski, F. Falcone, and S. Sahu. An efficient filtered scheme for some first order Hamilton-Jacobi-Bellman equations. Submitted to SIAM Journal on Scientific Computing (SISC). 2014.

- Chapter 2 is based on the conference preceding submitted paper [S15].

[S15] S. Sahu. High order filtered scheme for front propagation problems presented at HYP2014- XV International Conference on Hyperbolic Problems. Submitted to HYP2014 Bulletin of the Brazilian Mathematical Society.

- Chapter 3 is based on the submitted paper [FS15].

  [FS15] M. Falcone and S. Sahu. Coupled scheme for linear and Hamilton-Jacobi-Bellman equation. Submitted to Communications in Applied and Industrial Mathematics (CAIM), 2015.

- Chapter 4 is based on the submitted paper [CS15].

  [CS15] E. Cristiani and S. Sahu, On the micro-to-macro limit for first-order traffic flow models on networks, submitted to Networks and Heterogeneous Media (NHM), 2015.

Chapter 1

High-order numerical schemes

1.1 Introduction

We introduce a new class of "Filtered" schemes for some first-order non-linear HJB equations. The work follows recent ideas of Froese and Oberman [51] adn Oberman and Salvador [86]. Here we mainly study the time-dependent setting. Furthermore, specific corrections to the filtering idea are also needed in order to obtain high-order efficiency. The proposed schemes are not monotone but still satisfy some ϵ-monotone property. A general convergence result together with a precise error estimate is given, of the order of $\sqrt{\Delta x}$ where Δx is the mesh size. The framework allows to construct finite difference discretizations that are easy to implement and high-order in the domain where the solution is smooth. Numerical tests on several examples are given to validate the approach, also showing how the filtered technique can be applied to stabilize an otherwise unstable high-order scheme.

Our aim is to develop high-order and convergent schemes for first-order HJ equations of the following form

$$\partial_t v + H(x, \nabla v) = 0, \quad (t, x) \in [0, T] \times \mathbb{R}^d \tag{1.1}$$

$$v(0, x) = v_0(x), \quad x \in \mathbb{R}^d. \tag{1.2}$$

Basic assumptions on the Hamiltonian H and the initial data v_0 will be introduced in the next section. For more details about the present high order schemes refer readers

to the references already mentioned in the general introduction. In this chapter we give a very simple way to construct high–order schemes in a convergent framework. It is known (by Godunov's theorem) that a monotone scheme can be at most first order. Therefore it is necessary to look for non-monotone schemes. The difficulty is then to combine non-monotonicity of the scheme and convergence towards the viscosity solution of (3.1), and also to obtain error estimates. In our approach we will adapt a general idea of Froese and Oberman [51], that was presented for stationary second order Hamilton-Jacobi equations and based on the use of a "filter" function. The idea was also used to treat some stationary first order HJ equations in Oberman and Salvator [86].

Here we focus mainly on the case of time-dependent first order Hamilton-Jacobi equation (3.1). As suggested in [51] the scheme can be adapted to solve steady HJ equation by using a fixed point approach. The schemes are written in explicit time marching form which is well adapted to time-dependent equations, while the setting of [51] or [86] is better adapted to solve stationary equations. Let us emphasize that it is our experience that a direct application of the idea of [51] or [86], even if leading to convergent schemes, does not lead to second order schemes in general (similar filtering idea were already mentioned for instance in Osher and Shu [71, Remark 2.2], and see also Remark 1.3.1). One aim of the here is to explain in more detail some adaptations that where needed in order to achieve numerically the second order convergence, at least for main examples tested.

We use the same discontinuous filter function as in [86] for which the filtered scheme is still an "ϵ-monotone" scheme (see Eq.1.14). In our case we justify the use of this discontinuous filter to obtain a second order numerical behavior of the scheme in the L^∞ norm. It is our experience that using instead the continuous filter initially introduced in [51] leads to only first order behavior. (However in the case of steady equations - see in section 1.4, it is our experience that both filters give very similar results).

Furthermore, when using a central finite difference scheme together with the filtering idea, we introduce a limiting process that is needed in order to obtain high order efficiency and that is made precise in the case of front-propagation models. This limiting process was not needed in [51, 86] for the treatment of steady equations. Without the limiting process the scheme may switch back to first order after a few time steps (see for instance Example 2 in section 1.4).

Moreover, the filtered scheme (1.8) needs the use of a filtering parameter (hereafter denoted "ϵ") that must be chosen in order to switch between the high-order scheme and the monotone scheme in a convenient way. A natural upper bound for the parameter is given in [51, 86], of order $O(\sqrt{\Delta x})$. We give here a similar upper bound that is justified theoretically to ensure an error estimate of order $O(\sqrt{\Delta x})$. However in our case we give furthermore a lower bound on this parameter and some precise indications as how to fix the parameter depending of the data. In the end we advice using $\epsilon = c_1 \Delta x$ where c_1 is a constant depending of the data in order to obtain numerically a high order behavior, and therefore our choice is slightly different from the one of [86].

The approach also allows us to obtain new error estimates for filtered scheme for general time dependant HJ equations, of order $O(\sqrt{\Delta x})$ where Δx is the spatial mesh size, and under a standard CFL condition on the time step (this results is new compared to the works [51, 86]). This is similar to the Crandall-Lions error estimate for monotone schemes [34], because the scheme can be written as a perturbation of a monotone scheme.

1.2 Definitions and main results

1.2.1 Setting of the problem

Throughout the chapter $|\cdot|$ denotes the Euclidean norm on $\mathbb{R}^d$ ($d \geq 1$). The following classical assumptions will be considered:

(A1) v_0 is Lipschitz continuous function i.e. there exist $L_0 > 0$ such that for every $x\ , y \in \mathbb{R}^d$,

$$|v_0(x) - v_0(y)| \leq L_0 |x - y|. \tag{1.3}$$

(A2) $H : \mathbb{R}^d \times \mathbb{R}^d \to \mathbb{R}^d$ satisfies, for some constant $C \geq 0$, for all $p, q, x, y \in \mathbb{R}^d$:

$$|H(y,p) - H(x,p)| \leq C(1 + |p|)|y - x|, \tag{1.4}$$

and

$$|H(x,q) - H(x,p)| \leq C(1 + |x|)|q - p|. \tag{1.5}$$

Under assumptions (A1) and (A2) there exists a unique viscosity solution for (3.1) (see Ishii [72]). Furthermore v is locally Lipschitz continuous on $[0,T]\times\mathbb{R}^d$.

For clarity of presentation we focus on the one-dimensional case and consider the following simplified problem:

$$v_t + H(x, v_x) = 0, \quad (t,x) \in [0,T]\times\mathbb{R}, \tag{1.6}$$

$$v(0,x) = v_0(x), \quad x \in \mathbb{R}. \tag{1.7}$$

1.2.2 Construction of the filtered scheme

Let $\Delta t > 0$ be a time step (in the form of $\Delta t = \frac{T}{N}$ for some $N \geq 1$), and $\Delta x > 0$ be a space step. A uniform mesh is defined by $t_n := n\Delta t$, $n \in [0,\dots,N]$, and $x_j := j\Delta x$, $j \in \mathbb{Z}$.

The construction of a filtered scheme needs three ingredients:

- a monotone scheme, denoted S^M
- a high-order scheme, denoted S^A
- a bounded "filter" function, $F : \mathbb{R} \to \mathbb{R}$.

The high-order scheme need not be convergent nor stable; the letter A stands for "arbitrary order", following [51]. For a start, S^M will be based on a finite difference scheme. Later on we will also propose a definition of S^M based on a semi-Lagriangian scheme.

Then, the filtered scheme is defined by

$$u_j^{n+1} \equiv S^F(u^n)_j := S^M(u^n)_j + \epsilon\Delta t F\left(\frac{S^A(u^n)_j - S^M(u^n)_j}{\epsilon\Delta t}\right), \tag{1.8}$$

where $\epsilon = \epsilon_{\Delta t,\Delta x} > 0$ is a parameter that will satisfy

$$\lim_{(\Delta t,\Delta x)\to 0} \epsilon = 0. \tag{1.9}$$

More precision on the choice of ϵ will be given later on.

The scheme is initialized as follows:

$$u_j^0 := v_0(x_j), \quad \forall j \in \mathbb{Z}. \tag{1.10}$$

Now we make precise some requirements on S^M, S^A and F.

Definition of the monotone finite difference scheme S^M: Following Crandall and Lions [34], we consider a finite difference scheme written as $u^{n+1} = S^M(u^n)$ with

$$S^M(u^n)(x) := u^n(x) - \Delta t\ h^M(x, D^- u^n(x), D^+ u^n(x)), \tag{1.11}$$

with

$$D^{\pm} u(x) := \pm \frac{u(x \pm \Delta x) - u(x)}{\Delta x},$$

where h^M corresponds to a monotone numerical Hamiltonian that will be made precise below. We will denote also $S^M(u^n)_j := S^M(u^n)(x_j)$. Therefore the scheme also reads, for all $j \in \mathbb{Z}$, $\forall n \geq 0$:

$$u_j^{n+1} := u_j^n - \Delta t\ h^M(x_j, D^- u_j^n, D^+ u_j^n), \quad D^{\pm} u_j^n := \pm \frac{u_{j\pm1}^n - u_j^n}{\Delta x}. \tag{1.12}$$

(A3) - Assumptions on S^M:

(i) h^M is a Lipschitz continuous function.
(ii) (*consistency*) $\forall x$, $\forall u$, $h^M(x, p, p) = H(p)$.
(iii) (monotonicity) for any functions u, v,

$$u \leq v \Longrightarrow S^M(u) \leq S^M(v).$$

In pratice condition (A3)-(iii) is only required at mesh points and the condition reads

$$\Big(\forall j,\ u_j \leq v_j\Big) \quad \Rightarrow \quad \Big(\forall j,\ S^M(u)_j \leq S^M(v)_j\Big) \tag{1.13}$$

At this stage, we notice that under condition (A3) the filtered scheme is "ϵ-monotone" in the sense that

$$u_j \leq v_j,\ \forall j, \quad \Rightarrow \quad S^F(u)_j \leq S^F(v)_j + \epsilon\tau\, \|F\|_{L^\infty},\ \forall j. \tag{1.14}$$

with $\epsilon \to 0$ as $(\Delta t, \Delta x) \to 0$. This implies the convergence of the scheme by using Barles-Souganidis convergence theorem (see [10] and [2]).

Remark 1.2.1. *Under assumption (i), the consistency property (ii) is equivalent to say that, for any $v \in C^2([0,T]\times\mathbb{R})$, there exists a constant $C_M \geq 0$ independant of Δx such that*

$$\left| h^M(x, D^- v(x), D^+ v(x)) - H(x, v_x) \right| \leq C_M \Delta x \|\partial_{xx} v\|_\infty. \tag{1.15}$$

The same statement holds true if (1.15) is replaced by the following consistency error estimate:

$$\begin{aligned} \mathcal{E}_{S^M}(v)(t,x) &:= \left| \frac{v(t+\Delta t, x) - S^M(v(t,.))(x)}{\Delta t} - \big(v_t(t,x) + H(x, v_x(t,x))\big) \right| \\ &\leq C_M \Big(\Delta t \|\partial_{tt} v\|_\infty + \Delta x \|\partial_{xx} v\|_\infty \Big). \end{aligned} \tag{1.16}$$

Remark 1.2.2. *Assuming (i), it is easily shown that the monotonicity property (iii) is equivalent to say that $h^M = h^M(x, p^-, p^+)$ satisfies, a.e. $(x, p^-, p^+) \in \mathbb{R}^3$:*

$$\frac{\partial h^M}{\partial p^-} \geq 0, \quad \frac{\partial h^M}{\partial p^+} \leq 0, \tag{1.17}$$

and the CFL condition

$$\frac{\tau}{\Delta x} \left(\frac{\partial h^M}{\partial p^-}(x, p^-, p^+) - \frac{\partial h^M}{\partial p^+}(x, p^-, p^+) \right) \leq 1. \tag{1.18}$$

When using finite difference schemes, it is assumed that the CFL condition (1.18) is satisfied, and that can be written equivalently in the form

$$c_0 \frac{\Delta t}{\Delta x} \leq 1. \tag{1.19}$$

Proposition 1.2.1. *Let Hamiltonian H and initial data v_0 be Lipschitz continuous (satisfies (A1)-(A2)) and $v_j^0 = u_0(x_j)$. For fix $\Delta t > 0$ and $\Delta x > 0$, let the monotone finite difference scheme (1.11) (with numerical Hamiltonian satisfies (A3)) with standard CFL (1.19). Then there is a constant C such that for any $n \leq T/\Delta t$, we have*

$$|v^n(x_i) - u^n(x_i)| \leq C\sqrt{\Delta x}. \tag{1.20}$$

for $\Delta t \to 0$, $\Delta t = c\Delta x$.

Proof. For proof we refer reader to to [34]. □

As a pure convergence result, Crandall- Lions theory is generalized by the BarlesSouganidis theorem, although in the latter result no convergence estimate is obtained.

Example 1.2.1. *Let us consider the Lax-Friedrichs numerical Hamiltonian*

$$h^{M,LF}(x,p^-,p^+) := H(x,\frac{p^-+p^+}{2}) - \frac{c_0}{2}(p^+-p^-) \tag{1.21}$$

where $c_0 > 0$ *is a constant. The scheme is consistant; it is furthermore monotone under the conditions* $\max_{x,p}|\partial_p H(x,p)| \le c_0$, *and* $c_0\frac{\tau}{\Delta x} \le 1$.

Definition of the high-order scheme S^A*:* we consider an iterative scheme of "high-order" in the form $u^{n+1} = S^A(u^n)$, written as

$$S^A(u^n)(x) = u^n(x) - \tau h^A(x, D^{k,-}u^n(x), \dots, D^-u^n(x), D^+u^n(x), \dots, D^{k,+}u^n(x)),$$

where h^A corresponds to a "high-order" numerical Hamiltonian, and

$$D^{\ell,\pm}u(x) := \pm\frac{u(x\pm\ell\Delta x)-u(x)}{\Delta x} \quad \text{for} \quad \ell = 1,\dots,k$$

. To simplify the notations we may write (1.22) in the more compact form

$$S^A(u^n)(x) = u^n(x) - \tau h^A\big(x, D^{\pm}u^n(x)\big) \tag{1.22}$$

even if there is a dependency in $(D^{\ell,\pm}u^n(x))_{\ell=1,\dots,k}$.

(A4) - Assumptions on S^A:

(i) h^A *is a Lipschitz continuous function.*

(ii) *(high-order consistency) There exists* $k \ge 2$, *forall* $\ell \in [1,\dots,k]$, *for any function* $v = v(t,x)$ *of class* $C^{\ell+1}$, *there exists* $C_{A,\ell} \ge 0$,

$$\mathcal{E}_{S^A}(v)(t,x) := \left|\frac{v(t+\Delta t,x) - S^A(v(t,.))(x)}{\Delta t} - \big(v_t(t,x) + H(x,v_x(t,x))\big)\right| \tag{1.23}$$

$$\le C_{A,\ell}\Big(\Delta t^\ell \|\partial_t^{\ell+1}v\|_\infty + \Delta x^\ell \|\partial_x^{\ell+1}v\|_\infty\Big). \tag{1.24}$$

Here v_x^ℓ denotes the ℓ-th derivative of v w.r.t. x.

Remark 1.2.3. *The high-order consistency implies, for all $\ell \in [1, \dots, k]$, and for $v \in C^{\ell+1}(\mathbb{R})$,*

$$\left| h^A(x, \dots, D^- v, D^+ v, \dots) - H(x, v_x) \right| \leq \; C_{A,\ell} \|\partial_x^{\ell+1} v\|_\infty \Delta x^\ell.$$

Remark 1.2.4. (Centered scheme) *A typical example with $k = 2$ is obtained with the centered approximation in space and the TVD-RK2 scheme in time (or Heun scheme):*

$$S_0(u^n)_j := u_j^n - \Delta t H\left(x_j, \frac{u_{j+1}^n - u_{j-1}^n}{2\Delta x}\right), \tag{1.25a}$$

and

$$S^A(u) := \frac{1}{2}\left(u + S_0(S_0(u))\right). \tag{1.25b}$$

Of course there is no reason that the centered scheme be stable (as it will be shown in the numerical section). Using a filter will help stabilize the scheme.

Remark 1.2.5. *A similar example with $k = 3$ can be obtained with any third order finite difference approximation in space and the TVD-RK3 scheme in time [59].*

Definition of the filter function F. We recall that Froese and Oberman's filter function used in [51] was:

$$\tilde{F}(x) = sign(x)\max(1 - ||x| - 1|, 0) = \begin{cases} x & |x| \leq 1. \\ 0 & |x| \geq 2. \\ -x + 2 & 1 \leq x \leq 2. \\ -x - 2 & -2 \leq x \leq -1. \end{cases}$$

In the present work use another filter function which is also used by Oberman and Salvador in [86] simply as follows:

$$F(x) := x 1_{|x| \leq 1} = \begin{cases} x & \text{if } |x| \leq 1, \\ 0 & \text{otherwise.} \end{cases} \tag{1.26}$$

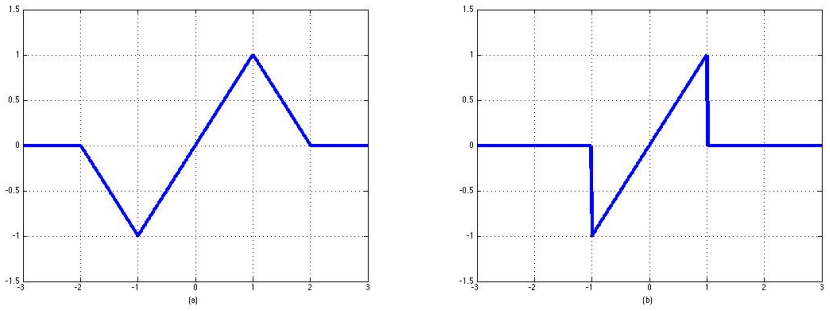

FIGURE 1.1: Froese and Oberman's filter (left), Oberman and Salvador's filter (right)

The idea of the present filter function is that it will keep the high-order scheme when $|h^A - h^M| \leq \epsilon$, because then

$$\frac{|S^A - S^M|}{\Delta t \epsilon} \leq 1 \text{ and } S^F = S^M + \Delta t \epsilon F(\frac{S^A - S^M}{\Delta t \epsilon}) \equiv S^A,$$

and otherwise $F = 0$ and $S^F = S^M$, i.e., the scheme is simply given by the monotone scheme itself. Clearly the main difference is the discontinuity at $x = -1, 1$. As mentionned in [86], use of a discontinuous filter may lead to difficulties when dealing with implicit schemes in order to show the existence of the numerical solution. However, here, we focus only on explicit schemes.

1.3 Convergence result

The following theorem gives several basic convergence results for the filtered scheme. Note that the high-order assumption (A4) will not be necessary to get the error estimates (i)-(ii). It will be only used to get a high-order consistency error estimate in the regular case (part (iii)). Globally the scheme will have just an $O(\sqrt{\Delta x})$ rate of convergence for Lipschitz continuous solutions because the jumps in the gradient prevent high-order accuracy on the kinks.

Theorem 1.3.1. *Assume (A1)-(A2), and v_0 bounded. We assume also that S^M satisfies (A3), and $|F| \leq 1$. Let u^n denote the filtered scheme (1.8). Let $v_j^n := v(t_n, x_j)$ where v is the exact solution of (1.6). Assume*

$$0 < \epsilon \leq c_0 \sqrt{\Delta x} \tag{1.27}$$

for some constant $c_0 > 0$. *(i) The scheme* u^n *satisfies the Crandall-Lions estimate*

$$\|u^n - v^n\|_\infty \leq C\sqrt{\Delta x}, \quad \forall\ n = 0, ..., N. \tag{1.28}$$

for some constant C *independent of* Δx.

(ii) (First-order convergence for classical solutions.) If furthermore the exact solution v *belongs to* $C^2([0,T] \times \mathbb{R})$, *and* $\epsilon \leq c_0 \Delta x$ *(instead of (1.27)). Then it holds*

$$\|u^n - v^n\|_\infty \leq C\Delta x, \quad n = 0, ..., N, \tag{1.29}$$

for some constant C *independent of* Δx.

(iii) (Local high-order consistency.) Let $\mathcal{N}$ *be a neighborhood of a point* $(t, x) \in (0, T) \times \mathbb{R}$. *Assume that* S^A *is a high-order scheme satisfying (A4) for some* $k \geq 2$. *Let* $1 \leq \ell \leq k$ *and* v *be a* $C^{\ell+1}$ *function on* $\mathcal{N}$. *Assume that*

$$(C_{A,1} + C_M) \left(\|v_{tt}\|_\infty \Delta t + \|v_{xx}\|_\infty \Delta x \right) \leq \epsilon. \tag{1.30}$$

Then, for sufficiently small $t_n - t$, $x_j - x$, Δt, Δx, *it holds*

$$S^F(v^n)_j = S^A(v^n)_j$$

and, in particular, a local high-order consistency error for the filtered scheme S^F*:*

$$\mathcal{E}_{S^F}(v^n)_j \equiv \mathcal{E}_{S^A}(v^n)_j = O(\Delta x^\ell)$$

(the consistency error $\mathcal{E}_{S^A}$ *is defined in (1.23)).*

Proof of Theorem 1.3.1: (*i*) Let $w_j^{n+1} = S^M(w^n)_j$ be defined with the monotone scheme only, with $w_j^0 = v_0(x_j) = u_j^0$. By definitions,

$$u_j^{n+1} - w_j^{n+1} \quad = \quad S^M(u^n)_j - S^M(w^n)_j + \epsilon \Delta t F(.)$$

Hence, by using the monotonicity of S^M,

$$\max_j |u_j^{n+1} - w_j^{n+1}| \quad \leq \quad \max_j |u_j^n - w_j^n| + \epsilon \Delta t,$$

and by recursion, for $n \leq N$,

$$\max_j |u_j^n - w_j^n| \quad \leq \quad \epsilon n \Delta t \leq T\epsilon.$$

On the other hand, by Crandall and Lions [34], an error estimate holds for the monotone scheme:

$$\max_j |w_j^n - v_j^n| \quad \leq \quad C\sqrt{\Delta x},$$

for some $C \geq 0$. By summing up the previous bounds, we deduce

$$\max_j |u_j^n - v_j^n| \quad \leq \quad C\sqrt{\Delta x} + T\epsilon,$$

and together with the assumption on ϵ, it gives the desired result.

(ii) Let $\mathcal{E}_j^n := \dfrac{v_j^{n+1} - S^M(v^n)_j}{\Delta t}$. If the solution is C^2 regular with bounded second order derivatives, then the consistency error is bounded by

$$|\mathcal{E}_j^n| \leq C_M(\Delta t + \Delta x). \tag{1.31}$$

Hence

$$\begin{aligned} |u_j^{n+1} - v_j^{n+1}| &= |S^M(u^n)_j - S^M(v^n)_j + \Delta t \mathcal{E}_j^n + \Delta t \epsilon F(.)| \\ &\leq \|u^n - v^n\|_\infty + \Delta t \|\mathcal{E}^n\|_\infty + \Delta t \epsilon. \end{aligned}$$

By recursion, for $n\Delta t \leq T$,

$$\|u^n - v^n\|_\infty \quad \leq \quad \|u^0 - v^0\|_\infty + T\left(\max_{0\leq k\leq N-1} \|\mathcal{E}^k\|_\infty + \epsilon\right).$$

Finally by using the assumption on ϵ, the bound (1.31) and the fact that $\Delta t = O(\Delta x)$ (using CFL condition (1.19)), we get the desired result.

(iii) To prove that $S^F(v^n)_j = S^A(v^n)_j$, one has to check that

$$\frac{|S^A(v^n)_j - S^M(v^n)_j|}{\epsilon \Delta t} \leq 1$$

as $(\Delta t, \Delta x) \to 0$. By using the consistency error definitions,

$$\begin{aligned}\frac{|S^A(v^n)_j - S^M(v^n)_j|}{\Delta t} &= \left| \frac{v_j^{n+1} - S^A(v^n)_j}{\Delta t} + v_t(t_n, x_j) + H(x_j, v_x(t_n, x_j)) \right. \\ &\qquad \left. - \left(\frac{v_j^{n+1} - S^M(v^n)_j}{\Delta t} + v_t(t_n, x_j) + H(x_j, v_x(t_n, x_j)) \right) \right| \\ &\leq |\mathcal{E}_{S^A}(v^n)_j| + |\mathcal{E}_{S^M}(v^n)_j| \\ &\leq (C_{A,1} + C_M)(\Delta t \|v_{tt}\|_\infty + \Delta x \|v_{xx}\|_\infty)\end{aligned}$$

Hence the desired result follows. □

Remark 1.3.1. (related approaches) *It is already known from the original work of Osher and Shu [71] that it is possible to modify and ENO scheme in order to obtain a convergent scheme. For instance, if $D^{\pm,A}u_j^n$ denotes a high-order finite difference derivative estimate (of ENO type), a projection on the first-order finite difference derivative $D^{\pm}u_j^n$ can be used, up to a controlled error (see in particular Remark 2.2 of [71]):*

$$\textit{instead of } \; D^{\pm,A}u_j^n, \quad \textit{use } P_{[D^{\pm}u_j^n, M\Delta x]}\left(D^{\pm,A}u_j^n\right)$$

where $P_{[a,b]}(y)$ is the projection defined by:

$$P_{[a,b]}(y) := \begin{cases} y & \textit{if } \; a-b \leq y \leq a+b \\ a-b & \textit{if } \; y \leq a-b \\ a+b & \textit{if } \; y \geq a+b \end{cases}$$

and $M > 0$ is some constant greater than the expected value $\frac{1}{2}|u_{xx}(t_n, x_j)|$. However, we emphasize that in our approach we do not consider a projection but a perturbation with a filter, which is sligthly different. Indeed, by using a projection into an interval of the form $[a - M\Delta x,\, a + M\Delta x]$ where $a = D^{\pm}u_i^n$, numerical tests show that we may choose too often one of the extremal values $a \pm M\Delta x$ which is then produces an overall too big error (worse than using the first-order finite differences).

Following the present approach, we would rather advise to use,

$$\textit{instead of } \; D^{\pm,A}u_j^n, \quad \textit{the value } \tilde{P}_{[D^{\pm}u_j^n, M\Delta x]}(D^{\pm,A}u_j^n)$$

where $\tilde{P}_{[a,b]}(y)$ *is defined by:*

$$\tilde{P}_{[a,b]}(y) := \begin{cases} y & \text{if } a-b \leq y \leq a+b \\ a & \text{if } y \notin [a-b, a+b] \end{cases}$$

Remark 1.3.2. Filtered semi-Lagrangian scheme. *Let us consider the case of*

$$H(x,p) := \min_{b\in B} \max_{a\in A} \{-f(x,a,b).p - \ell(x,a,b)\}, \tag{1.32}$$

where $A \subset \mathbb{R}^m$ *and* $B \subset \mathbb{R}^n$ *are non-empty compact sets (with* $m,n \geq 1$*),* $f : \mathbb{R}^d \times A \times B \to \mathbb{R}^d$ *and* $\ell : \mathbb{R}^d \times A \times B \to \mathbb{R}$ *are Lipschitz continuous w.r.t.* x*:* $\exists L \geq 0$*,* $\forall (a,b) \in A \times B$*,* $\forall x, y$*:*

$$\max\left(|f(x,a,b) - f(y,a,b)|, |\ell(x,a,b) - \ell(y,a,b)|\right) \ \leq \ L|x-y|. \tag{1.33}$$

(We notice that (A2) is satisfied for hamiltonian functions such as (1.32).) Let $[u]$ *denote the* P^1*-interpolation of* u *in dimension one on the mesh* (x_j)*, i.e.*

$$x \in [x_j, x_{j+1}] \quad \Rightarrow \quad [u](x) := \frac{x_{j+1}-x}{\Delta x} u_j + \frac{x-x_j}{\Delta x} u_{j+1}. \tag{1.34}$$

Then a monotone SL scheme can be defined as follows:

$$S^M(u^n)_j := \min_{a\in A} \max_{b\in B} \Big([u^n]\big(x_j + \Delta t f(x_j,a,b)\big) + \Delta t \ell(x_j,a,b) \Big). \tag{1.35}$$

A filtered scheme based on SL can then be defined by (1.8) and (1.35). Convergence result as well as error estimates could also be obtained in this framework. (For error estimates for the monotone SL scheme, we refer to [42, 102])

1.3.1 Adding a limiter

The basic filtered scheme (1.8) is designed to be of high-order where the solution is regular and when there is no viscosity aspects. However, for instance in the case of front propagation, it can be observed that the filter scheme may let small errors occur near extrema, when two possible directions of propagation occur in the same cell.

This is the case for instance near a minima for an eikonal equation. In order to improve the scheme near extrema, we propose to introduce a limiter before doing the filtering process. Limiting correction will be needed only when there is some viscosity aspect (it is not needed for advection).

Let us consider the case of front propagation, i.e., equation of type (1.6), now with

$$H(x, v_x) = \max_{a \in A} \left(f(x, a) v_x \right) \tag{1.36}$$

(i.e., no distributive cost in the Hamiltonian function).

In the one-dimensional case, a viscosity aspect may occur at a minima detected at mesh point x_i if

$$\min_a f(x_j, a) \leq 0 \quad \text{and} \quad \max_a f(x_j, a) \geq 0. \tag{1.37}$$

In that case, the solution should not go below the local minima around this point, i.e., we want

$$u_j^{n+1} \geq u_{min,j} := \min \left(u_{j-1}^n, u_j^n, u_{j+1}^n \right), \tag{1.38}$$

and, in the same way, we want to impose that

$$u_j^{n+1} \leq u_{max,j} := \max \left(u_{j-1}^n, u_j^n, u_{j+1}^n \right). \tag{1.39}$$

If we consider the high-order scheme to be of the form $u_j^{n+1} = u_j^n - \Delta t h^A(u^n)$, then the limiting process amount to saying that

$$h^A(u^n)_j \leq h_j^{max} := \frac{u_j^n - u_{min,j}}{\Delta t}.$$

and

$$h^A(u^n)_j \geq h_j^{min} := \frac{u_j^n - u_{max,j}}{\Delta t}.$$

This amounts to define a limited $\bar{h}^A$ such that, if (1.37) holds at mesh point x_j, then

$$\bar{h}^A(u^n)_j := \min \left(\max(h^A(u^n)_j,\, h_j^{min}),\, h_j^{max} \right).$$

and, otherwise,

$$\bar{h}_j^A :\equiv h_j^A.$$

Then the filtering process is the same, using $\bar{h}^A$ instead of h^A for the definition of the high-order hamiltonian.

For two dimensional equations a similar limiter could be developped in order to make the scheme more efficient at singular regions. However, for the numerical tests of the next section (in two dimensions) we will simply limit the scheme by using an equivalent of (1.38)-(1.39). Hence, instead of the scheme value $u_{ij}^{n+1} = S^A\left(u^n\right)_{ij}$ for the high-order scheme, we will update the value by

$$u_{ij}^{n+1} = \min\left(\max\left(S^A(u^n)_{ij}, u_{ij}^{min}\right), u_{ij}^{max}\right), \tag{1.40}$$

where $u_{ij}^{min} = \min\left(u_{ij}^n, u_{i\pm1,j}^n, u_{i,j\pm1}^n\right)$ and $u_{ij}^{max} = \max\left(u_{ij}^n, u_{i\pm1,j}^n, u_{i,j\pm1}^n\right)$.

1.3.2 Choice of the parameter ϵ : a simplified approach.

The scheme should switch to high-order scheme when some regularity of the data is detected, and in that case we should have

$$\left|\frac{S^A(v) - S^M(v)}{\epsilon\Delta t}\right| \;=\; \left|\frac{h^A(\cdot) - h^M(\cdot)}{\epsilon}\right| \;\leq\; 1.$$

In a region where a function $v = v(x)$ is regular enough, by using Taylor expansions, zero order terms in $h^A(x, D^{\pm}v)$ and $h^M(x, D^{\pm}v)$ vanish (they are both equal to $H(x, v_x(x))$) and it remains an estimate of order Δx. More precisely, by using the high-order property (A4) we have

$$h^A(x_j, D^{\pm}v_j) = H(x_j, v_x(x_j)) + O(\Delta x^2).$$

On the other hand, by using Taylor expansions,

$$Dv_j^{\pm} = v_x(x_j) \pm \frac{1}{2}v_{xx}(x_j)\Delta x + O(\Delta x^2),$$

Hence, denoting $h^M = h^M(x, u^-, u^+)$, it holds at points where h^M is regular,

$$h^M(x_j, Dv_j^-, Dv_j^+) = H(x_j, v_x(x_j)) + \frac{1}{2}v_{xx}(x_j)\left(\frac{\partial h_j^M}{\partial u^+} - \frac{\partial h_j^M}{\partial u^-}\right) + O(\Delta x^2).$$

Therefore,

$$|h^A(v) - h^M(v)| \quad = \quad \frac{1}{2}|v_{xx}(x_j)| \left| \frac{\partial h_j^M}{\partial u^+} - \frac{\partial h_j^M}{\partial u^-} \right| \Delta x + O(\Delta x^2).$$

Hence we will make the choice to take ϵ roughly such that

$$\frac{1}{2}|v_{xx}(x_j)| \left| \frac{\partial h_j^M}{\partial u^+} - \frac{\partial h_j^M}{\partial u^-} \right| \Delta x \leq \epsilon \tag{1.41}$$

(where $h_j^M = h^M(x_j, v_x(x_j), v_x(x_j))$). Therefore, if at some point x_j (1.41) holds, then the scheme will switch to the high-order scheme. Otherwise, when the expectations from h^M and h^A are different enough, the scheme will switch to the monotone scheme.

In conclusion we have upper and lower bound for the switching parameter ϵ:

- Choose $\epsilon \leq c_0\sqrt{\Delta x}$ for some constant $c_0 > 0$ in order that the convergence and error estimate result holds (see Theorem 1.3.1).
- Choose $\epsilon \geq c_1 \Delta x$, where c_1 is sufficiently large. This constant should be choosen roughly such that

  $$\frac{1}{2}\|v_{xx}\|_\infty \left\| \frac{\partial h^M}{\partial u^+}(., v_x, v_x) - \frac{\partial h^M}{\partial u^-}(., v_x, v_x) \right\|_\infty \leq c_1.$$

  where the range of values of v_x and v_{xx} can be estimated, in general, from the values of $(v_0)_x$, $(v_0)_{xx}$ and the Hamiltonian function H. Then the scheme is expected to switch to the high-order scheme where the solution is regular.

1.4 Numerical Test

In this section we present several numerical tests in one and two dimensions.

Unless otherwise precised, the filtered scheme will refer to the scheme where the high-order Hamiltonian is the centered scheme in space (see Remark 1.2.4), with Heun (RK2) scheme discretisation in time (see in particular Eqs. (1.25a)-(2.18b)). Hereafter this scheme will be referred as the "centered scheme". The monotone finite difference scheme and function h^M will be made precise for each example. For the filtered scheme, unless otherwise precised, the switching coefficient $\epsilon = 5\Delta x$. will be used. In practice $\epsilon = c_1 \Delta x$

with c_1 sufficiently large does not much change the numerical results in the following tests. All the tested filtered schemes (appart from the steady and obstacle equations) enters in the convergence framework of the previous section, so in particular there is a theoretical convergence of order $\sqrt{\Delta x}$ under the usual CFL condition.

In the tests, the filtered scheme will be in general compared to a second order ENO scheme (for precise definition, see Appendix A), as well as the centered (a priori unstable) scheme without filtering.

In several cases, local error in the L^2 norms are computed in some subdomain D, which, at a given time t_n, corresponds to

$$e_{L^2_{loc}} := \left(\Delta x \sum_{i, x_i \in D} |v(t_n, x_i) - u_i^n|^2 \right)^{1/2}$$

Examples 1 and 2 deal with one-dimensional HJ equations, examples 3 and 4 with two-dimensional HJ equations, and the last three examples will concern a one-dimensional steady equation and two nonlinear one-dimensional obstacle problems.

1.5 One dimentional Tests

1.5.1 Advection equation

Example 1.5.1. (Advection equation). *In this test we consider an sadvection equation in one dimension*

$$\begin{cases} v_t + v_x = 0, \quad t > 0, \ x \in (-2, 2), \\ v(0, x) = v_0(x), \quad x \in (-2, 2) \end{cases} \tag{1.42}$$

with periodic boundary condition on $(-2, 2)$*, terminal time* $T = 0.3$ *and the following initial data:*

$$v_0(x) = -\max\left(0, 1 - |x|^2\right)^4. \tag{1.43}$$

This "smooth" initial data is chosen in order to have at least a 3rd order continuous derivative at $x = \pm 1$. *The monotone upwind Hamiltonian is used* ($h^M(x, v^-, v^+) := v^-$).

Results are given in Table 1.1 for the errors in L^2 *norms, where is compared the CFD scheme (central finite difference scheme), the ENO scheme (second order ENO scheme) with RK2 in time, as described in Appendix A), and the Filter scheme using* $\epsilon = 4\Delta x$. *In this test the CFL number* $\left(= \frac{\tau}{\Delta x}\right)$ *is* 0.37. *Errors are numerically comparable in that case, all schemes are second order, also CFD scheme is numerically stable without filtering. More precisely we observe that CFD and Filter schemes give identical results, which means that the filtering has no effect here. So the filtering at least* does not deteriorate *the good behavior of the CFD scheme. (Results are similar for the* L^1 *and* L^∞ *errors.)*

A third order scheme. Then, we have also tested a third order filtered scheme. More precisely, to settle the third order scheme, the derivative v_x *was estimated using a third order backward difference:*

$$v_x(x_i) \equiv \frac{1}{\Delta x}\left(\frac{11}{6}v(x_i) - 3v(x_{i-1}) + \frac{3}{2}v(x_{i-2}) - \frac{1}{3}v(x_{i-3})\right) \equiv (\tilde{v}_x)_i.$$

and the corresponding high order Hamiltonian, simply $h^A(v)_i := H((\tilde{v}_x)_i)$. *The usual TVD-RK3 method was used for time discretisation, and is recalled in Appendix A (see for instance [59] and refs. therein).*

Results are given in Table 1.2, using CFL= 0.3. *It is indeed also observed near to third order convergence. This is only true for small enough CFL numbers though (CFL* $\leq$ 0.35*), otherwise it was numerically observed a switch to second order convergence.*

		Filter $\epsilon = 4\Delta x$		CFD		ENO2	
M	N	L^2 error	order	L^2 error	order	L^2 error	order
20	4	4.97E-02	-	4.97E-02	-	7.95E-02	-
40	8	1.26E-02	1.98	1.26E-02	1.98	2.29E-02	1.79
80	16	3.07E-03	2.03	3.07E-03	2.03	5.96E-03	1.95
160	32	7.66E-04	2.00	7.66E-04	2.00	1.51E-03	1.98
320	64	1.90E-04	2.01	1.90E-04	2.01	3.77E-04	2.00
640	128	4.76E-05	2.00	4.76E-05	2.00	9.41E-05	2.00

TABLE 1.1: (Example 2.3.1.) Global L^2 errors for Filter, Central Finite difference scheme (CFD) and ENO (2nd order) scheme with RK2 in time.

M	N	L^1 error	order	L^2 error	order	L^∞ error	order
20	4	1.12E-01	-	7.74E-01	-	8.82E-02	-
40	8	1.67E-02	2.78	1.19E-02	2.71	1.41E-02	2.64
80	16	2.21E-03	2.92	1.60E-03	2.89	1.86E-03	2.93
160	32	2.77E-04	2.99	2.07E-04	2.95	2.87E-04	2.69
320	64	3.43E-05	3.02	2.64E-05	2.97	4.78E-05	2.58
640	128	4.51E-06	2.93	3.43E-06	2.94	7.26E-06	2.72

TABLE 1.2: (Example 2.3.1.) Global Errors for the third order filter scheme ($\epsilon = 4\Delta x$).

1.5.2 Eikonal equation

Example 1.5.2. (Eikonal equation) *We consider the case of*

$$v_t + |v_x| = 0, \quad t \in (0,T),\ x \in (-2,2), \tag{1.44}$$

$$v(0,x) = v_0(x) := \max(0, 1-x^2)^4, \quad x \in (-2,2). \tag{1.45}$$

In Table 1.3, we compare the filtered scheme (with $\epsilon = 5\Delta x$) with the centered scheme and the ENO second order scheme, with CFL $= 0.37$ and terminal time $T = 0.3$. For the filtered scheme, the monotone hamiltonian used is $h^M(x, v^-, v^+) := max(v^-, -v^+)$.

As expected, we observe that the centered scheme alone is unstable. On the other hand, the filtered and ENO schemes are numerically comparable in that case, and second order convergent (the results are similar for the L^1 and the L^∞ errors).

Then, in Table 1.4, we consider the same PDE but with the following reversed initial data:

$$\tilde{v}_0(x) := -\max(0, 1-x^2)^4, \quad x \in (-2,2). \tag{1.46}$$

In that case the centered scheme alone is unbounded. The filtered scheme (with $\epsilon = 5\Delta x$) is second order. However, here, the limiter correction as described in section (1.3.1) was needed in order to get second order behavior. We also observe that the filtered scheme gives better results than the ENO scheme. (We have also numerically tested the ENO scheme with the same limiter correction but it does not improve the behavior of the ENO scheme alone).

In conclusion, this first example shows firstly, that the filtered scheme can stabilize an otherwise unstable scheme, and secondly that it can give the desired second order behavior.

		filtered ($\epsilon = 5\Delta x$)		centered		ENO2	
M	N	L^2 error	order	L^2 error	order	L^2 error	order
40	9	7.51E-03	-	1.18E-01	-	1.64E-02	-
80	17	3.36E-03	1.16	1.14E-01	0.06	4.38E-03	1.91
160	33	8.02E-04	2.07	1.13E-01	0.00	1.19E-03	1.87
320	65	1.80E-04	2.16	1.13E-01	0.00	3.22E-04	1.89
640	130	4.53E-05	1.99	1.13E-01	0.00	8.22E-05	1.97

TABLE 1.3: (Example 2.3.2. with initial data (1.45)) L^2 errors for filtered scheme, centered scheme, and ENO second order scheme

		filtered ($\epsilon = 5\Delta x$)		centered		ENO2	
M	N	error	order	error	order	error	order
40	9	1.27E-02	-	2.03E-02	-	2.60E-02	-
80	17	3.17E-03	2.00	8.96E-03	1.18	8.00E-03	1.70
160	33	7.90E-04	2.01	1.06E-02	-0.24	2.50E-03	1.68
320	65	1.97E-04	2.00	1.26E-01	-3.57	7.80E-04	1.68
640	130	4.92E-05	2.00	1.06E+02	-9.71	2.44E-04	1.67

TABLE 1.4: (Example 2.3.2. with initial data (1.46).) L^2 errors for filtered scheme, centered scheme, and ENO second order scheme.

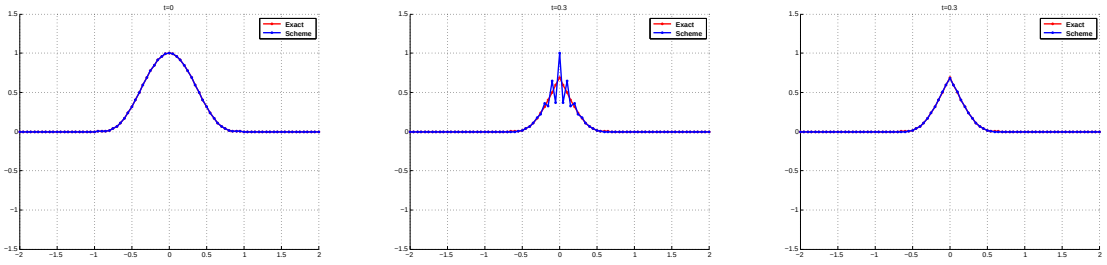

FIGURE 1.2: (Example 2.3.2.) With initial data (1.45) (left), and plots at time $T = 0.3$ with centered scheme - middle - and filtered scheme - right, using $M = 160$ mesh points.

1.5.3 Burger's equation

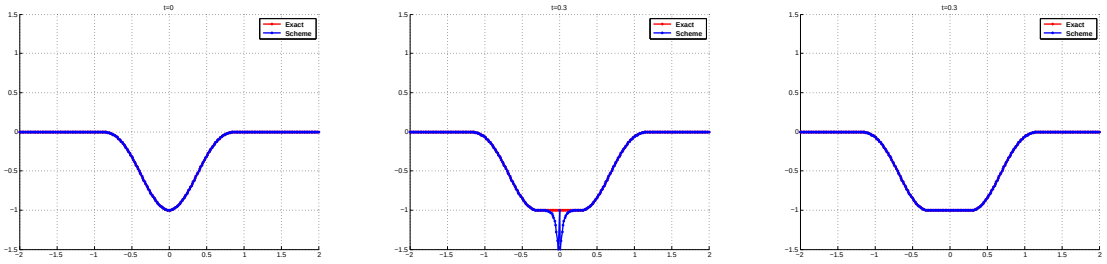

FIGURE 1.3: (Example 2.3.2. With initial data (1.46) (left), and plots at time $T = 0.3$ with centered scheme - middle - and filtered scheme - right, using $M = 160$ mesh points.

Example 1.5.3. (Burger's equation)

In this example an HJ equivalent of the nonlinear Burger's equation is considered:

$$v_t + \frac{1}{2}|v_x|^2 = 0, \quad t > 0, \ x \in (-2, 2) \tag{1.47a}$$

$$v(0, x) = v_0(x) := \max(0, 1 - x^2), \quad x \in (-2, 2) \tag{1.47b}$$

with Dirichlet boundary condition on $(-2, 2)$. *Exact solution is known.*[1]. *In order to test high order convergence we have considered the smoother initial data which is the one obtained from* (1.47) *at time* $t_0 := 0.1$, *i.e. :*

$$w_t + \frac{1}{2}|w_x|^2 = 0, \quad t > 0, \ x \in (-2, 2). \tag{1.48a}$$

$$w(0, x) := v(t_0, x), \quad x \in (-2, 2), \tag{1.48b}$$

with exact solution $w(t, x) = v(t + t_0, x)$.

An illustration is given in Fig. 1.4. For the filtered scheme, the monotone hamiltonian used is $h^M(x, v^-, v^+) := \frac{1}{2}(v^-)^2 \ 1_{v^->0} + \frac{1}{2}(v^+)^2 \ 1_{v^+<0}$.

Errors are given in Table (1.5), *using CFL*=0.37 *and terminal time* $T = 0.3$.

[1] It holds

$$v(t, x) = \frac{(\max(0, 1 - |\bar{x}|))^2}{2t} 1_{\{t > \frac{1}{2}\}} + \frac{(1 - 2t)^2 - |x|^2}{1 - 2t} \ 1_{\{1 \geq |x| \geq 1 - 2t\}}.$$

In conclusion we observe numerically that the filtered scheme keeps the good behavior of the centered scheme (here stable and almost second order).

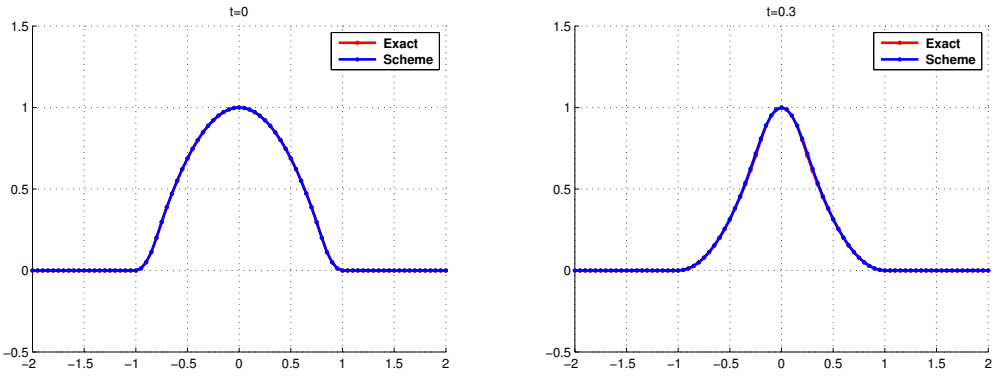

FIGURE 1.4: (Example 2.3.4) Plots at $t = 0$ and $t = 0.3$ with the filtered scheme.

		filtered ($\epsilon = 5\Delta x$)		centered		ENO2	
M	N	error	order	error	order	error	order
40	9	2.06E-02	-	2.07E-02	-	2.55E-02	-
80	17	6.24E-03	1.73	6.24E-03	1.73	8.24E-03	1.63
160	33	1.85E-03	1.76	1.85E-03	1.76	2.81E-03	1.55
320	65	5.51E-04	1.74	5.51E-04	1.74	1.03E-03	1.45
640	130	1.68E-04	1.71	1.68E-04	1.71	3.74E-04	1.47

TABLE 1.5: (Example 2.3.4) L^2 errors for filtered scheme, centered scheme, and ENO second order scheme.

1.6 Two dimensional tests

Example 1.6.1. (2D rotation) *We now apply filtered scheme to an advection equation in dimension 2:*

$$v_t - yv_x + xv_y = 0, \quad (x, y) \in \Omega, \ t > 0, \tag{1.49}$$

$$v(0, x, y) = v_0(x, y) := 0.5 - 0.5 \max\left(0, \frac{1 - (x-1)^2 - y^2}{1 - r_0^2}\right)^4 \tag{1.50}$$

where $\Omega := (-A, A)^2$ *(with* $A = 2.5$*),* $r_0 = 0.5$ *and with Dirichlet boundary condition* $v(t, x) = 0.5$, $x \in \partial\Omega$. *This initial condition is regular and such that the level set* $v_0(x, y) = 0$ *corresponds to a circle centered at* $(1, 0)$ *and of radius* r_0.

In this example the monotone numerical Hamiltonian is defined by

$$h^M(u_x^-, u_x^+, u_y^-, u_y^+) := \max(0, f_1(a,x,y))u_x^- + \min(0, f_1(a,x,y))u_x^+ + \max(0, f_2(a,x,y))u_y^- + \min(0, f_2(a,x,y))u_y^+ \quad (1.51)$$

and the high order scheme is the centered finite difference scheme in both spacial variables, and RK2 in time. The filtered scheme is otherwise the same as (1.8). However it is necessary to use a greater constant c_1 is the choice $\epsilon = c_1\Delta x$ in order to get (global) second order errors. We have used here $\epsilon = 20\Delta x$.

On the other hand the CFL condition is

$$\mu := c_0\left(\frac{\tau}{\Delta x} + \frac{\tau}{\Delta y}\right) \leq 1. \quad (1.52)$$

where here $c_0 = 2.5$ (an upper bound for the dynamics in the considered domain Ω). In this test the CFL number is $\mu := 0.37$.

Results are shown in Table 1.6 for terminal time time $T := \pi/2$. Although the centered scheme is a priori unstable, in this example it is numerically stable and of second order. So we observe that the filtered scheme keep this good behavior and is also or second order (ENO scheme gives comparable results here).

		filtered		centered		ENO	
Mx	Ny	L^2 error	order	L^2 error	order	L^2 error	order
20	20	5.05E-01	-	5.05E-01	-	6.99E-01	-
40	40	1.48E-01	1.77	1.48E-01	1.77	4.66E-01	0.58
80	80	3.77E-02	1.98	3.77E-02	1.98	2.04E-01	1.19
160	160	9.40E-03	2.00	9.40E-03	2.00	5.50E-02	1.89
320	320	2.34E-03	2.01	2.34E-03	2.01	1.29E-02	2.10

TABLE 1.6: (Example 2.3.5) Global L^2 errors for the filtered scheme, centered and second order ENO schemes (with CFL 0.37).

Example 1.6.2. (Eikonal equation) *In this example we consider the eikonal equation*

$$v_t + \|\nabla v\| = 0, \quad (x,y) \in \Omega, \ t > 0 \quad (1.53)$$

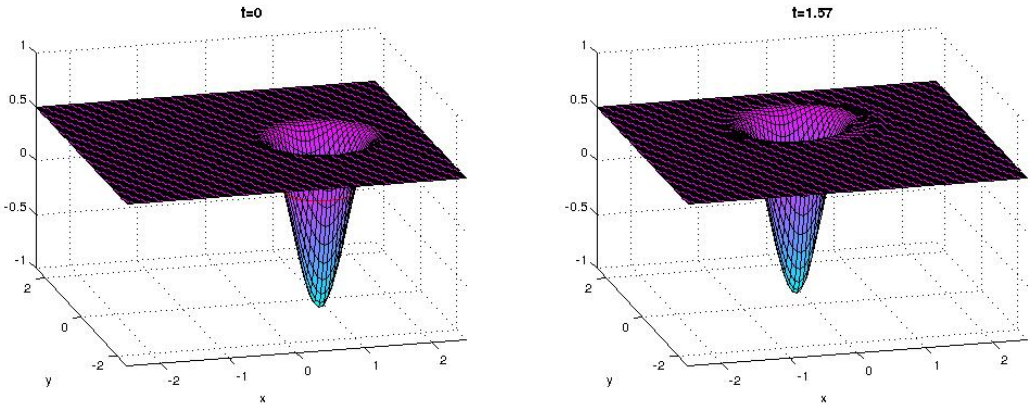

FIGURE 1.5: (Example 2.3.5) Filtered scheme, plots at time $t = 0$ (left) and $t = \pi/2$ (right) with $M = 80$ mesh points.

in the domain $\Omega := (-3, 3)^2$. *The initial data is defined by*

$$v_0(x, y) = \qquad (1.54)$$
$$0.5 - 0.5 \max\left(\max(0, \frac{1-(x-1)^2-y^2}{1-r_0^2})^4,\ \max(0, \frac{1-(x+1)^2-y^2}{1-r_0^2})^4 \right).$$

The zero-level set of v_0 *corresponds to two separates circles or radius* r_0 *and centered in* $A = (1, 0)$ *and* $B = (-1, 0)$ *respectively. Dirchlet boundary conditions are used as the previous example.*

The monotone hamiltonian h^M *used in the filtered scheme is in Lax-Friedriech form:*

$$\begin{aligned} h^M(x, u_1^-, u_1^+, u_2^-, u_2^+) &= H\left(x, \frac{u_1^- + u_1^+}{2}, \frac{u_2^- + u_2^+}{2}\right) \\ &\quad - \frac{C_x}{2}\left(u_1^+ - u_1^-\right) - \frac{C_y}{2}\left(u_2^+ - u_2^-\right), \end{aligned} \qquad (1.55)$$

where, here, $C_x = C_y = 1$. *We used the CFL condition* $\mu = 0.37$ *as in* (1.52). *Also, the simple limiter* (1.40) *was used for the filtered scheme as described in Section 1.3.1. It is needed in order to get a good second order behavior at extrema of the numerical solution. The filter coefficient is set to* $\epsilon = 20\Delta x$ *as in the previous example.*

Numerical results are given in Table 1.7, showing the global L^2 *errors for the filtered scheme, the centered scheme, and a second order ENO scheme, at time* $t = 0.6$. *We observe that the centered scheme has some unstabilities for fine mesh, while the filtered performs as expected.*

		filtered ($\epsilon = 20\Delta x$)		centered		ENO2	
Mx	Ny	L^2 error	order	L^2 error	order	L^2 error	order
25	25	5.39E-01	-	6.00E-01	-	5.84E-01	-
50	50	1.82E-01	1.57	2.25E-01	1.41	2.11E-01	1.47
100	100	3.72E-02	2.29	8.46E-02	1.41	6.88E-02	1.62
200	200	9.36E-03	1.99	3.53E-02	1.26	2.02E-02	1.76
400	400	2.36E-03	1.99	1.36E-01	-1.95	5.98E-03	1.76

TABLE 1.7: (Example 2.3.3) Global L^2 errors for filtered scheme, centered and second order ENO schemes.

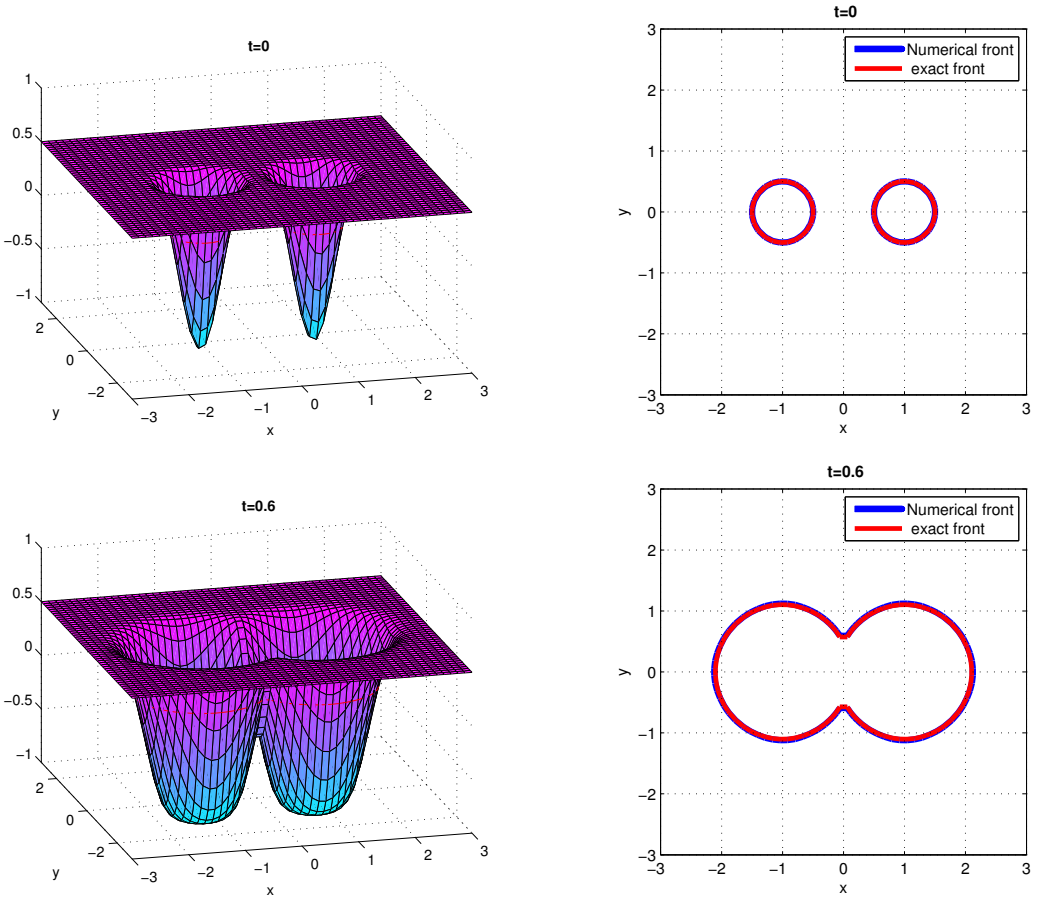

FIGURE 1.6: (Example 2.3.3) Plots at times $t = 0$ (top) and $t = \pi/2$ (bottom) for the filtered scheme with $M = 50$ mesh points. The figures to the right represent the 0-level sets.

Example 1.6.3. *In this example the considered HJ equation is*

$$v_t - yv_x + xv_y + \|\nabla v\| = 0, \quad (x,y) \in \Omega,\ t > 0, \tag{1.56}$$

with $\Omega = (-3,3)^2$*, and with the following initial data:*

$$v(0,x,y) = 0.5 - 0.5 \max\left(\max(0, \frac{1-(x-1)^2-y^2}{1-r_0^2})^4,\ \max(0, \frac{1-(x+1)^2-y^2}{1-r_0^2})^4 \right) \tag{1.57}$$

(together with Dirichlet boundary condition $v(t,x,y) = 0.5$ *for* $(x,y) \in \partial\Omega$*).*

Again we compare the filtered scheme (with $\epsilon = 5\Delta x$*) with the centered (a priori unstable) scheme and the second order ENO scheme.*

Numerical results are shown in Table 1.8, for terminal time $T = 0.75$ *and CFL* 0.37*. Local errors has been computed in the region* $|v(t,x,y)| \leq 0.1$ *and also away from the singular line* $x + y = 0$ *(i.e., for points such that furthermore* $|\frac{x+y}{\sqrt{2}}| \geq 0.1$*). In this example, the naive centered scheme is unstable (as expected), while the filtered scheme is stable and of second order.*

		filtered $\epsilon = 5\Delta x$		centered		ENO2	
Mx	Nx	L^2 error	order	L^2 error	order	L^2 error	order
25	25	1.02E-01	-	1.11E-01	-	1.14E-01	-
50	50	2.12E-02	2.45	1.99E-02	2.48	2.12E-02	2.43
100	100	9.02E-03	1.23	2.04E-02	-0.03	3.67E-03	2.53
200	200	1.90E-03	2.25	1.27E-02	0.69	8.61E-04	2.09
400	400	3.67E-04	2.38	1.13E-02	0.17	2.12E-04	2.02

TABLE 1.8: (Example 1.6.3) Local errors of filtered, centered and ENO scheme.

1.6.1 Steady equation

Example 1.6.4. (Steady eikonal equation) *We consider a steady eikonal equation with Dirichlet boundary condition, which is taken from Abgrall [2]:*

$$|v_x| = f(x) \quad x \in (0,1), \tag{1.58a}$$

$$v(0) = v(1) = 0, \tag{1.58b}$$

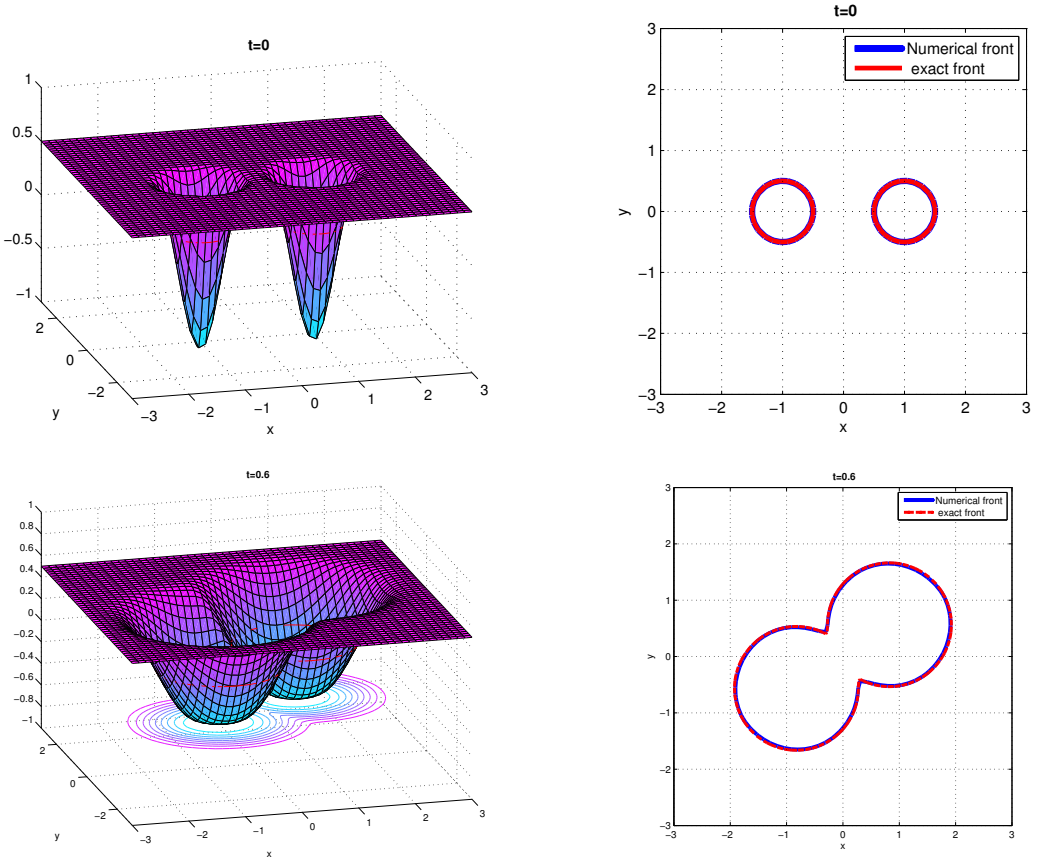

FIGURE 1.7: (Example (1.6.3)) Plots at times $t = 0$ (top) and $t = \pi/2$ (bottom) for the filtered scheme with $M = 50$ mesh points. The figures to the right represent the 0-level sets.

where $f(x) = 3x^2 + a$, *with* $a = \frac{1-2x_0^3}{2x_0-1}$ *and* $x_0 = \frac{\sqrt[3]{2}+2}{4\sqrt[3]{2}}$. *Exact solution is known:*

$$v(x) := \begin{cases} x^3 + ax & x \in [0, x_0], \\ 1 + a - ax - x^3 & x \in [x_0, 1]. \end{cases} \tag{1.59}$$

The steady solution for (1.58) *can be considered as the limit* $\lim_{t\to\infty} v(t,x)$ *where* v *is the solution of the time marching corresponding form:*

$$v_t + |v_x| = f(x) \quad x \in (0,1),\ t > 0, \tag{1.60a}$$

$$v(t,0) = v(t,1) = 0, \quad t > 0. \tag{1.60b}$$

In this example the upwind monotone scheme is used:

$$h^M(.)_j := \frac{u_j^{n+1} - u_j^n}{\tau} - \max\left\{\frac{u_j^n - u_{j-1}^n}{\Delta x}, \frac{u_j^n - u_{j+1}^n}{\Delta x}\right\} - \tau f(x_j),$$

the high order scheme will be the centered scheme, and the filtered scheme (1.8) *will be used with* $\epsilon = 5\Delta x$. *The iterations are stopped when the difference between too successive time step is small enough or a fixed number of iterations is passed, i.e., in this example,*

$$\|u^{n+1} - u^n\|_{L^\infty} := \max_i |u_i^{n+1} - u_i^n| \leq 10^{-6} \quad or \quad n \geq N_{max} := 5000. \tag{1.61}$$

As analyzed in [20] for ϵ*-monotone schemes, for a given mesh step, even if the iterations may not converge (because of the non monotony of the scheme), it can be shown to be close to a fixed point after enough iterations.*

	filtered		centered		filtered + ENO	
M	error	order	error	order	error	order
50	2.16E-03	-	NaN	-	5.29E-03	-
100	7.14E-04	1.60	NaN	-	1.35E-03	1.97
200	2.17E-04	1.72	NaN	-	3.42E-04	1.98
400	6.32E-05	1.78	NaN	-	8.61E-05	1.99
800	2.17E-05	1.54	NaN	-	2.16E-05	2.00

TABLE 1.9: (Example 2.3.8) Global errors for filtered scheme, compared with the centered (unstable) scheme, and a filtered ENO scheme.

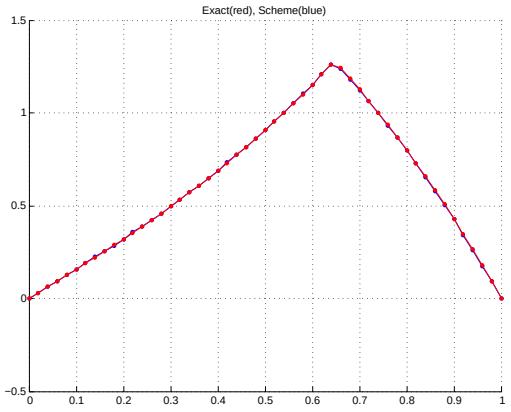

FIGURE 1.8: (Example 2.3.8) Filtered scheme for a steady equation, with $M = 50$ mesh points.

1.7 Obstacle problem

Example 1.7.1. (advection + obstacle) *Here we consider an obstacle problem, which is taken from [17]:*

$$min(v_t + v_x,\ v - g(x)) = 0, \quad t > 0, x \in [-1, 1], \tag{1.62}$$

$$v_0(x) = 0.5 + sin(\pi x) \quad x \in [-1, 1], \tag{1.63}$$

together with periodic boundary condition. The obstacle function is $g(x) := sin(\pi x)$. *In this case exact solution is given by:*

$$v(t,x) := \begin{cases} \max(v_0(x-at), g(x)) & \text{if } t < \frac{1}{3} \\ \max(v_0(x-at), g(x), -10_{x\in\ [0.5,1]}) & \text{if } t \in [\frac{1}{3}, \frac{1}{3}+\frac{1}{2}], \\ \max(v_0(x-at), g(x), 1_{x\in\ [-1,t-\frac{1}{3}-\frac{1}{2}]\cup[0.5,1]}) & \text{if } t \in [\frac{1}{3}+\frac{1}{2}, 1], \end{cases} \tag{1.64}$$

Results are given in Table 2.8, for terminal time $t = 0.5$. *Errors are computed away from singular points, i.e., in the region* $[-1,1] \setminus \left(\cup_{i=1,3} [s_i - \delta, s_i + \delta] \right)$ *(where* $s_1 = -0.1349733, s_2 = 0.5$ *and* $s_3 = 2/3$ *are the three singular points. Filtered scheme is numerically of second order (ENO gives comparable results here).*

Errors		filtered $\epsilon = 5\Delta x$		centered		ENO2	
M	N	error	order	error	order	error	order
40	20	7.93E-03	2.03	1.63E-02	1.54	2.14E-02	1.59
80	40	1.84E-03	2.10	2.98E-02	-0.87	7.75E-03	1.46
160	80	3.92E-04	2.24	1.46E-02	1.03	1.07E-03	2.86
320	160	9.67E-05	2.02	8.02E-03	0.86	2.72E-04	1.97
640	320	2.40E-05	2.01	4.10E-03	0.97	6.92E-05	1.98

TABLE 1.10: (Example 1.7.1) L^∞ errors away from singular points, for filtered scheme, centered scheme, and second order ENO scheme.

Example 1.7.2. (Eikonal + obstacle) *We consider an Eikonal equation with an obstacle term, also taken from [17]:*

$$min(v_t + |v_x|, v - g(x)) = 0, \quad t > 0, x \in [-1, 1], \tag{1.65}$$

$$v_0(x) = 0.5 + sin(\pi x) \quad x \in [-1, 1], \tag{1.66}$$

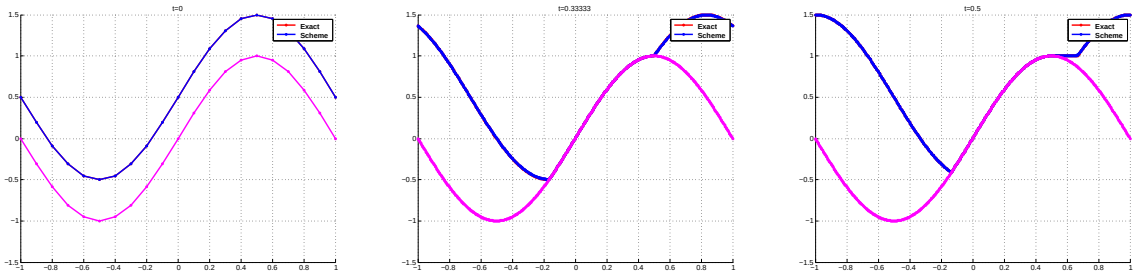

FIGURE 1.9: (Example 1.7.1) Plots at T=0(initial data), T=0.3, T=0.5.

with periodic boundary condition on $(-1, 1)$ *and* $g(x) = sin(\pi x)$*. In this case the exact solution is given by:*

$$v(t,x) = \max(\bar{v}(t,x), g(x)). \tag{1.67}$$

where $\bar{v}$ *is the solution of the Eikonal equation* $v_t + |v_x| = 0$*. The formula* $\bar{v}(t,x) = \min_{y\in[x-t,x+t]} v_0(y)$ *holds, which simplifies to*

$$v(t,x) := \begin{cases} v_0(x+t) & \text{if } x < -0.5 - t \\ -0.5 & \text{if } x \in [-0.5-t, -0.5+t], \\ \min(v_0(x-t), v_0(x+t)) & \text{if } x \geq -0.5 + t, \end{cases} \tag{1.68}$$

Results are given in Table 1.11 for terminal time $T = 0.2$*. Plots are also shown in Fig. 1.10 for different times (for* $t \geq \frac{1}{3}$ *solution remains unchanged).*

Errors	filtered		ENO2	
M	error	order	error	order
40	3.74E-03	-	6.85E-03	-
80	6.26E-04	2.58	2.12E-03	1.69
160	1.13E-04	2.47	6.80E-04	1.64
320	2.26E-05	2.32	2.18E-04	1.64
640	5.50E-06	2.04	6.96E-05	1.65

TABLE 1.11: (Example 1.7.2) Filtered scheme and ENO scheme at time $t = 0.2$

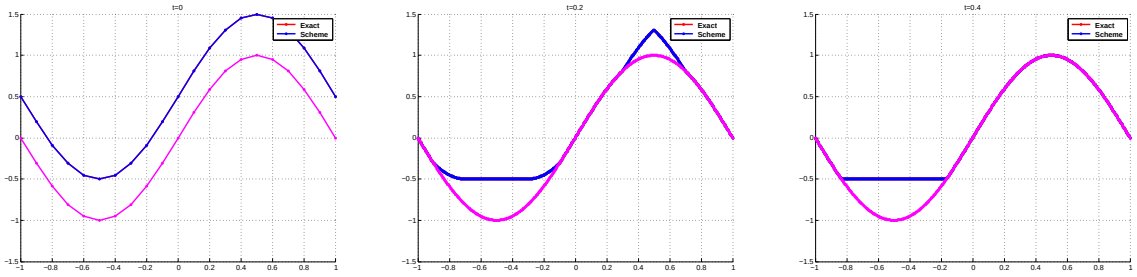

FIGURE 1.10: (Example 1.7.2) Plots at times $t = 0$, $t = 0.2$ and $t = 0.4$. The dark line is the numerical solution, similar to the exact solution, and the ligth line is the obstacle function.

Chapter 2

High-order approximation schemes for front propagation

2.1 Introduction

The main aim of this chapter is to solve front propagation problem by the high-order filtered scheme presented in the chapter 1. The idea of level set formulation to propagate curves and surfaces has been introduced by Osher and Sethian [89] for computing and analyzing the motion of the interface in two and three dimensions. The advantages of this approach are well known by now. It treats self-intersections, topological changes, kinks and it is easily extended to capture hypersurfaces in higher dimensions. Propagating interfaces occur in a wide variety of settings, including examples from fluid mechanics, image processing, shape of soap bubbles, oil drop floating on water, computer animations, manufacture of computer chips, airbag inflation (a comprehensive presentation is contained in [88] and [100]). The techniques used to approximate these problems are based mainly on finite difference schemes [100] and SL schemes [42]. It is important to notice that monotone finite difference schemes (analyzed by Crandall and Lions in [34]) converge to the solution which has to be understood in the viscosity sense but are in general limited to at most first-order accuracy. Higher order finite difference schemes such as ENO schemes [71] have also been developed but a general convergence proof for them is still missing. For more details we refer readers to the references already mentioned in the general introduction. Here we use the recent class of filtered

finite difference schemes studied in [19] in order to show that they are effective also for singular problems like front propagation problems. It is important to note that filtered schemes were introduced in the [51] for second order elliptic PDE's and satisfy an ϵ-monotonicity property which is enough to obtain a convergence result and an a priori estimate. Finally, let us also mention that ϵ-monotone semi-Lagrangian schemes were studied for steady equations in [20]). In this chapter we develop a specific application of the scheme proposed and analyzed in [19] to front propagation problems. The approach is based on the level-set method which leads in the isotropic case to a classical evolutive first-order HJ equation. We will apply to this equation high-order "filtered schemes", for these which the strong monotonicity property will not be satisfied. However, a weak ϵ-monotonicity property applies and this is enough to obtain a convergence result and a precise error estimate. In the last section we present several examples where we solve front propagation problems by high filtered scheme in two and three dimensions showing the accuracy of our method.
We first give some notations and definitions for the model problem and then we present many numerical tests based on high-order filtered scheme.

2.2 Definitions and notations

Let $\phi : \mathbb{R}^d \to \mathbb{R}$ denotes a real valued function implicitly or explicitly defined on $\mathbb{R}^d$, where d is typically equal to 2 or 3. A level set associated to ϕ is geometrically defined as points (in $\mathbb{R}$), a curve (in $\mathbb{R}^2$) or a surface (in $\mathbb{R}^3$) given by

$$\Gamma := \{x \in \mathbb{R}^d |\ \phi(x) = c\} \tag{2.1}$$

for some constant c i.e. $\phi|_\Gamma = c$. The function ϕ is called level set function associated to Γ. A typical choice is $c = 0$ and we refer to Γ as an interface, described by the zero level set. The following sets are associated to the interface $\Gamma_0 := \{x \in \mathbb{R}^d |\ \phi(x) = 0\}$

$$\Omega^- := \{x \in \mathbb{R}^d |\ \phi(x) < 0\}, \quad \Omega^+ := \{x \in \mathbb{R}^d |\ \phi(x) > 0\} \tag{2.2}$$

are known as interior and exterior region respectively. Note that $dim(\Gamma) = d - 1$. This gives a normal direction of evolution point outward with respect to Ω and the interior region will grow in time. Reversing the sign of ϕ we obtain an inward evolution and the

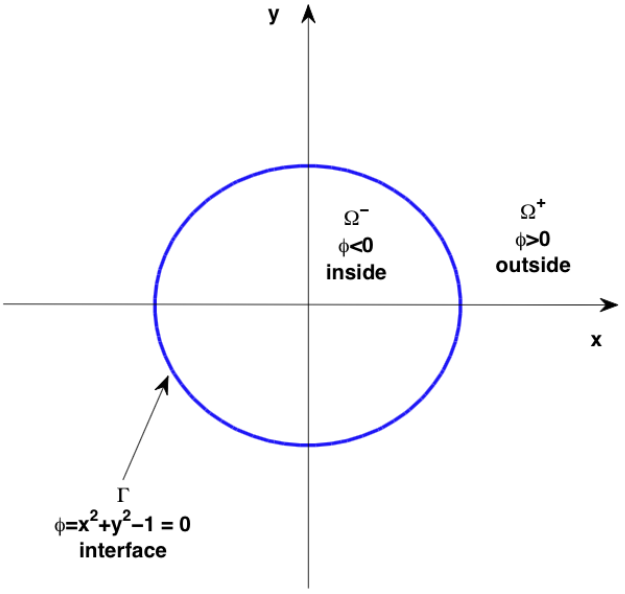

FIGURE 2.1: Implicit representation of the curve $x^2 + y^2 = 1$.

curve (surface) will shrink. When the interface is represented by an explicit function ϕ then it is easy to parametrize Γ_0.

For example. $\phi(\bar{x}) = |\bar{x}|^2 - 1$ gives the circle of radius 1. in the Fig. 2.1, where the interface defined by the $\phi(\bar{x}) = 0$. The interior region is the unit open disk $\Omega^- = \{\bar{x} \in \mathbb{R}^2 |\ |\bar{x}| < 1\}$ and exterior region is $\Omega^+ = \{\bar{x} \in \mathbb{R}^2 |\ |\bar{x}| > 1\}$. Explicit representation of the surface is simply the unit circle defined by $\partial\Omega = \{\bar{x} \in \mathbb{R}^2 |\ |\bar{x}| = 1\}$. However, in many physical applications, the interface can be defined only in implicit form. Implicitly surfaces can undergo some dynamics, say, under the influence of an external velocity field for e.g. soap bubble in a steady wind current.

2.2.1 Front Propagation Problem

The associated level set function ϕ is also time-dependent hence zero level set denotes by

$$\Gamma_t = \partial\Omega_t = \{x \in \mathbb{R}^d |\ \phi(t, x) = 0\}. \tag{2.3}$$

This gives a normal direction of evolution point outward with respect to Ω_t and the interior region grow in time. Reversing the sign of ϕ we will obtain an inward evolution

and the curve (surface) will shrink. If we regard the moving curves as an interface separating two regions, the front at time t should consist of only the set of all points located a distance t from the initial curve. This is known as Huygens principle construction (see [99]). Let $x(t)$ be the path of a point on the propagation front i.e. x is a point on Γ_0 at $t = 0$. The stipulation that the zero level set of the evolving function ϕ always match the equation

$$\frac{dx}{dt} = f(t, x)\vec{n},$$

where $\frac{dx}{dt}$ is normal to the front $x(t)$ and f is scalar. The zero level set of the evolutive function ϕ will coincide with the propagating hypersurface and this implies that

$$\phi(x(t), t) = 0$$

By chain rule we have

$$\frac{\partial \phi}{\partial t} + \nabla \phi(x(t), t) \cdot \frac{dx}{dt} = 0. \tag{2.4}$$

Since f is a scalar speed in the outward normal direction, therefore

$$\frac{dx}{dt} \cdot n = f, \text{ where } n = \frac{\nabla \phi}{|\nabla \phi|}.$$

Hence the evolution equation for ϕ becomes

$$\frac{\partial \phi}{\partial t} + f|\nabla \phi| = 0, \tag{2.5}$$

$$\text{given } \phi(0, x) = \phi_0(x). \tag{2.6}$$

For certain forms of the speed function f, this is our time dependent level set equation, which is a standard time dependent HJ equation. This approach is simple and clever way to describe an interface operating on two or more regions with different physical phases. Depending upon the choice of normal (exterior/ interior), and the choice of f we can describe the growth of a phase and its reduction. There are three major cases of interest:

- $f(t, x)$, isotropic velocity depending upon (t, x)
- $f(x, k(x))$, velocity depending upon both x and the front curvature at x

- $f(x, \vec{n}(x))$, anisotropic velocity depending on both x and the normal at x

We focus on the isotropic case where Γ_0 is the only available data and $f = f(t, x)$ is given. For this problem a typical choice for the initial profile is signed distance i.e.

$$\bar{d}(x, \Gamma_0) = \begin{cases} d(x, \Gamma_t) & x \in \Omega_0^c, \\ -d(x, \Gamma_t) & x \in \Omega_0. \end{cases} \tag{2.7}$$

Let us note that problem (2.5) is simplifies if the evolution is monotone (either increasing or decreasing). This happens when the velocity f has constant sign. Note that the signed distance function has to be Lipschitz continuous. For monotone evolution the level set formulation can converted from the time dependent PDE to a stationary problem. More precisely $f(x) > 0$ for all $x \in \mathbb{R}^d$, then (2.5) can be written as a stationary form by introducing the function

$$\phi(t, x) = T(x) - t \tag{2.8}$$

and then we can recover the interface by the knowledge of T at any time using

$$\Gamma_t = \left\{ x \in \mathbb{R}^d : T(x) = t \right\}.$$

Formally substituting (2.8) in (2.5) we obtain

$$f(x)|\nabla T| = 1. \tag{2.9}$$

Note that Dirichlet boundry condition $T(x) = 0$ on $\partial\Omega_0$ is quite natural to considering that $T(x)$ represents the time needed by the interface to reach the point x and we can reformulate the boundary value problem as

$$\begin{cases} f(x)|\nabla T| = 1, & x \in \mathbb{R}^d / \Omega_0 \\ T(x) = 0, & x \in \partial\Omega_0, \end{cases} \tag{2.10}$$

where Ω_0 is a subset of $\mathbb{R}^d$ such that $\partial\Omega_0 = \Gamma_0$. This stationary approach is linked to minimum time problem. Here we briefly explain the minimum time problem (the interested reader can find in the appendix of [6] and [40] more details on this link). Let

us consider the following controlled dynamical system

$$\begin{cases} \dot{y}(t)) = f(y)\alpha(t) \quad t \in (0, +\infty) \\ y(0) = x, \end{cases} \tag{2.11}$$

where $f : \mathbb{R}^d \to \mathbb{R}$, $f > 0$ is Lipschitz continuous and taking the values in a compact set $A \subset \mathbb{R}^m$ and with the measurable control $\alpha \in \mathcal{A} = \{\alpha \in L^\infty(R^+; A)\}$. We denote $y_x(., \alpha(.))$ the solution of (2.11) corresponding to the control $\alpha \in \mathcal{A}$. Here we consider $B(0, 1)$, whihch is a unit ball centered at origin. This choice means that the controller can move the state of the system with speed $f > 0$ (which depends on the position of the system itself) in every direction he wants. We can define for every x and α the minimum time to hit the target $\mathcal{T}$ as

$$t(x, \alpha) = \inf_s \left\{ t \in \mathbb{R}^+ : y_x(t, \alpha) \in \mathcal{T} \right\}$$

The problem is to determine the minimum time function

$$T(x) = \inf_{\alpha \in \mathcal{A}} t(x, \alpha) \tag{2.12}$$

and its domain of the definition $\mathcal{R}$, called reachable set,

$$\mathcal{R} = \left\{ x \in \mathbb{R}^d : \ T(x) < +\infty \right\} \tag{2.13}$$

$$= \left\{ x \in \mathbb{R}^d : \ \exists \ \bar{\alpha} \in \mathcal{A} \text{ and } \bar{t} \in [0, +\infty] \text{ such that } y_x(\bar{t}, \bar{\alpha}) \in \mathcal{T} \right\}. \tag{2.14}$$

But in our case it can reach the target from every initial position x so that $\mathcal{R} = \mathbb{R}^d$. Note that T satisfies (2.10) (see [6]) since by the definition. Always assuming that the solution trajectory $y_x(., \alpha)$ is unique (the Carathedory conditions are satisfied).

The connection between front propagation and minimum time problem can also be exploited for numerical purposes, once characteristics of the front problem (also termed as rays) are identified with optimal trajectories. Moreover, it is possible to treat the propagation in presence of obstacles using a natural interpretation in terms of state constraints. For solving such front propagation problems many schemes has been given

we refer reader to [5, 6, 40, 42, 43]. In conclusion we have two kind of formulations.

Level set Formulation	**Stationary Formulation**
$\frac{\partial \phi}{\partial t} + f\lvert\nabla\phi\rvert = 0,$	$\lvert\nabla T\rvert f = 1,$
Front $= \Gamma(t) = \{(x,y)\lvert\ \phi(x,y,t) = 0\}$	Front $= \Gamma(t) = \{(x,y)\lvert\ T(x,y) = t\}$
applies for arbitrary f	requires $f > 0$ or $f < 0$.

In the next section we present some numerical tests. for the model problem (2.5) The main goal is to obtain high-order scheme when the solution is smooth. In chapter 1 we proposed a general way to mix a first-order scheme (monotone) with a high-order (non-monotone) scheme for time dependent HJB equations with the convergence result.

2.3 Numerical test

We solve (2.5) by high-order filtered scheme (1.8). Let us consider the two dimensional case, of the level set equation (2.5), which can be written as

$$\phi_t + H(\phi_x, \phi_y) = 0, \tag{2.15}$$

where H is the classical Hamiltonian and it is standard HJ equation. We keep the notations from the chapter 1. Now we present filtered scheme in dimension two.
Let $\Delta t > 0$ be a constant time steps, and $t_n = n\Delta t$, $n \in [0 \dots N]$, and $\Delta x > 0$ be a step size of a spatial grid. Let $(x_i, y_j) = (i\Delta x, j\Delta x)$ denote a uniform mesh with $i, j \in \mathbb{Z}$. Hence the filtered scheme is :

$$\phi_{ij}^{n+1} = S^M(\phi^n)_{ij} + \epsilon\Delta t F\left(\frac{S^A(\phi^n)_{ij} - S^M(\phi^n)_{ij}}{\epsilon\Delta t}\right), \tag{2.16}$$

where F is the filter function (1.26), ϵ is the switching parameter (section 1.3.2 from chapter 2), S^M is monotone scheme (1.11) where h^M is Lax-Friedrich monotone flux

$$h^{M,LF}\left(\phi_1^-\phi_1^+, \phi_2^-, \phi_2^+\right) = H\left(\frac{\phi_1^- + \phi_1^+}{2}, \frac{\phi_2^- + \phi_2^+}{2}\right) - \frac{C_x}{2}\left(\phi_1^+ - \phi_1^-\right) - \frac{C_y}{2}\left(\phi_2^+ - \phi_2^-\right), \tag{2.17}$$

$$C_x = \max_{A\leq\phi_1\leq B} |H_{\phi_1}(\phi_1,\phi_2)|, \quad C_y = \max_{A\leq\phi_2\leq B} |H_{\phi_2}(\phi_1,\phi_2)|,$$

$H_i(\phi_1,\phi_2)$ is the partial derivative of H with respect to i-th argument, or the Lipschitz constant of H with respect to the i-th argument $A = (\phi_1^-,\phi_1^+)$ and $B = (\phi_2^-,\phi_2^+)$ with with the CFL condition (1.18). S^A is high-order scheme which is the same as in previous chapter i.e. centered scheme in space (see Remark 1.2.4), with Heun (RK2) scheme discretization in time (see in particular Eqs. (1.25a)-(2.18b)).

$$S^{A,1}(\phi_{ij}^n) := \phi_{ij}^n - \Delta t h\left(\frac{\phi_{(i+1)j}-\phi_{(i-1)j}}{2\Delta x}, \frac{\phi_{i(j+1)}-\phi_{i(j-1)}}{2\Delta x}\right), \tag{2.18a}$$

and

$$S^A(\phi_{ij}) := \frac{1}{2}\left(\phi_{ij}^n + S^{A,1}(S^{A,1}(\phi_{ij}^n))\right). \tag{2.18b}$$

Hereafter in all the numerical test we use the "centered scheme" (2.18) as high-order scheme and (1.12) scheme as monotone with the same filtered function (1.26). As we have already discussed in the chapter 1 for the choice of switching parameter ϵ we have numerically observed that taking $\epsilon = c_1\Delta x$ with c_1 sufficiently large does not change much the numerical results in the following so we will precise the value of c_1 in each example. In this case of front propagation, it can be observed that the filter scheme may produce small errors occur the near extrema, when two possible directions of propagation occur in the same cell. For improving the order in all numerical tests before doing the filtering process. limiter correction will be needed. In limiter correction (see section 1.3.1 in chapter 1). In general tables below in the numerical tests filtered scheme will be compared to a second order ENO scheme (for precise ENO scheme, see Appendix A), as well as the centered (a priori unstable) scheme without filtering. In front merging case when front merg then regularity lost. In that case one can not have high order everywhere so local error in the L^2 norms are computed in some subdomain D, at a given time t_n, corresponds to

$$e_{L^2_{loc}} := \left(\Delta x \sum_{\{i,\ x_i\in D\}} |v(t_n,x_i) - u_i^n|^2\right)^{1/2}$$

and similarly L^1 and Ł$^\infty$ errors also comparable. We fixed CFL is $\mu = c_0\left(\frac{\tau}{\Delta x}+\frac{\tau}{\Delta x}\right) = 0.37$.

2.3.1 Evolution of regular front

Example 2.3.1. (Evolution of regular front) *In this example the initial condition is given by the distance function $\bar{d}$ (as in (2.7)) from the initial configuration of the front*

$$\Gamma_0 = \left\{ (x,y) \in \Omega \mid 0.5 - 0.5 \max\left(0, \frac{1-x^2-y^2}{1-r_0^2}\right)^4 = 0 \right\}, \tag{2.19}$$

where $\Omega = (-2,2)^2$ and here $f(x,y) = 1$ in (2.5) and $T = 0.6$ with Drichlet boundary condition. We are solving front propagation problem and we choose switching parameter $\epsilon = 10\Delta x$. In this example the evolution in the outward direction and interior region will grow in time and front expand. After evolution front will remains smooth. We compare filtered scheme with central finite difference scheme and second order ENO scheme with TVD RK2 in time. In the table 2.1 we are calculating global errors. Here viscous aspect occurs so in order to have high-order behavior we need to use limiter correction (see section 1.3.1 of chapter 1). In the Fig. 2.2 several level curves for ϕ are shown.

		filtered ($\epsilon = 10\Delta x$)		centered		ENO2	
M	N	L^2 error	order	L^2 error	order	L^2 error	order
25	25	1.69E-01	-	2.15E-01	-	2.49E-01	-
50	50	5.03E-02	1.75	7.50E-02	1.52	8.49E-02	1.55
100	100	1.22E-02	2.04	2.55E-02	1.55	2.48E-02	1.78
200	200	3.03E-03	2.02	9.36E-03	1.45	7.24E-03	1.77
400	400	7.57E-04	2.00	2.58E-02	-1.46	2.13E-03	1.76

TABLE 2.1: Example 2.3.1, L^2 errors for filtered scheme, centered scheme, and ENO second order scheme.

2.3.2 Merging of regular fronts

Example 2.3.2. Merging of two disconnected fronts *Again the initial condition is given by the distance function $\bar{d}$ (as in (2.7)) from the initial configuration of the front*

$$\Gamma_0 = \left\{ (x,y) \in \Omega \mid \phi_0(x,y) = 0 \right\},$$

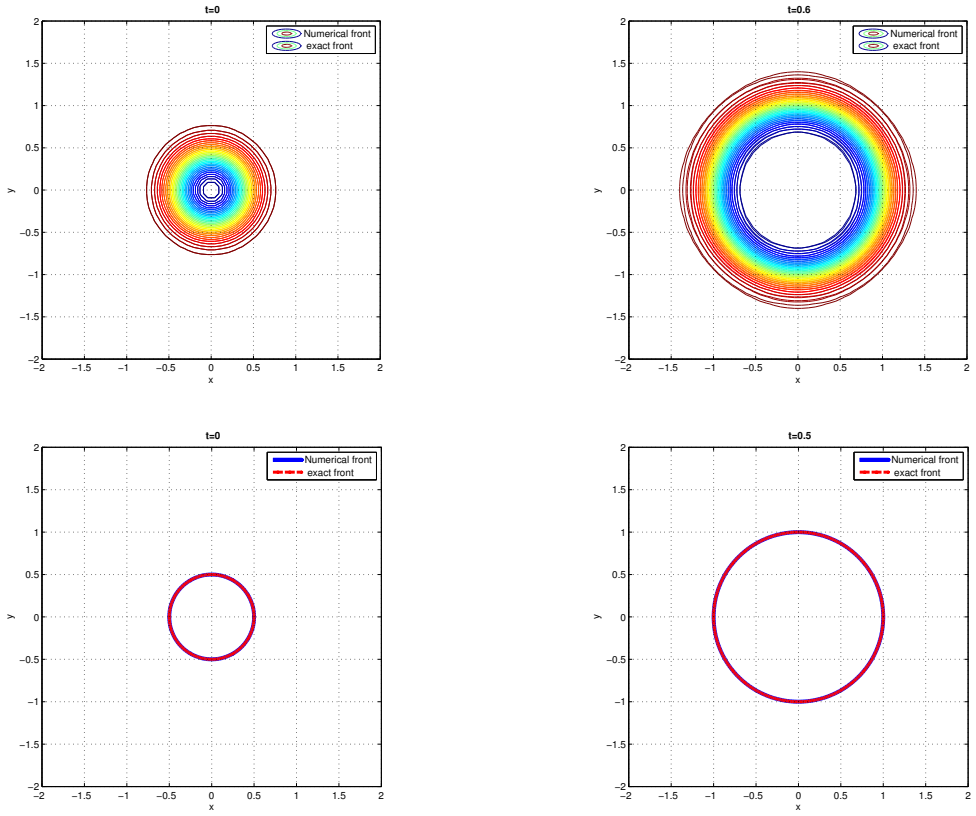

FIGURE 2.2: Example 2.3.1, on the left we have initial configuration circle of radius $r_0 = 0.5$ and on the right expanded front at time $T = 0.6$ and CFL is 0.37.

where $\phi_0(x,y) = \min(\phi_1(x,y), \phi_2(x,y))$

$$\phi_1(x,y) = r_0 - r_0 \max\left(0, \frac{1-(x-1)^2-y^2}{1-r_0^2}\right)^4,$$

$$\phi_2(x,y) = r_0 - r_0 \max\left(0, \frac{1-(x+1)^2-y^2}{1-r_0^2}\right)^4,$$

are two disconnected smooth fronts which are centered at $(1,0)$ *and* $(-1,0)$ *with radius* $r_0 = 0.5$ *respectively. Computations are done on the domain* $\Omega = (-3,3)^2$ *with Drichlet boundary conditions. Here initial data corresponds to the mixing of two fronts. As front evolve and merge. They lost their regularity. So this example is less regular than the previous one. CFL number and switching parameter* ϵ *are the same as in Example 2.3.1. In the table 2.2 local errors have been computed away from the singular strip* $|x| \leq \epsilon_1$ *and* $|y| \leq \epsilon_1$ *where* $\epsilon_1 = 0.1$*. In this example, the naive centered scheme is unstable (as expected), while the filtered scheme is stable and of second order. In Fig. 2.3 we can*

observe a very nice merging.

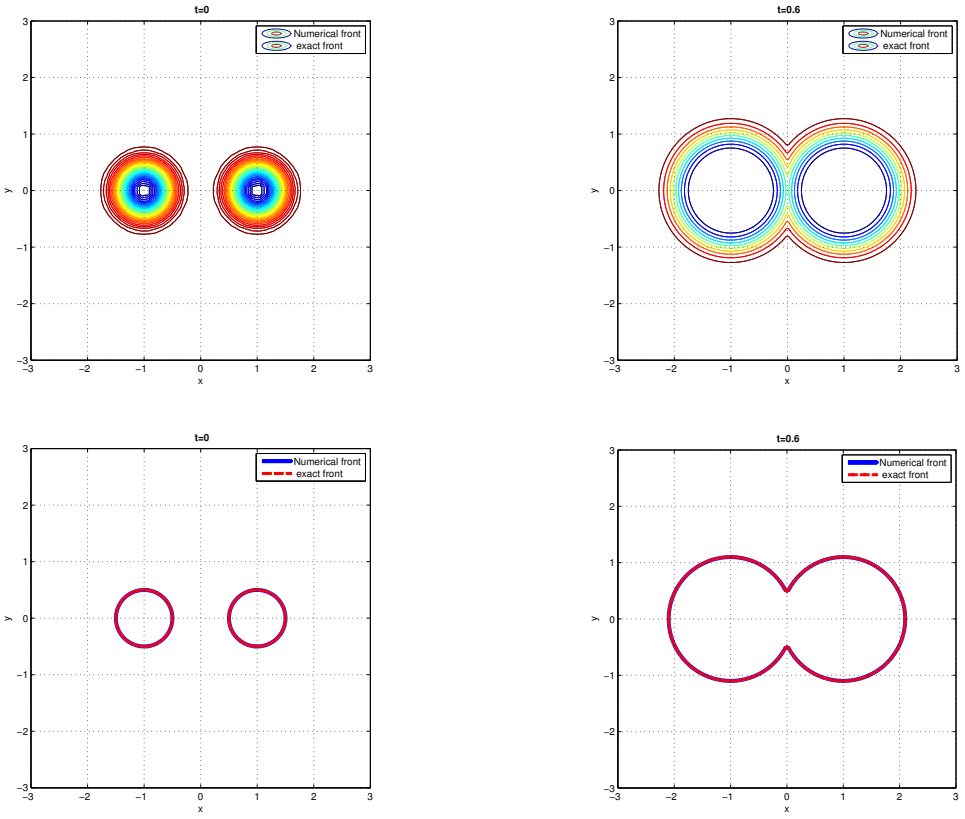

FIGURE 2.3: Example 2.3.2, on the left we have initial configuration circle of radius $r_0 = 0.5$ and on the right expanded front at time $T = 0.6$.

		filtered ($\epsilon = 10\Delta x$)		centered		ENO2	
M	N	L^2 error	order	L^2 error	order	L^2 error	order
50	50	1.14E-02	1.80	1.95E-01	1.30	1.32E-02	0.98
100	100	2.76E-03	2.04	7.31E-02	1.42	4.47E-03	1.56
200	200	6.97E-04	1.99	2.96E-02	1.30	1.25E-03	1.84
400	400	1.67E-04	2.06	1.36E-01	-2.20	2.64E-04	2.24

TABLE 2.2: Example 2.3.2, local L^2 errors for filtered scheme, centered scheme, and ENO second order scheme

Example 2.3.3. Merging of five regular fronts : *The motivation of presenting this example is that if we have more than two fronts expanding and merging even then filtered scheme is locally high-order. The initial condition is given by the distance function* $\bar{d}$ *(as in (2.7)) from the initial configuration of the front*

$$\Gamma_{k0} = \{(x, y) \in \Omega \mid \phi(x, y) = 0\},$$

where

$$\phi(x,y) = \min\{\phi_k(x,y) : k = 1,...,5\}$$

$$\phi_k(x,y) = r_0 - r_0 \max\left(0, \frac{1-(x-x_k)^2-(y-y_k)^2}{1-r_0^2}\right)^4, \text{ for } k = 1,...,5$$

where $r_0 = 0.25$ *and centers* (x_k, y_k) *are* $(1,0)$, $(-1,0)$, $(0,0)$, $(0,-1)$, $(0,1)$ *for* $k = 1,...,5$ *respectively. We are solving front propagation problem for* $f(x,y) = 1$ *and we choose switching parameter* $\epsilon = 10\Delta x$. *Computations are done on the domain* $\Omega = (-4,4)^2$. *In the Fig. 2.7 good merging is observed. Errors calculated away from singularities (we removed strips* $|x+y| \le \epsilon_1$, $|x-y| \le \epsilon_1$ *and* $\epsilon_1 = 0.2$ *from the domain). Filtered scheme gives the desired second order behavior.*

		filtered ($\epsilon = 10\Delta x$)		centered		ENO2	
M	N	L^2 error	order	L^2 error	order	L^2 error	order
50	50	4.76E-02	1.56	1.02E-01	0.65	6.35E-02	1.53
100	100	1.06E-02	2.16	5.94E-02	0.78	2.10E-02	1.60
200	200	2.83E-03	1.91	2.10E-01	-1.82	6.41E-03	1.71
400	400	7.05E-04	2.01	7.28E-02	1.53	1.87E-03	1.77

TABLE 2.3: Example 2.3.3, local L^2 errors for filtered scheme, centered scheme, and ENO second order scheme.

2.3.3 Evolution of non-smooth front

Example 2.3.4. Evolution of front with sharp corners : *The initial condition is given by the distance function* $\bar{d}$ *(as in (2.7)) from the initial configuration of the front*

$$\Gamma_0 = \{(x,y) \in \Omega \mid \phi(x,y) = 0\},$$

where $\phi(x,y) = \|(x,y)\|_\infty - r_0$ *is a square centered at origin with the sides* $r_0 = 1$. *Computations are done on the domain* $\Omega = (-1.5, 1.5)^2$ *with Dirichlet boundary condition and* $f(x,y) = 1$. *In this example the evolution in the outward direction and interior region will grow in time. Also front expand. Note that initially front has sharp corners but after evolution it becomes smoother. In the table 2.4 we compare filtered scheme with central finite difference scheme and second order ENO scheme with TVD RK2 in time and switching parameter is* $\epsilon = 10\Delta x$. *As expected naive centered scheme alone is not stable but when it is filtered with monotone scheme then the filtered scheme is stable and*

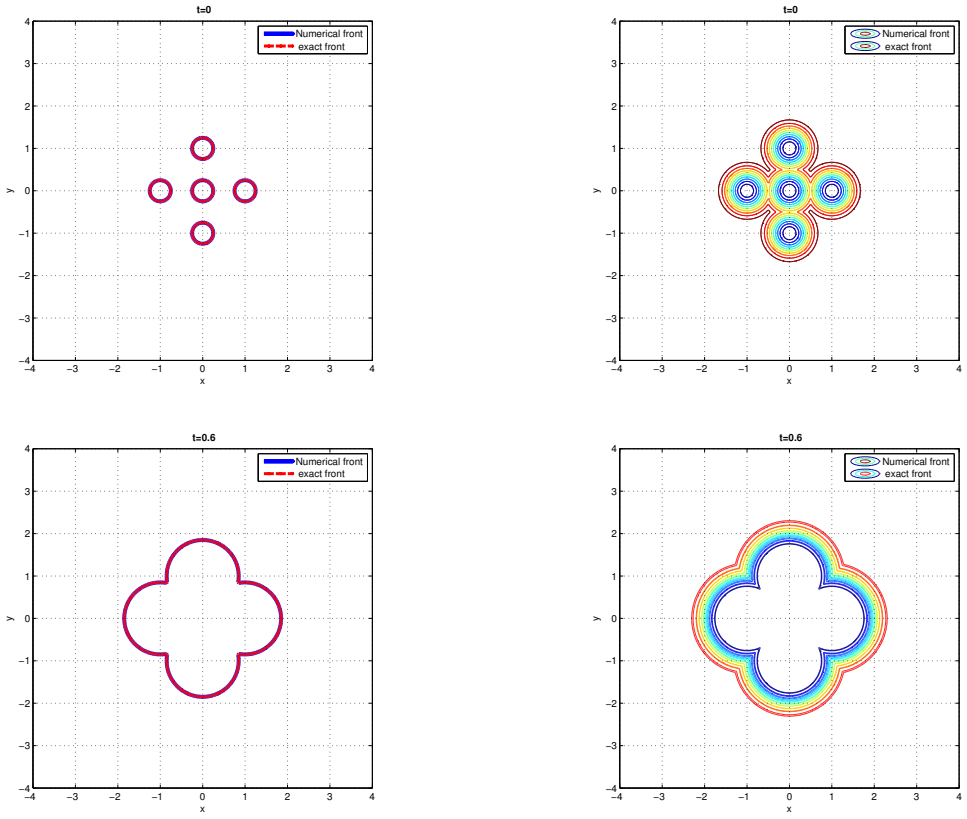

FIGURE 2.4: (Example 2.3.3) plots at time $T = 0$ (top) and $T = 0.6$ (bottom) for the filtered scheme with mesh point $M = N = 100$.

of high-order (without limiter scheme switches to first-order at extremes). In the Fig. 2.5 initially at $T = 0$ front has sharp corners and when front expands then corners of the squares become smoother. We present the error tables for small time $T = 0.25$ (For the longer time run front expands and becomes a circle). In this example we present the full error tables (L^1, L^2 and L^∞) for filtered scheme.

Errors		(L_1-Error)		L_2-Error)		L_∞-Error)	
M	N	error	order	error	order	error	order
100	100	6.89E-03	2.23	6.65E-03	2.12	9.36E-03	2.09
200	200	1.80E-03	1.93	1.84E-03	1.86	3.53E-03	1.41
400	400	3.02E-04	2.58	3.56E-04	2.37	1.10E-03	1.68
800	800	7.52E-05	2.01	8.72E-05	2.03	2.20E-04	2.32

TABLE 2.4: Example 2.3.4, local errors filtered scheme and RK2 in time where $\epsilon = 10\Delta x$ and with CFL=0.37.

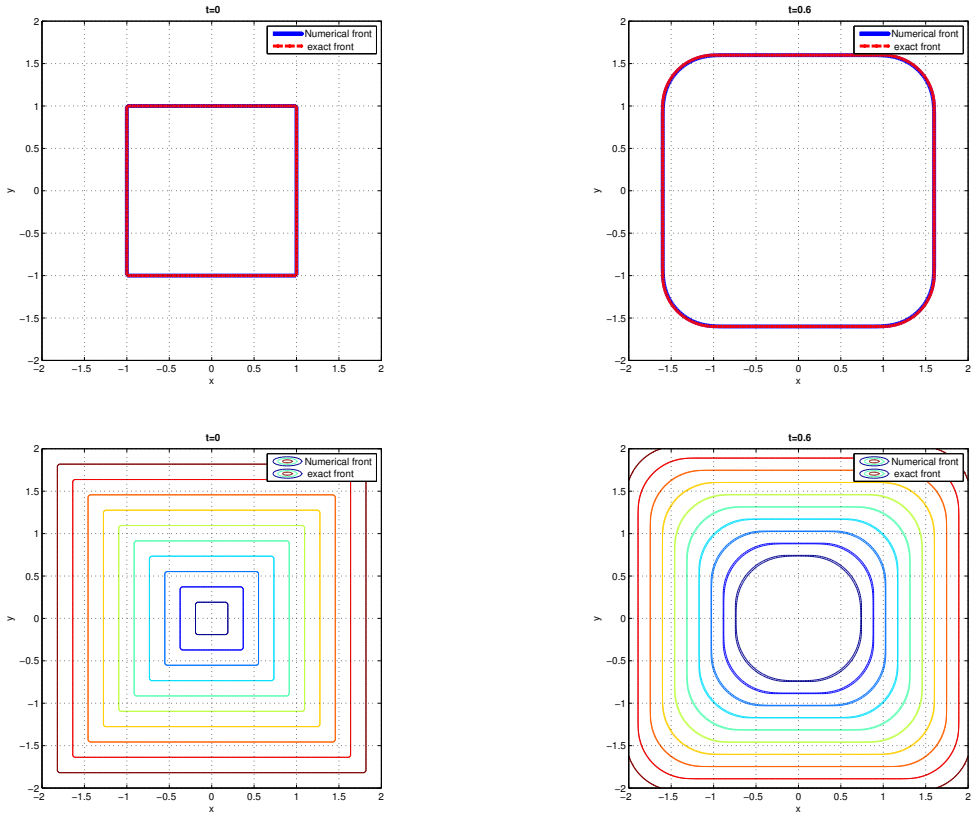

FIGURE 2.5: (Example 2.3.3) plots at time $T = 0$ (top) and $T = 0.6$ (bottom) for the filtered scheme with mesh point $M = N = 100$.

2.3.4 Merging of one smooth and one non-smooth front

Example 2.3.5. One smooth and one non smooth front mergeing : *In this example the initial condition is given by the distance function* $\bar{d}$ *(as in* (2.7)*) from the initial configuration of the front.*

$$\Gamma_0 = \{(x, y) \in \Omega \mid \phi_0(x, y) = 0\},$$

where $\phi_0(x, y) = \min(\phi_1(x, y), \phi_2(x, y))$, $\phi_1(x, y) = \|(x, y) - (0.5, 0)\|_\infty - r_0$ *and*

$$\phi_2(x, y) = r_0 - r_0 \max\left(0, \frac{1 - (x - 0.5)^2 - y^2}{1 - r_0^2}\right)^4,$$

where $r_0 = 0.25$ *and computations are done on the domain* $\Omega = (-2, 2)^2$ *with Dirichlet boundary condition and* $f(x, y) = 1$*. In this example we have one regular front and one front with sharp corners. After evolution fronts merge. In the table 2.5 we compare*

filtered scheme with centered scheme and second order ENO scheme with TVD RK2 in time. Switching parameter is $\epsilon = 10\Delta x$. *In the Fig. 2.6 we have one smooth front and one front with sharp corners and when front expands then corners of the square become smoother and circle will also expand. When both the fronts merge, the regularity is lost. Errors are calculated away from singularities (we removed the strip* $|x| \leq \epsilon_1$ *and* $\epsilon_1 = 0.2$ *from the domain). Filtered scheme is locally high order.*

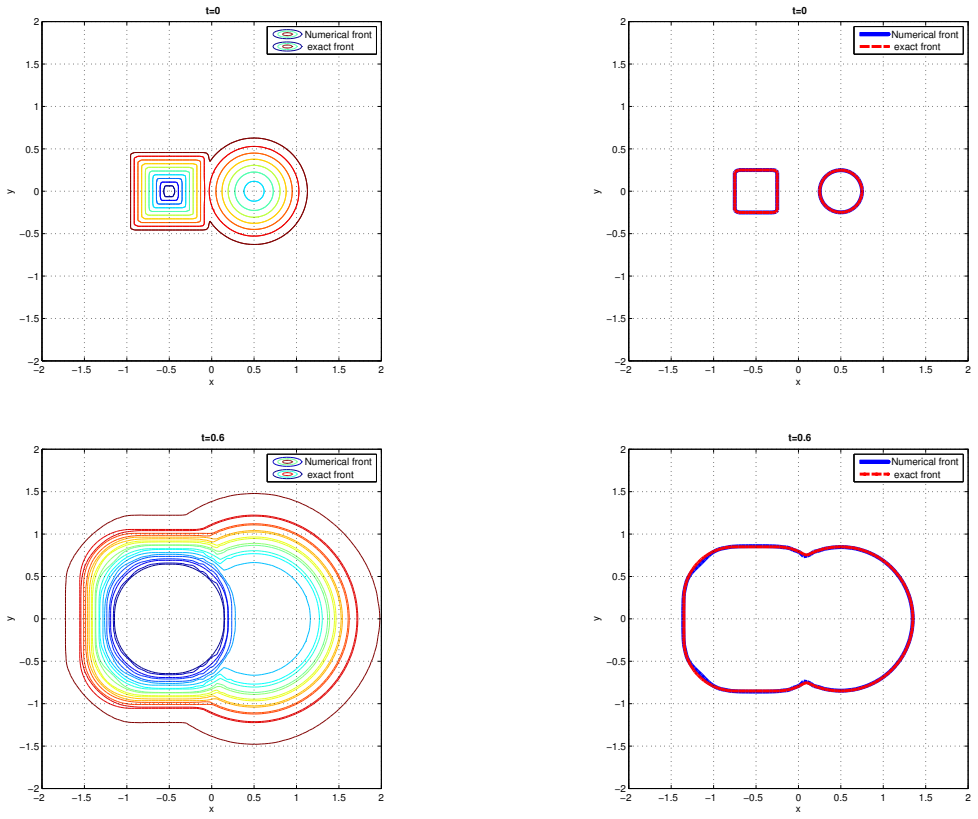

FIGURE 2.6: Example 2.3.5, plots at time $T = 0$ (top) and $T = 0.6$ (bottom) for the filtered scheme with mesh point $M = N = 100$.

		filtered ($\epsilon = 10\Delta x$)		centered		ENO2	
M	N	L^2 error	order	L^2 error	order	L^2 error	order
50	50	8.25E-04	2.54	6.80E-02	1.24	1.44E-03	2.52
100	100	2.51E-04	1.72	7.01E-02	-0.04	3.48E-04	2.05
200	200	6.30E-05	2.00	2.30E-01	-1.71	8.27E-05	2.07
400	400	1.57E-05	2.01	2.73E+00	-3.57	2.03E-05	2.03

TABLE 2.5: Example 2.3.5, local L^2 errors for filtered scheme, centered scheme, and ENO second order scheme and $T = 0.6$.

Till now all above examples solved for the constant velocity $f(x, y) = 1$. Now we present some examples with variable velocity.

Example 2.3.6. *In the examples below, we are solving* (2.5) *with Dirichlet boundary condition, and CFL number is 0.37 in the same domain considered in Example* 2.3.1 *with the initial profile as in* (2.19)*. Moreover, we assume the velocity* $f(x, y)$ *to be Lipschitz continuous. The numerical tests are performed for the following different variable velocities.*

(*i*) $f(x, y) = |x|$ *in the Fig.* 2.7 *solved by filtered scheme with* $\epsilon = 20\Delta x$*. For this example T=1.*

(*ii*) $f(x, y) = |y|$ *in the Fig.* 2.8 *solved by filtered scheme with* $\epsilon = 20\Delta x$*. For this example T=1.*

(*iii*) $f(x, y) = |x| + |y|$ *in the Fig.* 2.9 *solved by filtered scheme with* $\epsilon = 20\Delta x$*. For this example T=0.8.*

(*iv*) $f(x, y) = (f_1, f_2) = (cos(\frac{\pi}{6}), sin(\frac{\pi}{6}))$ *in the Fig.* 2.10 *solved by filtered scheme with* $\epsilon = 20\Delta x$ *and* $T = 0.6$.

(*v*) $f(x, y) = (f_1, f_2) = (|x|cos(\frac{\pi}{6}), |y|sin(\frac{\pi}{6}))$ *in the Fig.* 2.11 *solved by filtered scheme with* $\epsilon = 20\Delta x$ *and* $T = 0.6$.

(*vi*) $f(x, y) = (f_1, f_2) = (|x|cos(\frac{\pi}{6}), |x|sin(\frac{\pi}{6}))$ *in the Fig.* 2.12 *solved by filtered scheme with* $\epsilon = 20\Delta x$ *and* $T = 0.6$.

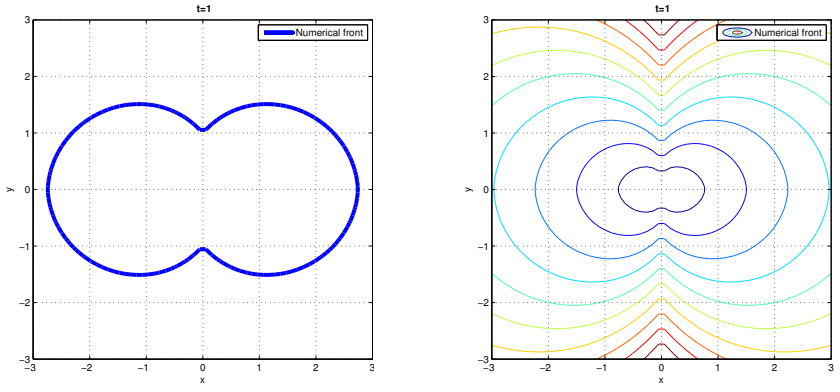

FIGURE 2.7: Example 2.3.6 (*i*) , $f(x, y) = |x|$ and T=1 solved by filtered scheme.

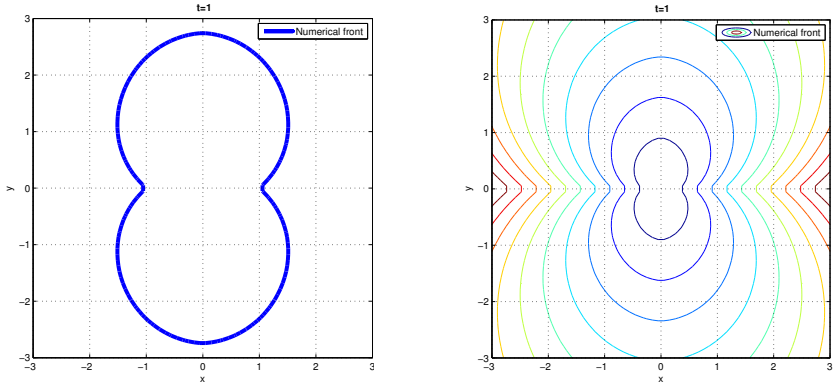

FIGURE 2.8: Example 2.3.6 (ii), $f(x,y) = |y|$ and T=1 solved by filtered scheme.

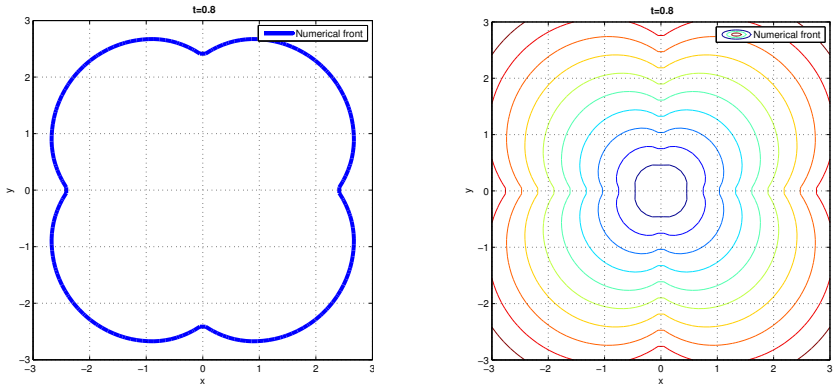

FIGURE 2.9: Example 2.3.6 (iii), $f(x,y) = |x| + |y|$ solved by filtered scheme and T=0.8.

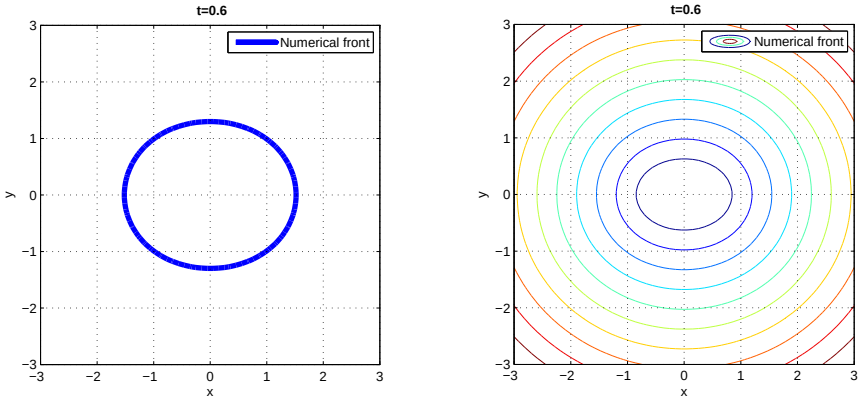

FIGURE 2.10: Example 2.3.6 (iv), $f(x,y) = (cos(\frac{\pi}{6}), sin(\frac{\pi}{6}))$ solved by filtered scheme and T=0.6.

The Fig. 2.7 and 2.8 show the direction of velocity of propagation $f(x,y)$ in the direction of x and y axis respectively which is not the case in the Fig. 2.9, 2.10, 2.11 and 2.12

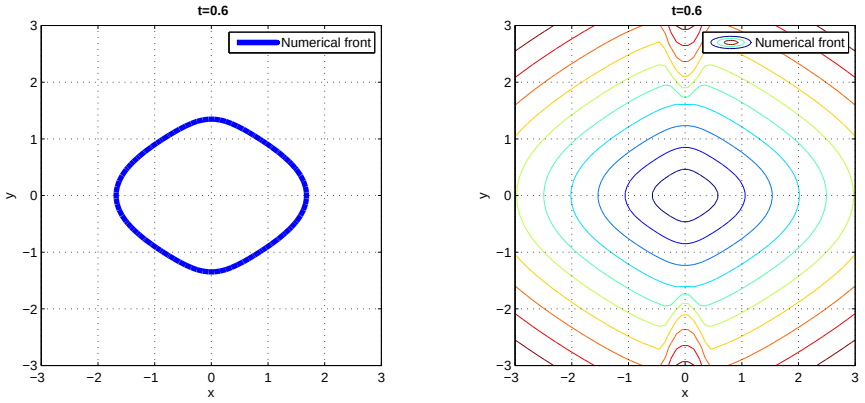

FIGURE 2.11: Example 2.3.6 (v), $f(x,y) = (|x|cos(\frac{\pi}{6}), |y|sin(\frac{\pi}{6}))$ solved by filtered scheme and T=0.6.

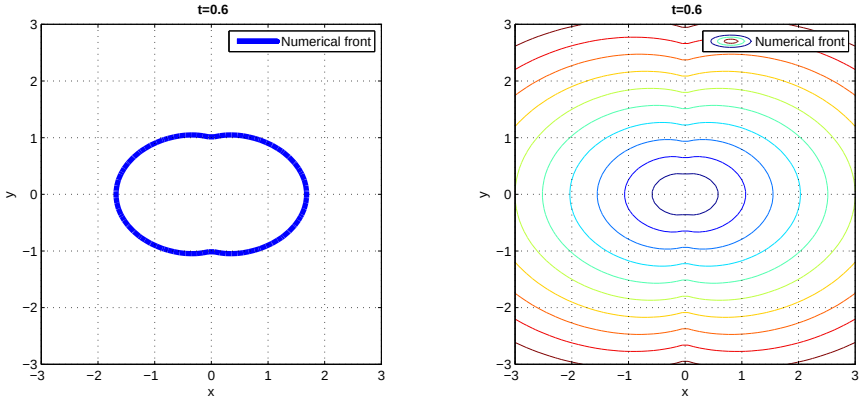

FIGURE 2.12: Example 2.3.6 (vi), $f(x,y) = (|x|cos(\frac{\pi}{6}), |y|sin(\frac{\pi}{6}))$ solved by filtered scheme and T=0.6.

and filtered scheme shows nice results.

Now we present some numerical examples in 3D. We extend filtered scheme (1.8) with the limiter 1.3.1 to 3D same manner as in 2D with the same filter function 1.26. In the examples below we observed that ENO scheme is slow compared to the filtered scheme and switching parameter $\epsilon = 20\Delta x$.

2.3.5 Evolution of fronts in 3D

Example 2.3.7. Regular Front in 3D : *In this example the initial condition is given by the distance function* $\bar{d}$ *(as in (2.7)) from the initial configuration of the front*

$$\Gamma_0 = \{(x,y,z) \in \Omega \mid \phi(x,y,z) = 0\},$$

where

$$\phi(x,y,z) = r_0 - r_0 \max\left(0, \frac{1-(x-0.5)^2-y^2+z^2}{1-r_0^2}\right)^4, \tag{2.20}$$

where $r_0 = 0.25$. *Computations are done on the domain* $\Omega = (-2,2)^3$ *with Dirichlet boundary condition. We are solving front propagation problem where* $f(x,y) = 1$ *and we choose switching parameter* $\epsilon = 20\Delta x$. *In the table 2.6 we can see centered finite difference is not stable (as expected) and filtered scheme is stable and have second order behavior. Filtered scheme is faster and somewhere better than ENO scheme. Here the calculation of errors is global.*

Errors			filtered ($\epsilon = 20\Delta x$)		centered		ENO	
M	N	P	L^2 error	order	L^2 error	order	L^2 error	order
50	50	50	5.61E-02	2.25	7.97E-002	1.70	1.08E-01	1.76
100	100	100	1.43E-02	1.97	4.08E-002	0.97	3.09E-02	1.81
200	200	200	3.64E-03	1.98	6.10E-001	-3.90	9.04E-03	1.77

TABLE 2.6: (Example 2.3.7) global errors for filtered scheme, centered scheme, and ENO second order scheme.

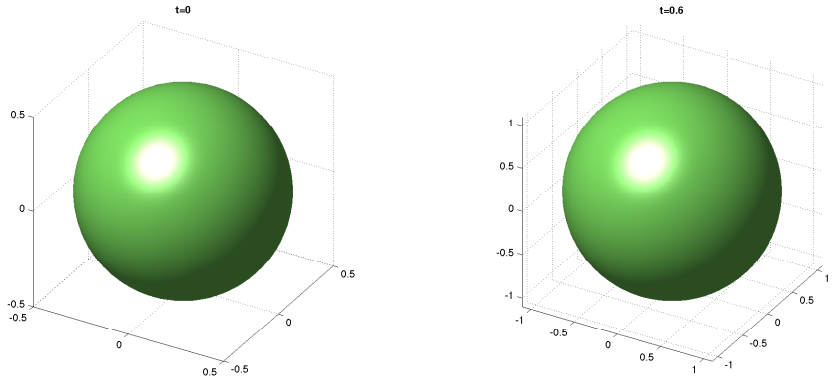

FIGURE 2.13: Example 2.3.7, plots at time $T = 0$ (left) and $T = 0.6$ (right) for the filtered scheme with mesh point $M = N = P = 100$.

2.3.6 Merging of regular fronts in 3D

Example 2.3.8. Merging of two regular fronts : *In this example the initial condition is given by the distance function* $\bar{d}$ *(as in (2.7)) from the initial configuration*

of the front. We start with two smooth fronts (spheres) i.e.

$$\Gamma_0 = \{(x, y, z) \in \Omega \mid \phi_0(x, y, z) = 0\},$$

ss where $\phi_0(x, y, z) = \min(\phi_1(x, y, z), \phi_2(x, y, z))$

$$\phi_1(x, y, z) = r_0 - r_0 \max\left(0, \frac{1 - (x-1)^2 - y^2 - z^2}{1 - r_0^2}\right)^4,$$

$$\phi_2(x, y, z) = r_0 - r_0 \max\left(0, \frac{1 - (x+1)^2 - y^2 - z^2}{1 - r_0^2}\right)^4,$$

where $r_0 = 0.25$ *and computations are done on the domain* $\Omega = (-2, 2)^3$ *with Dirichlet boundary condition.* $f(x, y) = 1$ *and we choose switching parameter* $\epsilon = 20\Delta x$*. The centered scheme is not stable (as expected) and filtered scheme is stable and have second order behavior and faster and somewhere better than ENO scheme. In the table 2.8 error calculations are local away from singularity (we eliminate the ball* $B(P, \epsilon_1)$ *of radius* $\epsilon_1 = 0.2$ *and* P *is the point where two fronts touches).*

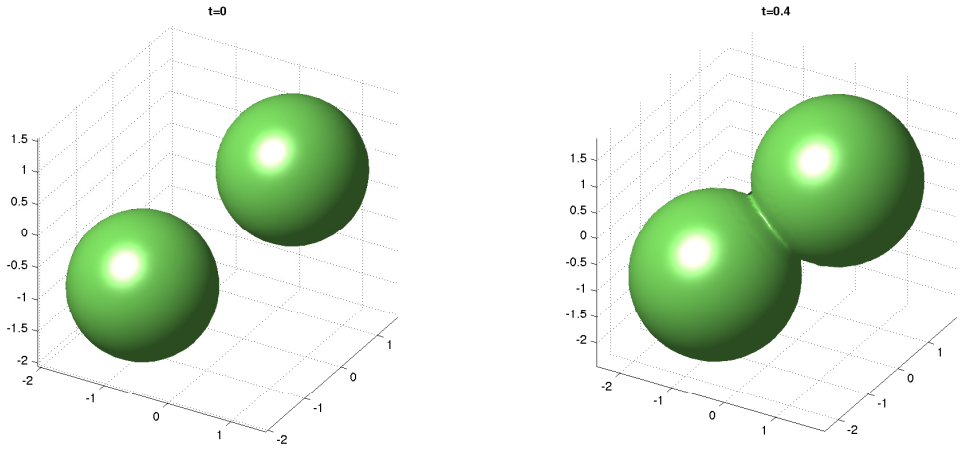

FIGURE 2.14: Example 2.3.8, plots at time $T = 0$ (left) and $T = 0.6$ (right) for the filtered scheme with mesh point $M = N = P = 100$.

Example 2.3.9. *The motivation of this example is that if we have more than two fronts (even in three dimensional space) then filtered scheme is still of second order. In this*

Errors			(filtered $\epsilon = 20\Delta x$)		(centered)		(ENO)	
M	N	P	L^2 error	order	L^2 error	order	L^2 error	order
50	50	50	7.48E-02	2.07	1.31E-001	1.42	1.54E-01	1.68
100	100	100	2.15E-02	1.80	7.64E-002	0.78	4.60E-02	1.75
200	200	200	4.75E-03	2.18	2.55E+01	-3.03	1.24E-02	1.89

TABLE 2.7: (Example 2.3.8) local errors for filtered scheme, centered scheme, and ENO second order scheme.

example we have five fronts

$$\phi_k(x,y,z) = r_0 - r_0 \max\left(0, \frac{1-(x-x_k)^2-(y-y_k)^2-(z-z_k)^2}{1-r_0^2}\right)^4, \ k = 1,..,5,$$

where $r_0 = 0.25$ *and centers* (x_k, y_k, z_k) *are* $(1,0,0)$, $(-1,0,0)$, $(-1,0,0)$, $(0,-1,0)$, $(0,1,0)$ *for* $k = 1,...,5$ *respectively. Computations are done on the domain* $\Omega = (-2,2)^3$ *with Dirichlet boundary condition. In the table 2.8 error calculations are local away from singularities and schemes switch to first-order. We eliminate the ball* $B(P_k, \epsilon_1)$ *of radius* $\epsilon_1 = 0.2$ *and* P_k *are the points where fronts touches for* $k = 1,...,5$ *respectively. It is clear from the figure 2.15 that the singularities propagate, hence one cannot expect to have high-order (thats why filtered scheme switches to first-order). However, filtered scheme is better than ENO somewhere and we can see nice merging.*

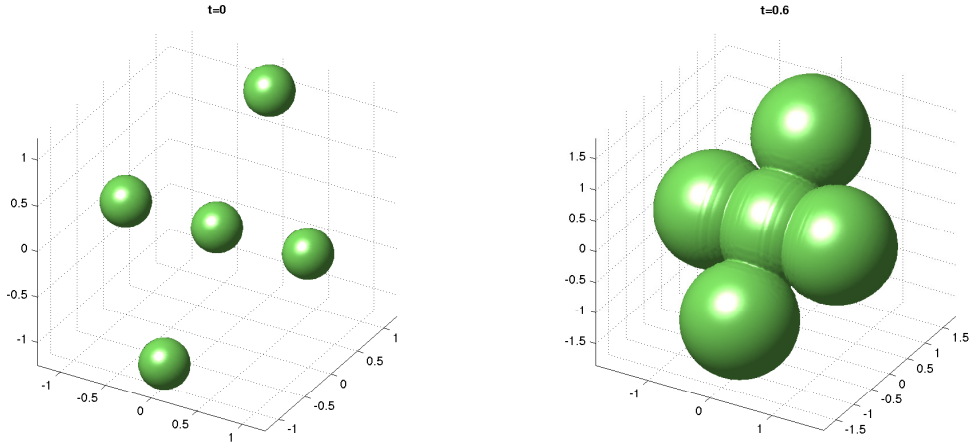

FIGURE 2.15: Example 2.3.8, plots at time $T = 0$ (left) and $T = 0.6$ (right) for the filtered scheme with mesh point $M = N = P = 100$

Example 2.3.10. *In this example we extend all 2D Example 2.3.6 with variable velocities in dimension three. We are solving (2.5) equation in 3D with Dirichlet boundary*

Errors			(filtered $\epsilon = 20\Delta x$)		(centered)		(ENO)	
M	N	P	L^2 error	order	L^2 error	order	L^2 error	order
25	25	25	1.43E-01	-	1.69E-01	-	1.30E-01	-
50	50	50	6.37E-02	1.17	1.54E-01	0.14	4.18E-02	1.64
100	100	100	1.50E-02	2.09	1.46E-01	0.08	1.20E-02	1.79
200	200	200	3.95E-03	1.92	2.57E+01	-7.46	3.75E-03	1.68

TABLE 2.8: (Example 2.3.8), local errors for filtered scheme, centered scheme, and ENO second order scheme.

condition, Time T= 0.5 and CFL number is 0.37 in the same domain as considered in Example 2.3.1 with the initial profile is (2.20) as in Example (2.3.7). Moreover, we assume the velocity $f(x, y, z)$ to be Lipschitz continuous. The numerical tests are performed for the following different variable velocities.

(*i*) $f(x, y, z) = |x|$ *in the Fig. 2.18 solved by filtered scheme with* $\epsilon = 20\Delta x$.

(*ii*) $f(x, y, z) = |y|$ *in the Fig. 2.16 solved by filtered scheme with* $\epsilon = 20\Delta x$.

(*iii*) $f(x, y, z) = |x| + |y|$ *in the Fig. 2.17 solved by filtered scheme with* $\epsilon = 20\Delta x$ *for this example T=1.*

(*iv*) $f(x, y, z) = x^2 + y$ *in the Fig. 2.19 solved by filtered scheme with* $\epsilon = 20\Delta x$.

In all the figures below we plot solution with first order scheme and with filtered scheme. We observe nice behavior of filtered scheme.

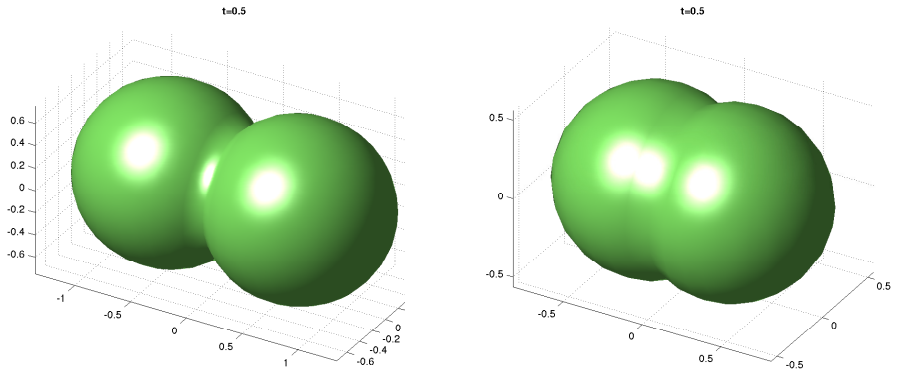

FIGURE 2.16: Example 2.3.10, $f(x, y, z) = |x|$ in the bottom and T=0.5 solved by filtered scheme.

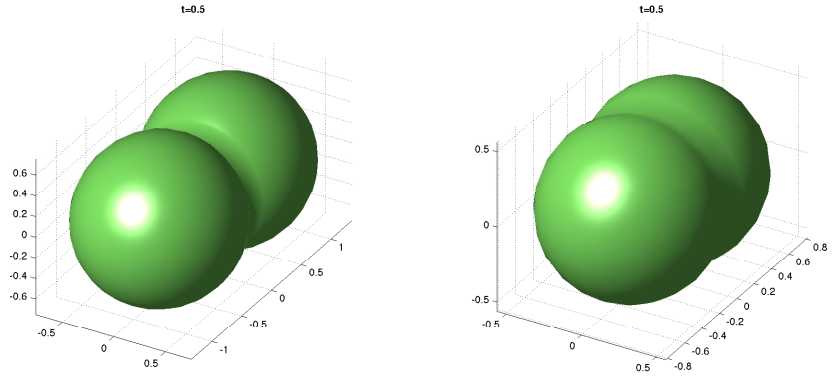

FIGURE 2.17: Example 2.3.10, $f(x, y, z) = |y|$ solved by filtered scheme and T=0.5. First picture with first-order numerical scheme and second one with filtered scheme with $\epsilon = 20\Delta x$

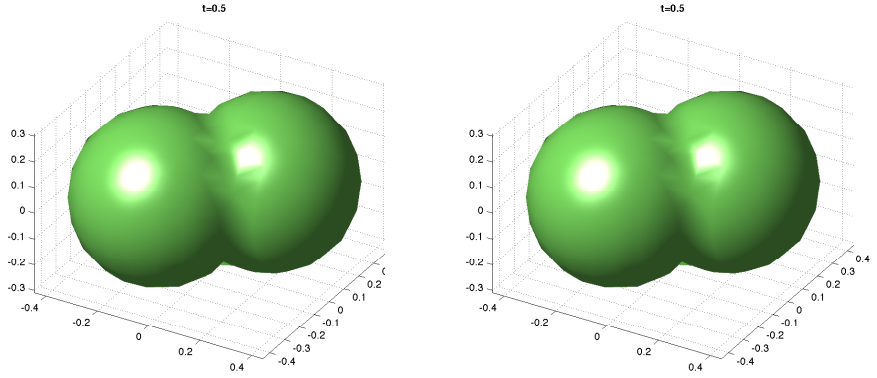

FIGURE 2.18: Example 2.3.10, $f(x, y, z) = |x| + |y|$ solved by filtered scheme and T=0.8. First picture with first-order numerical scheme and second one with filtered scheme with $\epsilon = 20\Delta x$

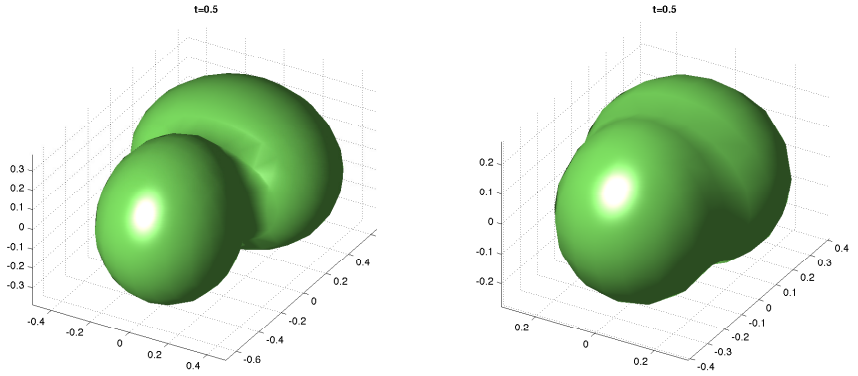

FIGURE 2.19: Example 2.3.10, $f(x, y, z) = x^2 + y$ solved by filtered scheme and T=0.5 with first-order numerical scheme and second one with filtered scheme with $\epsilon = 20\Delta x$

Chapter 3

Coupled schemes for Hamilton-Jacobi equations

3.1 Introduction

We propose a new numerical approximation for Hamilton-Jacobi-Bellman equations which is based on the coupling of two schemes with different properties. The approach is general and can in principle be applied to couple many different schemes, for example one can couple an accurate method for the regions where the solution is smooth with another method which is more adapt to treat discontinuities and/or jumps in the gradients. Clearly one has to decide where to apply the first or the second method and this is done by means of an indicator parameter which has to be computed in every cell at every time step. In this chapter we investigate in particular, the coupling between an anti-dissipative scheme which has been proposed in order to deal with discontinuous solutions and a semi-Lagrangian scheme which is more adapt to deal with Lipschitz continuous and can be more accurate for regular solutions provided a high-order local interpolation operator is used for the space reconstruction. We will introduce the indicator parameter for this coupling, show how to couple the two schemes which typically use two different grids reconstructions and prove some properties of the resulting coupled scheme. In the last section we will show some 1-dimensional tests which illustrate the properties of the coupled scheme. In this chapter our aim is to propose a new method to build schemes for first order time dependent HJ equations coupling two schemes for viscosity solution

which have different properties. We will consider the following model problem

$$\partial_t v + H(x, \nabla v) = 0, \quad (t, x) \in [0, T] \times \mathbb{R} \tag{3.1}$$

$$v(0, x) = v_0(x), \quad x \in \mathbb{R}. \tag{3.2}$$

where the hamiltonian H is convex in the gradient. A typical example comes from optimal control theory where $H(x, \nabla v) = \max_{\alpha \in A}\{f(x, \alpha)v_x(t, x)\}$ and a represents the control, it is well known that in this framework the solution v of the equation (3.1) corresponds to the value function of an optimization problem [6, 9]. Typically the solution is Lipschitz continuous if the data are Lipschitz continuous but also discontinuous solutions can be considered and they actually appear in several applications to control problems with state constraints, games and image processing. This is our main motivation to deal here with discontinuous initial conditions and in general the coupled scheme will be designed in order to be able to track discontinuous solutions. However, since the typical situation is to have a piecewise regular solution which only has discontinuities or jumps of the derivatives at isolated points it is natural to try to diversify the method in the subdomains where the solution is regular and in the cells where the solution exhibits this kind of singularities. To this end we will couple two schemes which have been already proposed in the literature and for which we know a number of properties which will turn to be useful for the construction of the coupled scheme. Let us also mention that hybrid schemes for hyperbolic conservation laws have been proposed in the literature to capture shocks for hyperbolic conservation laws and contact discontinuities for the compressible Euler system (see chapter 22 in the book by Laney [76] for more informations and references). The coupled scheme proposed here follows the same ideas although our goal is to solve HJ equations and the schemes chosen for the coupling are different.

It is well known that, in the one dimensional case, there is a strong link between Hamilton-Jacobi (HJ) equations and hyperbolic conservation laws. Namely, the viscosity solution of the evolutive HJ equation is the primitive of the entropy solution of the corresponding hyperbolic conservation law with the same Hamiltonian. There are several schemes developed for hyperbolic conservation law (see references [34, 59, 63, 64]. Most of the numerical ideas to solve hyperbolic conservation law can be extended to HJ equations. In the last decades many numerical schemes have been proposed for HJ

equations using different techniques, for example, finite differences, markov chain, semi-Lagrangian (SL) [2, 34, 42], these schemes have been shown to be stable and convergent under mild regularity assumptions on the solution and to be first order accurate for the approximation of Lipschitz continuous solutions. We also mention that more recently [19] a new class of high-order filtered schemes has been proposed, this schemes converge to the viscosity solution and a precise error estimate has been proved for regular viscosity solution. However, as we said, it can be interesting to deal with discontinuous viscosity solutions so these schemes have to be adapted in order to obtain reasonable approximations which do not diffuse too much around the discontinuities of Dv and/or v and do not oscillate.

For discontinuous solutions an anti-dissipative (AD) scheme has been proposed [13] and a convergence result has been proved in one dimension [15, 16]. That scheme has been initially proposed for hyperbolic conservation laws [38, 96] and then extended to Hamilton-Jacobi equations in one dimension. Another class of schemes which have been shown to be rather effective is that of SL scheme (see Falcone and Ferretti book [42] for a comprehensive presentation of this approach). SL scheme gives good results and are naturally multidimensional, they can be very accurate in the regions of regularity for the solution provided a high-order local reconstruction in space is used. Despite these interesting features SL schemes are not efficient for discontinuous initial data since they use a local interpolation operator for the computation at the foot of the characteristic. In this chapter we present a new scheme for (3.1) based on the coupling between the Ultrabee scheme (an AD scheme) and a first order SL scheme. We intend to take the advantage of the properties of the two methods introducing an indicator parameter σ_j which will be computed in every cell C_j in order to detect if there is a singularity there. Then, according to the value of σ_j, we will use the SL scheme if the solution is regular enough switching to the AD scheme when a discontinuity is detected.

3.2 Background results for the uncoupled schemes.

In this section we recall SL scheme which studied by Ferretti and Falcone and works very well when solution of HJ equation is smooth in [41]. Also we will recall Antidiffusive (Ultrabee) scheme which Modified by Bokanowski and Zidani [13].

3.2.1 Semi-Lagrangian (SL) Schemes [42]

A SL method, is based on two basic steps: the reconstruction of the solution on a fixed grid and numerical integration along the lines of the same characteristics; remember that the idea of using the aspect numerical method of characteristics was proposed for the first time by Courant, Isaacson and Rees in the [33]. In 1 dimension the CIR scheme precisely gives the first order upwind scheme when applied to the advection equation imposing the CFL condition $v_{max}\Delta t/\Delta x \leq 1$ where v_{max} is the upper bound for the modulus of the velocity. However, these methods are still stable for large time steps so they do not need the typical CFL condition required by finite difference methods. This is particularly important to run simulations which want to investigate the long time behavior of the solution. In the framework of HJ, SL schemes have been developed initially for the solution of Bellman equations associated with optimal control problems. This schemes can be interpreted as a discretization of the dynamic programming principle.
The typical *assumptions on* H are:

1. $H(\cdot,\cdot,\cdot)$ is uniformly continuous in all the variables.
2. $H(x,v,\cdot)$ is convex and coercive.
3. $H(x,\cdot,Dv)$ is monotone.

Under these assumptions we have the representation Hopf-Lax formula for the solution

$$v(x,t+\Delta t) = \min_{a\in\mathbb{R}}\{v(x-a\Delta t,t) + \Delta t H^*(a)\}$$

where

$$H^*(a) = \sup\{a\cdot p - H(p)\}$$

is the Legendre transform of Hamiltonian H. Note that the formula is the extension of the classical representation formula for the linear advection equation. Let $I_1[u]$ denote the P_1-interpolation of a function u in dimension one on the mesh $G = \{x_j\}$, i.e.

$$I_1[u](x) = \frac{x_{j+1}-x}{\Delta x}u_j + \frac{x-x_j}{\Delta x}u_{j+1} \quad \text{for } x\in[x_j,x_{j+1}] \tag{3.3}$$

Hence the SL scheme for (3.1) is

$$u_j^{n+1} = \min_{a\in R}\{I[u^n](x_j - a\Delta t)\Delta t H^*(a)\} \tag{3.4}$$

SL scheme is monotone stable and works for large Courant number. Converges and error estimate has been proven (see [42] for precise results).

3.2.2 Ultra-Bee scheme for HJB equations [13]

In this section we recall the anti-dissipative scheme (AD) which is the "Ultrabee" scheme of Roe [96]. For modified Ultrabee scheme we refer the work of [13]. The Ultrabee scheme is non monotone but it has the interesting property to transport exactly a particular space of step functions in the case of linear advection when the speed is constant.

Let Δt be a constant time step and $t_n = n\Delta t$ for $n \geq 0$. Given two velocity functions $f^g : \mathbb{R} \to \mathbb{R}$, $g = m, M$, we set the following notation for the corresponding CFL numbers at a node x_j:

$$\nu_j^m := \frac{\Delta t}{\Delta x} f_m(x_j) \text{ and } \nu_j^M := \frac{\Delta t}{\Delta x} f_M(x_j),\ j \in \mathbb{Z} \tag{3.5}$$

Then we can define the vectors, $\nu^m = \{\nu_j^m, j \in \mathbb{Z}\}$, $\nu^M = \{\nu_j^M, j \in \mathbb{Z}\}$. Let us define the exact average values of the approximate solution at time t_n:

$$\overline{u}_j^n = \frac{1}{\Delta x}\int_{j-1/2}^{j+1/2} u(t_n, x)dx\ , j \in \mathbb{Z},\ n \in \mathbb{N} \tag{3.6}$$

Denoting by $\|f\|_\infty$ the L^∞ norm of a bounded function defined on $\mathbb{R}$ we define the CFL condition

$$\max\left(\|f_m\|_\infty, \|f_M\|_\infty\right)\frac{\Delta t}{\Delta x} \leq 1. \tag{3.7}$$

Here we recall the steps of the algorithm for the

Algorithm for the Ultrabee Scheme (UB)

Initialization. Compute the initial averages $\{\overline{u}_j^0\}_{j\in\mathbb{Z}}$ as above

For $n \geq 0$,

Main cycle

Step 1. Compute $u^{n+1} = \{u_j^{n+1}\}_{j\in\mathbb{Z}}$ by:

Step 2. For every $j \in \mathbb{Z}$, we define the "fluxes" $u^n_{j\pm 1/2}(\nu_j)$ for $\nu_j \in \{\nu_j^m, \nu_j^M\}$ as follows: if $\nu_j \geq 0$, we set

$$u^n_{j+1/2}(\nu) := \begin{cases} \min\left(\max\left(\overline{u}^n_{j+1}, b_j^+(\nu_j)\right), B_j^+\right) & \text{if } \nu_j > 0 \\ \overline{u}^n_{j+1} & \text{if } \nu_j = 0 \text{ and } \quad \overline{u}^n_j \neq \overline{u}^n_{j-1} \\ \overline{u}^n_j & \text{if } \nu_j = 0 \text{ and } \quad \overline{u}^n_j = \overline{u}^n_{j-1} \end{cases} \tag{3.8}$$

where

$$\begin{cases} b_j^+(\nu) := \max\left(\overline{u}^n_j, \overline{u}^n_{j-1}\right) + \frac{1}{\nu_j}\left(\overline{u}^n_j - \max\left(\overline{u}^n_j, \overline{u}^n_{j-1}\right)\right), \\ B_j^+(\nu) := \min\left(\overline{u}^n_j, \overline{u}^n_{j-1}\right) + \frac{1}{\nu_j}\left(\overline{u}^n_j - \min\left(\overline{u}^n_j, \overline{u}^n_{j-1}\right)\right), \end{cases} \tag{3.9}$$

if $\nu_j \leq 0$, we set

$$u^n_{j-1/2}(\nu) := \begin{cases} \min\left(\max\left(\overline{u}^n_{j-1}, b_j^-(\nu_j)\right), B_j^-\right) & \text{if } \nu_j < 0 \\ \overline{u}^n_{j-1} & \text{if } \nu_j = 0 \text{ and } \quad \overline{u}^n_j \neq \overline{u}^n_{j+1} \\ \overline{u}^n_j & \text{if } \nu_j = 0 \text{ and } \quad \overline{u}^n_j = \overline{u}^n_{j+1} \end{cases} \tag{3.10}$$

where

$$\begin{cases} b_j^-(\nu) := \max\left(\overline{u}^n_j, \overline{u}^n_{j+1}\right) + \frac{1}{\nu_j}\left(\overline{u}^n_j - \max\left(\overline{u}^n_j, \overline{u}^n_{j+1}\right)\right), \\ B_j^-(\nu) := \min\left(\overline{u}^n_j, \overline{u}^n_{j+1}\right) + \frac{1}{\nu_j}\left(\overline{u}^n_j - \min\left(\overline{u}^n_j, \overline{u}^n_{j+1}\right)\right), \end{cases} \tag{3.11}$$

Step 3. For $\nu_j \in \left\{\nu_j^m, \nu_j^M\right\}$, we define

$$\overline{u}^{n+1}_j = \overline{u}^n_j - \nu_j\left(u^n_{j+1/2}(\nu) - u^n_{j-1/2}(\nu)\right) \tag{3.12}$$

Step 4. Finally, we set $\overline{u}^{n+1}_j := \min\left(\overline{u}^{n+1}_j(\nu_j^m), \overline{u}^{n+1}_j(\nu_j^M)\right)$, $j \in \mathbb{Z}$.

For simplicity and considering all the cases, we will use the following short notation for the Ultrabee scheme

$$\overline{u}^{n+1}_j = S_j^{UB}(\overline{u}^n) := \left(\min\left(\overline{u}^{n+1}_j(\nu^m), \overline{u}^{n+1}_j(\nu^M)\right)\right)_{j\in\mathbb{Z}} \tag{3.13}$$

For the advection equation: in [38] it has been proved that under the CFL condition $0 \leq \nu_j \leq 1$, for all j, Ultrabee scheme is consistent, L^∞ stable and TVD. Let us also mention the form of flux which used in [38] i.e.

$$u^n_{j+1/2} := \overline{u}^n_j + \frac{1-\nu_j}{\phi_j}(\overline{u}^n_{j+1} - \overline{u}^n_j), \tag{3.14}$$

where ϕ_j is defined as

$$\phi_j = \begin{cases} \max\left(0, \min\left(\frac{2r_j}{\nu_j}, \frac{2}{1-\nu_j}\right)\right), & \text{if} \quad \overline{u}^n_{j+1} = \overline{u}^n_j \quad \text{and} \quad \nu_j \neq 1 \\ 0, & \text{otherwise,} \end{cases} \tag{3.15}$$

where $r_j = \frac{\overline{u}^n_j - \overline{u}^n_{j-1}}{\overline{u}^n_{j+1} - \overline{u}^n_j}$ and by replacing $j = j-1$ we can compute $u^n_{j-1/2}$.

3.3 Construction of the Coupled Scheme (CS)

As we said, AD schemes are based on previous results for conservation laws and they typically require a projection onto a discontinuous reconstruction at every step. This choice seems to be clever for the regions where the solution is non regular but rather unfortunate where the solution is regular. Then a natural idea is to couple the features of two schemes: a scheme (S_1) well adapted for regular (at least Lipschitz continuous) solutions with an AD scheme (S_2) which allows for accurate result at the jumps. Thus we expect to get advantages coupling the two schemes, to this end we should be able to detect the regularity regions and the singular regions.

SL scheme uses a local interpolation operator to recover the value of the numerical solution at the foot of characteristics which are not grid points themselves. In their standard version, SL schemes do not use cell averages. On the contrary AD schemes is based on cell average values. For the coupling, we need values on two different grids G^{SL} and G^{AD} with space step Δx which are defined below:

$$G^{SL} = \{x_j = j\Delta x : j = \mathbb{Z}\},$$

$$G^{AD} = \{\overline{x}_j : \overline{x}_j = x_j + \frac{\Delta x}{2},\ j \in \mathbb{Z}\}$$

For simplicity we will often use the short cut for the nodes of the two grids which are shifted by $\Delta x/2$, calling $\bullet$-nodes the nodes of G^{SL} and $\times$-nodes the nodes of G^{AD}. Where u^n_j denotes an approximation of the $u(x_j, t_n)$, $\overline{u}^n_j$ denotes an approximation of the $\overline{u}(\overline{x}_j, t_n)$, where $t_n = n\Delta t$, $\Delta t > 0$. In what follows we drop the time index n and denote for simplicity $u_j = u^n_j$. At every step, we divide our domain into two regions, one where our approximate solution is continuous and the other where we detect discontinuities. To construct the CS scheme we need following definitions.

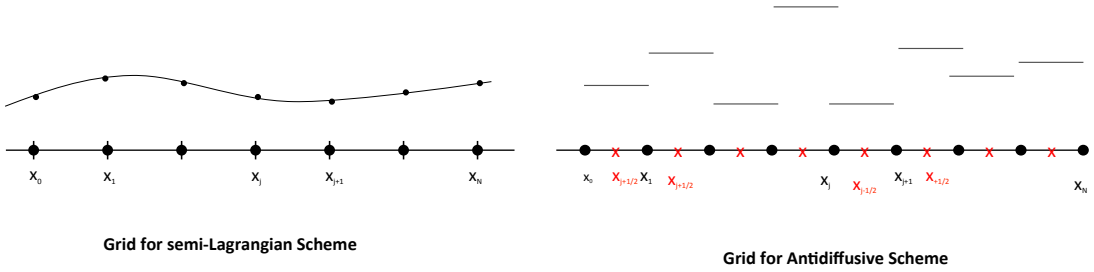

Let us define the *regularity indicators*, $P_j : \mathbb{Z} \to \mathbb{R}$

$$P_j := Du_j^n \equiv \frac{u_{j-1}^n - u_{j+1}^n}{2\Delta x} \text{ and } \overline{P}_j := \frac{\overline{u}_{j-1}^n - \overline{u}_{j+1}^n}{2\Delta x}, \tag{3.16}$$

By the above indicators we will detect the cells where the solution is regular in the two schemes, for simplicity we will just give the definition for P_j, the definitions for $\overline{P}_j$ are analogous.

Definition 1. *A cell $C_j = [x_j, x_{j+1})$ is said to be a* regular cell *if we have $|P_j| < \delta$ or $Du_j^n Du_{j-1}^n > 0$ and $Du_{j+1}^n Du_j^n > 0$.*

For example in the case of transport equation, we know the solution which is $u(x,t) = u_o(x-ct)$, so can set our threshold with the help of the initial condition $\delta = ||Du_j^0||_\infty - \epsilon$, $\epsilon > 0$.

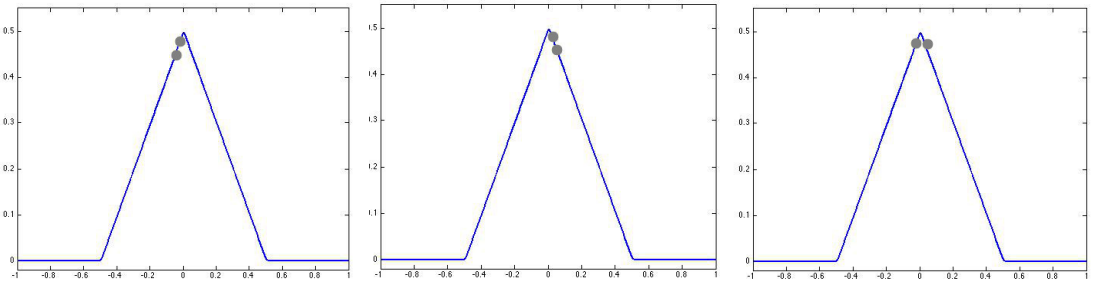

FIGURE 3.1: A sketch of three possible situations around a jump in the derivative.

Definition 2. *A cell C_j is said to be* a singular cell *if it is not a regular cell. We denote the set of singular cells by $\mathcal{C}_s$.*

Definition 3. *The* singular region *$\mathcal{R}_s$ is defined by the union of the following cells:*
a) all the singular cells

b) the neighbouring cells C_{j+1}, C_{j-1} to $C_j \in \mathcal{C}_s$ provided they are not in $\mathcal{C}_s$and their neighbour on the left or on the right is in $\mathcal{C}_s$, i.e. we look for C_{j+2} and C_{j-2} and

$$\text{if } \; C_{j+2} \in \mathcal{C}_s \Rightarrow C_{j+1} \in \mathcal{C}_s$$

$$\text{similarly, if } \; C_{j-2} \in \mathcal{C}_s \Rightarrow C_{j-1} \in \mathcal{C}_s$$

Definition 4. *The set $\mathcal{R}_r = [a,b] \setminus \mathcal{R}_s$ is called the* regular region.

Now we have a singular region $\mathcal{R}_s$ where we set $\sigma_j \equiv 0$ and in the regularity region $\mathcal{R}_r$ set $\sigma_j \equiv 1$. Since the schemes are working on different grids when the indicator says that we have to switch from SL to AD (or viceversa) we need to define the values on the other grid . To this end we define two local projection operators.

Definition 5 (*Local Projection Operator for SL).* *We define the local projection operator $P_{loc}^{SL} : \mathbb{R}^2 \to \mathbb{R}$ by a map which defines the new value u_j at x_j starting from the values $(\overline{u}_{j-1/2}, \overline{u}_{j+1/2})$,*

$$P_{loc}^{SL}(\overline{u}_{j-1/2}, \overline{u}_{j+1/2}) := \frac{\overline{u}_{j-1/2} + \overline{u}_{j+1/2}}{2} = u_j \tag{3.17}$$

Definition 6 (*Local Projection Operator for AD).* *We define the local projection operator $P_{loc}^{AD} : \mathbb{R}^2 \to \mathbb{R}$ by a map which defines the new value $\overline{u}_j$ at $x_{j+1/2}$ starting from the values (u_j, u_{j+1}),*

$$P_{loc}^{AD}(u_j, u_{j+1}) := \frac{u_j + u_{j+1}}{2} = \overline{u}_{j+1/2}. \tag{3.18}$$

Note that the projection operators are based on the average and they must be used locally whenever in a cell we switch from one scheme to the other. From the local definition we can also define a global projection operator which applies the local definition to every cell, i.e.

$$u^n = P^{SL}(\overline{u}^n) \text{ will mean } u_j^n = P_{loc}^{SL}(\overline{u}_{j-1/2}^n, \overline{u}_{j+1/2}^n), \forall j \tag{3.19}$$

and

$$\overline{u}^n = P^{AD}(u^n) \text{ will mean } \overline{u}_{j+1/2}^n = P_{loc}^{AD}(u_j^n, u_{j+1}^n), \forall j \tag{3.20}$$

We will describe the algorithm which couples the the two scheme and formally works on the two grids, although in practice we do not need to have a global algorithm everywhere and we just compute in every node according to the scheme which is selected by the

indicator σ_j^n which is computed only at the $\bullet$-nodes (remember that the $\times$-nodes are shifted by $\Delta x/2$ with respect to the $\bullet$-nodes)

Algorithm for the Coupled Scheme SL+UB

*Step 1.*On every x_j, we compute the initial data w_j^0 on every x_j and $\overline{x}_j$.

For $n \geq 0$

Step 2. We compute Du_{j-1}^n, Du_j^n, Du_{j+1}^n and Du_{j+2}^n and check $\forall\ j \in \mathbb{Z}$,

$$Du_{j-1}^n Du_j^n > 0, \quad Du_j^n Du_{j+1}^n > 0 \text{ and } \ ||Du_j^n||_\infty > \delta\ .$$

Step 3. If Step 2 is true then go to Step 4

Step 4. For every node x_j, we set

$$\sigma_j^n = 1$$

and compute

$$w_j^{n+1/2} = \sigma_j^n S_j^{SL}[w^n] + (1-\sigma_j^n) S_j^{AD}[w^n] = S_j^{SL}[w^n],$$

otherwise go to Step 5

Step 5. Check that $Du_j^n Du_{j+1}^n > 0,\ Du_{j-1}^n Du_{j-2}^n > 0$ and $||Du_{j-1}^n||_\infty > \delta$.

Step 6. If Step 5 is true then set

$$\sigma_j^n = 0$$

and apply P_{loc}^{AD} at the node $\overline{x}_j$,

$$P_{loc}^{AD}(u_j^n, u_{j+1}^n) = \frac{u_j^n + u_{j+1}^n}{2} = \overline{u}_j^n.$$

then we compute

$$w_j^{n+1/2} = \sigma_j^n S_j^{SL}[w^n] + (1-\sigma_j^n) S_j^{AD}[w^n] = S_j^{AD}[w^n]. \tag{3.21}$$

Step 7 If Step 5 is false then apply P_{loc}^{SL} at x_j

$$P_{loc}^{SL}(\overline{u}_j, \overline{u}_{j+1}^n) = \frac{\overline{u}_j^n + \overline{u}_{j+1}^n}{2} = u_j^n$$

Set

$$\sigma_j^n = 1$$

and compute

$$w_j^{n+1/2} = \sigma_j^n S_j^{SL}[w^n] + (1-\sigma_j^n) S_j^{AD}[w^n] = S_j^{SL}[w^n], \tag{3.22}$$

Step 8 (Filling the holes procedure)
For all the •-nodes where $\sigma_j^n = 0$ we need to project by P_{loc}^{SL} defined in (3.17) using the values in $w_j^{n+1/2}$;
at the ×-nodes not computed by the SL-scheme we need to project by P_{loc}^{SL} defined in (3.18) using the values in $w_j^{n+1/2}$. This will finally produce the new approximate solution w^{n+1}.

Then we go back to Step 2. □

Note that for all the •-nodes where $\sigma_j^n = 1$ we have the value computed by the SL-scheme so we will need to give a value only to the •-nodes where $\sigma_j^n = 0$, this is done via the projection operator P_{loc}^{SL}. In a similar way, at the ×-nodes belonging to a regular cell we will not have a value computed by the AD-scheme so we have to assign a value by the projection operator P_{loc}^{AD}. The filling procedure is included in the scheme just to simplify the presentation, in practice at every time step we will not need to project to assign a value to the node if the scheme applied that node will not change with respect to the scheme applied to compute the previous time step since in that case we already have the necessary informations. Whenever there is a switch of σ_j^n we need to project. In section 3.5 we will see that the coupled scheme (CS) described above is working well for the linear case and also for (3.1). In both cases we will be able to define a proper regularity threshold δ.

3.4 Properties of the coupled SL+UB scheme

In this section we focus our attention on the properties for coupled scheme defined at the end of the previous section. We will prove these properties for the advection problem, the extension to the non linear problem is still under study. At the end of the chapter

we will show some tests for linear and Hamilton-Jacobi equations which shows that the coupling procedure is also effective for nonlinear problems and deserves further analysis in that direction.

Let us start introducing some definitions.

Definition 7. *The* Discrete Total Variation *of an approximate solution* u^n *is*

$$TV(u^n) = \sum_{j\in\mathbb{Z}} |u^n_{j+1} - u^n_j|. \tag{3.23}$$

Definition 8. *We say that* the scheme is Total Variation Diminishing (TVD) *if for all* $n \geq 0$,

$$TV(u^{n+1}) \leq TV(u^n). \tag{3.24}$$

Now we also recall that a scheme written in Harten's incremental form [63]

$$u^{n+1}_j = u^n_j - c_{j-\frac{1}{2}}(u^n_j - u^n_{j-1}) + D_{j+\frac{1}{2}}(u^n_{j+1} - u^n_j), \tag{3.25}$$

$C_{j-\frac{1}{2}},\ D_{j+\frac{1}{2}} \in \mathbb{R}$, is TVD if and only if the following conditions are satisfied for all j:

$$0 \leq C_{j-\frac{1}{2}},\ 0 \leq D_{j+\frac{1}{2}} \text{ and } C_{j-\frac{1}{2}} + D_{j+\frac{1}{2}} \leq 1.$$

Definition 9. *The scheme* (3.12) *is* L^∞- stable *if the following conditions hold*

$$\nu_j \geq 0 \quad \Rightarrow \min(u^n_j, u^n_{j-1}) \leq u^{n+1}_j \leq \max(u^n_j, u^n_{j-1}), \tag{3.26}$$

$$\nu_j \leq 0 \quad \Rightarrow \min(u^n_j, u^n_{j+1}) \leq u^{n+1}_j \leq \max(u^n_j, u^n_{j+1}). \tag{3.27}$$

It is clear that above definition of L^∞- stability implies the standard definition of L^∞-stability i.e.

$$\|u^{n+1}\|_{L^\infty} \leq \|u^n\|_{L^\infty} \tag{3.28}$$

Definition 10. *We say that scheme* (3.12) *is* consistent *if all the fluxes* $u^{n,L}_{j+\frac{1}{2}}$ *and* $u^{n,R}_{j+\frac{1}{2}}$ *satisfy:*

$$\nu_j > 0 \quad \Rightarrow \min(u_j^n, u_j^{n+1}) \leq u^{n,L}_{j+\frac{1}{2}} \leq \max(u_j^n, u_{j-1}^n), \tag{3.29}$$

$$\nu_j < 0 \quad \Rightarrow \min(u_j^n, u_j^{n+1}) \leq u^{n,R}_{j+\frac{1}{2}} \leq \max(\overline{u}_j^n, \overline{u}_{j+1}^n). \tag{3.30}$$

Properties of the CS for the linear advection equation

Let us consider the following model problem

$$\begin{cases} v_t + cv_x = 0, \ t \in [0,T], \ x \in \mathbb{R} \quad c > 0 \ \text{ and constant}, \\ v(0,x) = v_0(x) \end{cases} \tag{3.31}$$

We consider the coupled scheme:

$$w_j^{n+1/2} = \sigma_j^n S_j^{SL}[w^n] + (1-\sigma_j^n) S_j^{AD}[w^n], \tag{3.32}$$

with the projection (3.17) or (3.18) (as explained in the coupled scheme algorithm we use projection when it needed). When we are always in regular region then above coupled scheme is coincide with the SL scheme. Let $x_j - c\Delta t \in (x_{j-1}, x_j]$ and $\nu = c\frac{\Delta t}{\Delta x}$ then we have following SL scheme

$$u_j^{n+1} = S_j^{SL}(u^n) := \nu u_{j-1}^n + (1-\nu) u_j^n \tag{3.33}$$

Note that, despite being obtained through a different procedure, the result precisely coincides with the upwind discretization for $\nu = 1$. Although Δt can in general be rather big ans SL schemes typically work for large Courant numbers here we will set $\nu = 1$ because the coupling is made with the Ultrabee scheme which needs that condition for stability.

For proving several properties of scheme we have to consider three cases.

Case 1 As we explained in the algorithm, when at time t_n we are in the regular region and there is no switch at the node x_j, we have $\sigma_j^n = \sigma_j^{n-1} = 1$ and we keep computing by the SL scheme on that node. Thus the resulting scheme automatically follows all the properties of SL schemes.

Case 2 Similarly, when $\sigma_j^n = \sigma_j^{n-1} = 0$ we continue to apply the AD scheme. Thus the resulting scheme is AD (here in particular Ultrabee) scheme and its satisfied all the properties for AD scheme.

Case 3 The scheme switches from one scheme to the other, i.e. $\sigma_j^n \neq \sigma_j^{n-1}$. We need to project the values from one grid to the other by the local projection operators (3.17) or (3.18) and check the properties of the resulting coupled scheme.

Note that the following properties of the projection operators will play an important role: As the definition of projection operator we have

$$\min(u_j^n, u_{j+1}^n) \leq \overline{u}_j^n = P_{loc}^{AD}(u_{j+1}^n, u_j^n) = \frac{u_j^n + u_{j+1}^n}{2} \leq \max(u_j^n, u_{j+1}^n) \tag{3.34}$$

$$\min(\overline{u}_j^n, \overline{u}_{j+1}^n) \leq \overline{u}_j^n = P_{loc}^{SL}(\overline{u}_{j+1}^n, \overline{u}_j^n) = \frac{\overline{u}_j^n + \overline{u}_{j+1}^n}{2} \leq \max(\overline{u}_j^n, \overline{u}_{j+1}^n) \tag{3.35}$$

1. *L^∞-stability of the coupled SL+UB scheme.* Let us consider the three cases.

   Case 1: In this case, we are at the node x_j the SL scheme which is known to be L^∞-stable (see [42]), so the property is true.

   Case 2: Also in this case, the property follows from the fact that the Ultrabee scheme is L^∞-stable (see [15]), this implies scheme L^∞ stability as in (3.26).

   Case 3: If we switch from one scheme to another then we need to use local projection operator (3.17) or (3.18). For instance, consider the situation when there is a switch from SL to the Ultrabee scheme. More precisely, the point (t_n, x_{j-1}) has been computed by SL scheme because σ_{j-1}^{n-1}=1) i.e.

   $$w_{j-1}^n = w_{j-1}^{n-1/2} = S_{j-1}^{SL}[w^{n-1}] = S_{j-1}^{SL}[u^{n-1}] \tag{3.36}$$

   Now we need to switch to the Ultrabee scheme, hence the local projection operator P_{loc}^{AD} (see (3.18)) is needed. This gives

   $$P_{loc}^{AD}(w_{j-1}^n, w_j^n) = P_{loc}^{AD}(u_j^n, u_{j+1}^n) = \frac{u_j^n + u_{j+1}^n}{2} = \overline{u}_j^n, \tag{3.37}$$

   and since $\sigma_j^n = 0$ and we have

   $$w_j^{n+1/2} = S_j^{AD}[w^n] = S_{j-1}^{SL}[\overline{u}^n] \tag{3.38}$$

Then the L^∞ bound is satisfied by (3.34) and the stablity property of the Ultrabee scheme. In the same way we can prove, that when the scheme switches from Ultrabee to SL scheme, the L^∞ stability is bound is satisfied by (3.35) and the SL stability property.

2. *The Coupled SL+UB scheme is TVD.*

We prove the TVD property for the three cases.

Case 1: $\sigma_j^n = \sigma_j^{n-1} = 1$. We need to prove that the semi-Lagrangian scheme based on P_1-interpolation (SL-P^1) is TVD. We have then,

$$w_j^{n+1} = w_j^{n+1/2} = S_j^{SL}[w^n] = S_j^{SL}[u^n] \tag{3.39}$$

$$u_j^{n+1} = \nu u_{j-1}^n + (1-\nu)u_j^n \text{ with } \nu \in (0,1] \tag{3.40}$$

$$|u_{j+1}^n - u_j^n| = |\nu u_j^{n-1} + (1-\nu)u_{j+1}^{n-1} - (\nu u_{j-1}^{n-1} + (1-\nu)u_j^{n-1})|$$

$$|u_{j+1}^n - u_j^n| = |\nu(u_j^{n-1} - u_{j-1}^{n-1}) + (1-\nu)(u_{j+1}^{n-1} - u_j^{n-1})|$$

$$\sum_j |u_{j+1}^n - u_j^n| \leq \sum_j |\nu(u_j^{n-1} - u_{j-1}^{n-1}) + (1-\nu)(u_{j+1}^{n-1} - u_j^{n-1})|$$

$$TV(u^n) \leq |\nu| TV(u^{n-1}) + |(1-\nu)| TV(u^{n-1})$$

$\nu \in (0,1]$ which implies

$$TV(w^n) = TV(u^n) \leq TV(u^{n-1}) = TV(w^{n-1}) \tag{3.41}$$

Hence SL-P^1 scheme is TVD.

Case 2: We assume that $\nu > 0$, using the L^∞-stability property and we have

$$w_j^{n+1/2} = S_j^{AD}[w^n] = S_{j-1}^{SL}[\overline{u}^n] \tag{3.42}$$

so we can also write

$$\overline{u}_j^{n+1} = \overline{u}_j^n - C_{j-1/2}(\overline{u}_j^n - \overline{u}_{j-1}^n)$$

with $C_{j-1/2} \in [0,1]$, and we can write (3.25) with $D_{j+1/2} = 0$ Hence we have the incremental form (3.25) with $C_{j+1/2} + D_{j+1/2} \leq 1$ since one of the coefficient $C_{j+1/2}$ or $D_{J+1/2}$ always vanishes. Thus the scheme is TVD.

Case 3: The scheme switches from one scheme to the other, i.e. $\sigma_j^n \neq \sigma_j^{n-1}$. For instance, consider the situation (same as we did in the case 3 of L^∞ stability proof) when there is a switch from SL to the Ultrabee scheme. More precisely, the point (t_n, x_{j-1}) has been computed by SL scheme because σ_{j-1}^{n-1}=1, i.e.

$$w_{j-1}^n = w_{j-1}^{n-1/2} = S_{j-1}^{SL}[w^{n-1}] = S_{j-1}^{SL}[u^{n-1}] \tag{3.43}$$

Now we need to switch to the Ultrabee scheme, hence the local projection operator P_{loc}^{AD} (see (3.18)) is needed. This gives

$$P_{loc}^{AD}(w_{j-1}^n, w_j^n) = P_{loc}^{AD}(u_j^n, u_{j+1}^n) = \frac{u_j^n + u_{j+1}^n}{2} = \overline{u}_j^n, \tag{3.44}$$

and since $\sigma_j^n = 0$ and we have

$$w_j^{n+1/2} = S_j^{AD}[w^n] = S_{j-1}^{SL}[\overline{u}^n] \tag{3.45}$$

Hence coupled scheme is TVD thanks to local projection operator. In the same manner we can prove when we switch from Ultrabee to SL scheme.

3. *The Coupled scheme SL+UB is consistent.*

Case 1: $\sigma_j = 1$ we already know that SL scheme is consistent . For more details we refer reader to see [42]

Case 2: if $\sigma_j = 0$ Ultrabee scheme is consistent. Thus implies scheme L^∞ stable as in (3.29) (For more details we refer reader to see [15]).

Case 3 and 4 : When we switch from one scheme to the other, the scheme resultant scheme is also consistent thanks to projection operator and the fact that they work on different nodes. Thus the coupled scheme is consistent.

3.5 Numerical tests

In this section we present several numerical tests in dimension one. In the following examples we solve advection equation (with constant and variable velocities) and HJ equation (3.1) by a coupled scheme based on the SL scheme (3.4) with P^1 local reconstruction and the Ultrabee scheme (3.13) presented in the sections 4.3.1. In order to show the differences between the original building methods and the couples scheme we consider several initial conditions with various degree of regularity and we follow their evolutions in time over an interval Ω. We will compute the errors in $L^1(\Omega)$, $L^2(\Omega)$ and, in some cases, in $L^\infty(\Omega_{reg})$ to show also the behavior in the regularity region.

3.5.1 Advection equation

Example 3.5.1. *We consider advection equation*

$$v_t + f(x)v_x = 0, \quad (t,x) \in \Omega, \tag{3.46}$$

$$v_0(x) = v(0,x), \tag{3.47}$$

where $f(x)$ is the velocity and $v_0(x)$ is initial data with bounded support. We consider three different v_0 with different regularity. For all three initial data, domain $\Omega = [0,2] \times (-2,2)$. We fix CFL is 0.9 and $f(x) = 1$. In all the tables below error calculation is global.

1 *Initial data v_0 is smooth data i.e.*

$$v(0,x) = v_0(x) = \begin{cases} (1-(1-|x|^2))^4 & |x| \leq 1 \\ 0 & otherwise, \end{cases} \tag{3.48}$$

In this case it is clear that solution remains smooth hence SL-P^1 scheme have good behavior unlike Ultrabee. So we expect coupled scheme to switch to SL-P^1 scheme everywhere. In fact in the error calculation we get exactly the same table for SL-P^1 and coupled scheme which is the expected result. In the Fig. 3.2 we have shown solution of (3.46) at time $t = 20\Delta t$ where time step $\Delta t = 0.045$ for the initial data (3.48). Fig. 3.3 shows the plots of σ for different time $t = 10\Delta t,\ 20\Delta t,\ 30\Delta$ where $\Delta t = 0.045$ (as we mentioned solution is smooth so $\sigma = 1$ for all the t). To sum-up for the advection with constant

velocity if initial data is smooth then indicator function σ is able to switch to the correct scheme. Table 3.1 and 3.2 are the error tables of Ultrabee and coupled (here same as SL-P^1) scheme respectively.

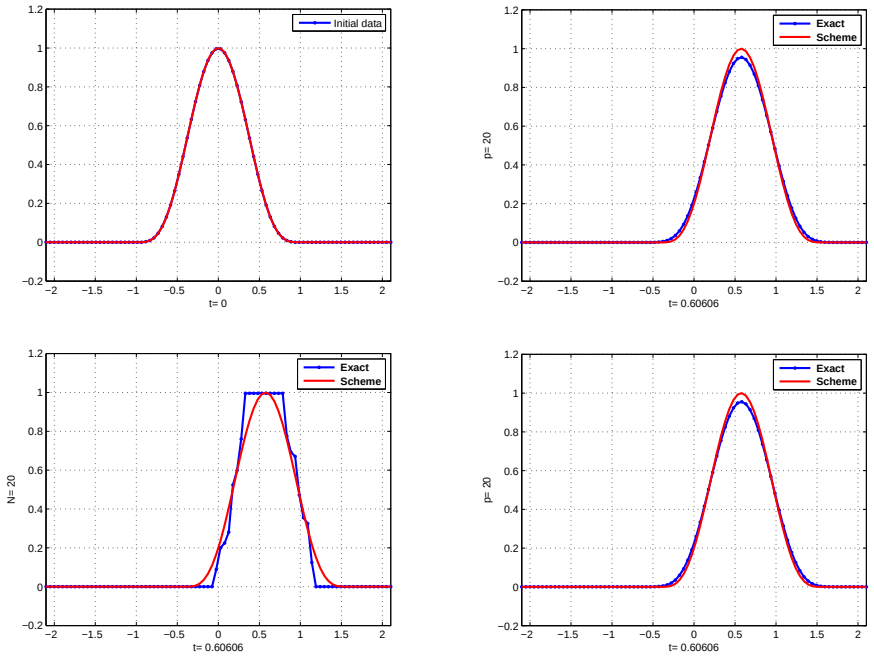

FIGURE 3.2: (Example 3.5.1), on the top left is the plot of initial data (3.48) and on the top right SL-P^1 scheme. In the second row plot of Ultrabee and coupled scheme respectively at $t = 20\Delta t$ where $\Delta t = 0.045$.

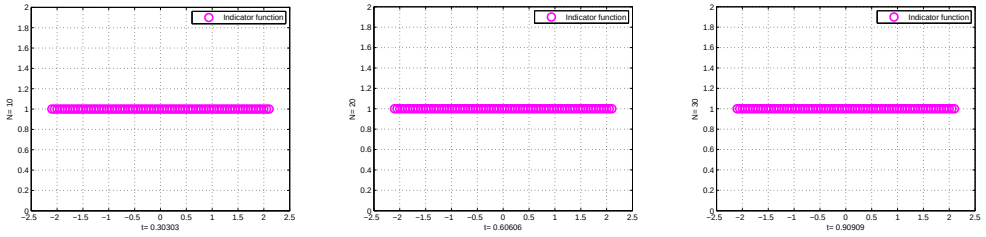

FIGURE 3.3: (Example 3.5.1), the plot of the indicator function σ for (3.48) at different time steps $t = 10\Delta t,\ 20\Delta t,\ 30\Delta t$ where $\Delta t = 0.045$.

2 *Initial data v_0 is Lipschitz continuous i.e.*

$$v(0,x) = v_0(x) = \begin{cases} 1 - |x| & \text{if} \quad |x| \leq 1 \\ 0 & \text{otherwise,} \end{cases} \tag{3.49}$$

Δt	Δx	L^1 Error	L^2 Error	L^∞ Error
0.181818	0.210526	9.04E-002	8.49E-002	1.10E-001
0.090909	0.102564	4.32E-002	4.27E-002	7.68E-002
0.045455	0.050633	2.17E-002	2.22E-002	5.56E-002
0.022472	0.025157	1.27E-002	1.27E-002	3.59E-002
0.011236	0.012539	6.49E-003	6.68E-003	2.20E-002
0.005634	0.006260	3.34E-003	3.50E-003	1.09E-002

TABLE 3.1: (Example 3.5.1), errors for the Ultrabee scheme with initial condition (3.48) at time $t = 20\Delta t$ where $\Delta t = 0.045$.

Δt	Δx	L^1 Error	L^2 Error	L^∞ Error
0.181818	0.210526	7.36E-002	5.93E-002	7.44E-002
0.090909	0.102564	3.49E-002	2.84E-002	3.64E-002
0.045455	0.050633	1.67E-002	1.37E-002	1.75E-002
0.022472	0.025157	8.87E-003	7.28E-003	9.31E-003
0.011236	0.012539	4.38E-003	3.60E-003	4.60E-003
0.005634	0.006260	2.14E-003	1.76E-003	2.25E-003

TABLE 3.2: (Example 3.5.1), errors for the coupled SL-P^1 + UB scheme with initial condition (3.48) at time $t = 20\Delta t$ where $\Delta t = 0.045$.

For this case we expect coupled scheme to detect the sharp point and switch to Ultrabee. In the Fig. 3.4 we have shown solution of (3.46) at time $t = 20\Delta t$ where time step $\Delta t = 0.045$ for the initial data (3.49). Fig. 3.5 contain the plots of σ for different time $t = 10\Delta t,\ 20\Delta t,\ 30\Delta$ where $\Delta t = 0.045$ and it is clear that indicator function σ detects discontinuity. Table 3.3, 3.4 and 3.5 are the error tables of coupled SL-P^1, Ultrabee and coupled scheme respectively.

Δt	Δx	L^1 Error	L^2 Error	L^∞ Error
0.181818	0.210526	5.10E-002	6.06E-002	1.17E-001
0.090909	0.102564	1.91E-002	2.35E-002	4.60E-002
0.045455	0.050633	8.96E-003	1.37E-002	3.37E-002
0.022472	0.025157	4.74E-003	8.68E-003	3.18E-002
0.011236	0.012539	2.33E-003	5.12E-003	2.40E-002
0.005634	0.006260	1.13E-003	2.97E-003	1.26E-002

TABLE 3.3: (Example 3.5.1), errors for the SL-P^1 scheme with initial condition (3.49) at $t = 20\Delta t$ where $\Delta t = 0.045$.

3 *Initial data v_0 is discontinuous function:*

$$v(0,x) = v_0(x) = \begin{cases} 1 & \text{if} \quad |x| \leq 1 \\ 0 & \text{otherwise,} \end{cases} \tag{3.50}$$

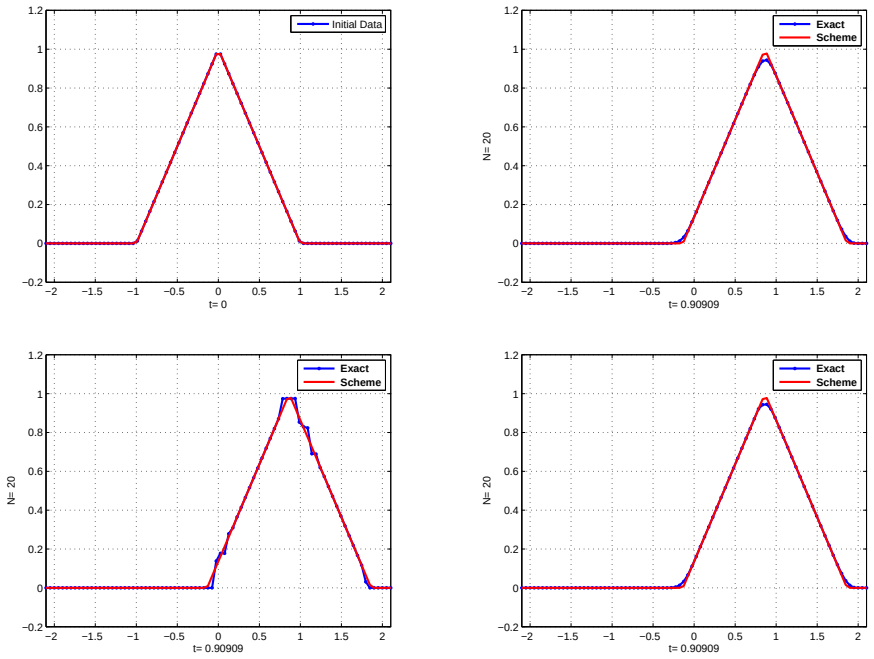

FIGURE 3.4: (Example 3.5.1), on the top left is the plot of initial data (3.49) and on top right SL-P^1 scheme. In the second row plot of Ultrabee and coupled scheme at $t = 20\Delta t$ where $\Delta t = 0.045$.

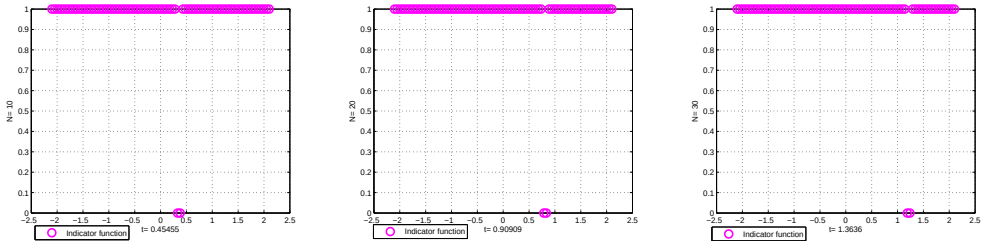

FIGURE 3.5: (Example 3.5.1), the plot of the indicator function σ for (3.49) initial data at $t = 10\Delta t,\ 20\Delta t,\ 30\Delta t$ where $\Delta t = 0.045$.

Δt	Δx	L^1 Error	L^2 Error	L^∞ Error
0.181818	0.210526	9.17E-002	8.75E-002	1.15E-001
0.090909	0.102564	4.07E-002	4.85E-002	1.05E-001
0.045455	0.050633	2.30E-002	2.94E-002	6.04E-002
0.022472	0.025157	1.29E-002	1.67E-002	3.86E-002
0.011236	0.012539	6.19E-003	8.48E-003	2.56E-002
0.005634	0.006260	2.88E-003	4.48E-003	2.20E-002

TABLE 3.4: (Example 3.5.1), errors for the Ultrabee scheme with initial condition (3.49) at $t = 20\Delta t$ where $\Delta t = 0.045$.

Here initial data is discontinuous we expect coupled scheme to switch to Ultrabee when discontinuity detects. In the Fig. 3.6 we have shown solution of (3.46) *at time* $t = 20\Delta t$

Δt	Δx	L^1 Error	L^2 Error	L^∞ Error
0.181818	0.210526	5.79E-002	6.34E-002	1.17E-001
0.090909	0.102564	1.91E-002	2.36E-002	4.15E-001
0.045455	0.050633	8.35E-003	1.32E-002	3.29E-002
0.022472	0.025157	4.19E-003	7.89E-003	2.73E-002
0.011236	0.012539	1.97E-003	4.46E-003	1.99E-002
0.005634	0.006260	9.34E-003	2.48E-003	1.34E-002

TABLE 3.5: (Example 3.5.1), errors for the coupled SL-P^1 + UB scheme with initial condition (3.49) at $t = 20\Delta t$ where $\Delta t = 0.045$.

where time step $\Delta t = 0.045$ *for the initial data* (3.50). *Fig. 3.7 shows the plots of* σ *for different time* $t = 10\Delta t,\ 20\Delta t,\ 30\Delta t = 0.45$. *It is clear in the Fig. 3.7 that indicator function* σ *detects discontinuity correctly. Tables 3.6, 3.7 and 3.8 are the error tables of SL-*P^1*, Ultrabee and coupled scheme respectively.*

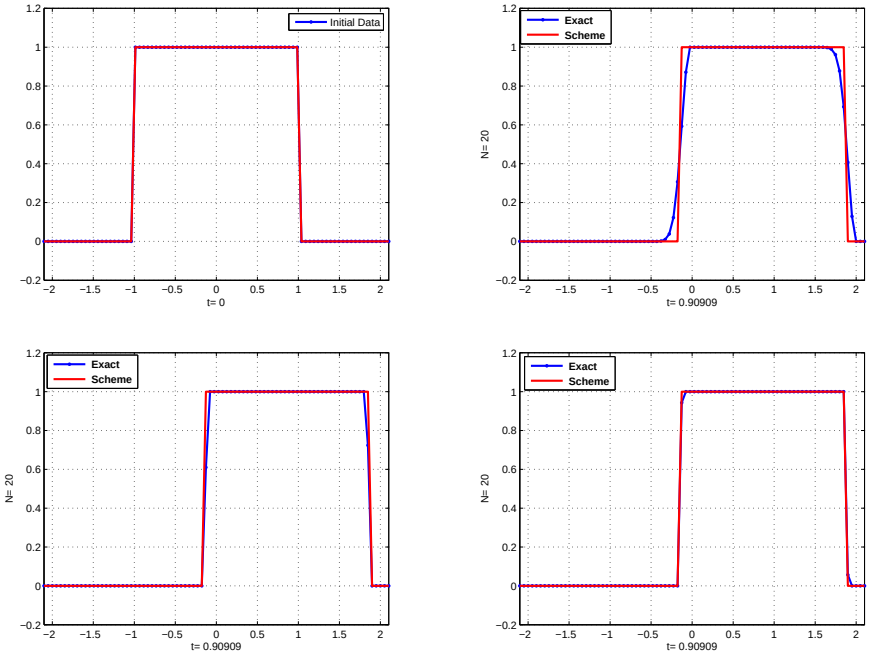

FIGURE 3.6: (Example 3.5.1), on the top left is the plot of initial data (3.49) and on top right SL-P^1 scheme. In the second row plot of Ultrabee and coupled scheme at $t = 20\Delta t$ where $\Delta t = 0.045$.

3.5.2 Advection equation with variable velocity

Example 3.5.2. *In this example we consider advection equation with variable velocity* $f(x) = -(x - \bar{x})$, *where* $\bar{x} = 1.1$. *This example has been taken from the book of Falcone*

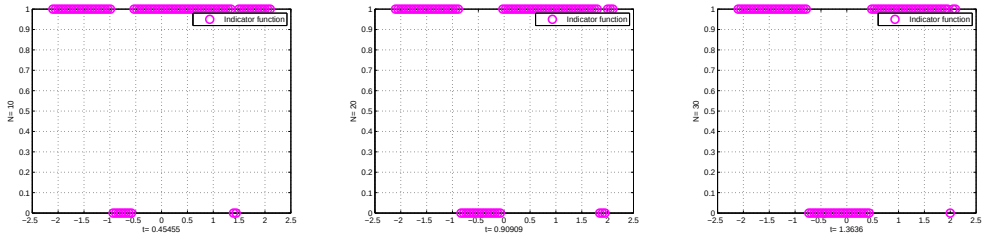

FIGURE 3.7: (Example 3.5.1), the plot of the indicator function σ for (3.49) initial data at $t = 10\Delta t,\ 20\Delta t,\ 30\Delta t$ where $\Delta t = 0.045$.

Δt	Δx	L^1 Error	L^2 Error	L^∞ Error
0.181818	0.210526	2.53E-001	3.32E-001	5.56E-001
0.090909	0.102564	1.43E-001	1.99E-001	3.38E-001
0.045455	0.050633	1.03E-001	1.72E-001	4.07E-001
0.022472	0.025157	7.57E-002	1.47E-001	4.05E-001
0.011236	0.012539	5.37E-002	1.25E-001	4.38E-001
0.005634	0.006260	3.77E-002	1.05E-001	4.61E-001

TABLE 3.6: (Example 3.5.1), errors for the SL-P^1 scheme with initial condition (3.50) at $t = 20\Delta t$ where $\Delta t = 0.045$.

Δt	Δx	L^1 Error	L^2 Error	L^∞ Error
0.181818	0.210526	7.02E-002	1.12E-001	2.12E-001
0.090909	0.102564	6.84E-002	1.51E-001	3.56E-001
0.045455	0.050633	3.38E-002	1.08E-001	3.90E-001
0.022472	0.025157	1.68E-002	8.32E-002	4.96E-001
0.011236	0.012539	8.36E-003	6.24E-002	5.44E-001
0.005634	0.006260	4.17E-003	3.73E-002	3.33E-001

TABLE 3.7: (Example 3.5.1), errors for the Ultrabee scheme with initial condition (3.50) at $t = 20\Delta t$ where $\Delta t = 0.045$.

Δt	Δx	L^1 Error	L^2 Error	L^∞ Error
0.181818	0.210526	1.08E-001	1.04E-002	1.37E-001
0.090909	0.102564	4.66E-003	2.36E-002	2.27E-002
0.045455	0.050633	5.75E-003	1.32E-002	5.68E-002
0.022472	0.025157	8.20E-003	7.89E-003	1.63E-001
0.011236	0.012539	5.28E-003	4.46E-003	2.11E-001
0.005634	0.006260	2.03E-017	2.48E-016	1.55E-015

TABLE 3.8: (Example 3.5.1), errors for the coupled SL-P^1 + UB scheme with initial condition (3.50) at $t = 20\Delta t$ where $\Delta t = 0.045$.

and Ferretti [42]. We consider smooth initial data which has bounded second derivative

i.e.

$$v(0,x) = v_0(x) = \max(0, 1 - 16(x - 0.25)^2)^2 \tag{3.51}$$

Here we fix CFL 0.6 and computations are done on the domain $\Omega = [0,1] \times (0,1)$. *As solution is smooth so we expect to our coupled scheme to be SL-*P^1 *everywhere. In the Fig. 3.8 we have shown solution of* (3.51) *at time* $t = 20\Delta t$ *and where time step* $\Delta t = 0.015385$. *Fig. 3.9 is the plot of* σ *for different time* $t = 10\Delta t,\ 20\Delta t,\ 30\Delta t$.

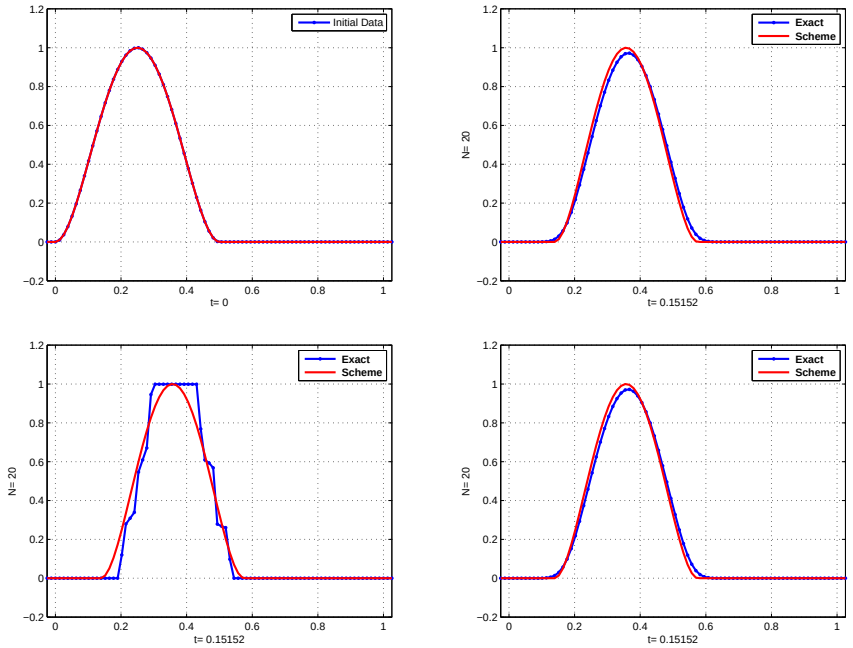

FIGURE 3.8: Example 3.5.2, on the top left is the plot of initial data (3.48) and on top right SL-P^1 scheme. In the second row plot of Ultrabee and coupled scheme at $t = 20\Delta t$ where $\Delta t = 0.015385$.

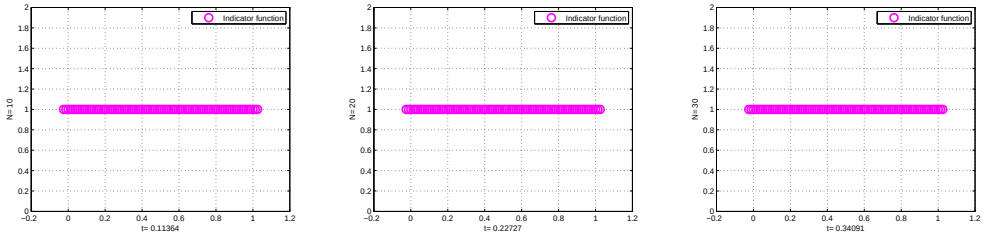

FIGURE 3.9: Example 3.5.2, the plot of the indicator function σ for (3.51) initial data for $\Delta t = 0.015385$ and $t = 5\Delta t,\ 10\Delta t,\ 20\Delta t$.

Δt	Δx	L^1 Error	L^2 Error	L^∞ Error
0.066667	0.111111	1.34E-001	2.62E-001	7.18E-001
0.031250	0.052632	1.35E-001	2.55E-001	6.79E-001
0.015385	0.025641	1.50E-001	2.87E-001	8.26E-001
0.007576	0.012658	1.64E-001	3.20E-001	9.10E-001
0.003774	0.006289	1.74E-001	3.44E-001	9.62E-001

Example 3.5.2, errors for the SL-P^1 scheme with initial condition (3.51) at $t = 20\Delta t$ where $\Delta t = 0.015385$.

Δt	Δx	L^1 Error	L^2 Error	L^∞ Error
0.031250	0.052632	5.07E-002	1.04E-001	3.04E-001
0.015385	0.025641	5.98E-002	1.15E-001	3.44E-001
0.007576	0.012658	3.08E-002	5.85E-002	2.12E-001
0.003774	0.006289	1.95E-002	3.72E-002	1.33E-001
0.001880	0.003135	1.58E-002	3.01E-002	1.18E-001
0.000939	0.001565	1.54E-002	2.74E-002	9.67E-002

TABLE 3.9: (Example 3.5.2), errors for the Ultrabee scheme with initial condition (3.51) at $t = 20\Delta t$ where $\Delta t = 0.015385$.

Δt	Δx	L^1 Error	L^2 Error	L^∞ Error
0.031250	0.052632	2.98E-002	4.50E-002	9.51E-002
0.015385	0.025641	1.95E-002	3.09E-002	6.63E-002
0.007576	0.012658	1.53E-002	2.52E-002	5.86E-002
0.003774	0.006289	1.52E-002	2.56E-002	6.16E-002
0.001880	0.003135	1.50E-002	2.53E-002	6.16E-002
0.000939	0.001565	1.51E-002	2.57E-002	6.29E-002

TABLE 3.10: (Example 3.5.2), errors for the coupled SL-P^1 + UB scheme with initial condition (3.51) at $t = 20\Delta t$ where $\Delta t = 0.015385$.

3.5.3 HJ equation

Example 3.5.3. *In the example below we solve HJ equation*

$$v_t + |f(x)v_x| = 0 \quad (t, x) \in \Omega. \tag{3.52}$$

We solve above HJ equation for the initial data (3.48) *and* (3.50). *We fix CFL* $= 0.6$ *and* $f(x) = 1$ *and the domain* $\Omega = [-2, 2] \times [0, 0.5]$. *All error calculations are global.*

Firstly we consider smooth initial data (3.48) *and in this case initialy solution is smooth but later on regularity will be lost. So in the beginning we expect coupled scheme to be*

SL-P^1 scheme and when some non smoothness detect scheme must switch to Ultrabee scheme. Fig. 3.13 shows the desired result i.e. till $t = 10\Delta x$ solution is smooth (i.e. $\sigma = 1$) and after that regularity lost ($\sigma = 0$). In Fig. 3.10, 3.11 and 3.12 are the plots at different time steps for initial data (3.48). Table 3.11, 3.12 and 3.13 are the error tables of SL-P^1, Ultrabee and coupled scheme respectively at time $t = 20\Delta t$ and $\Delta t = 0.014706$.

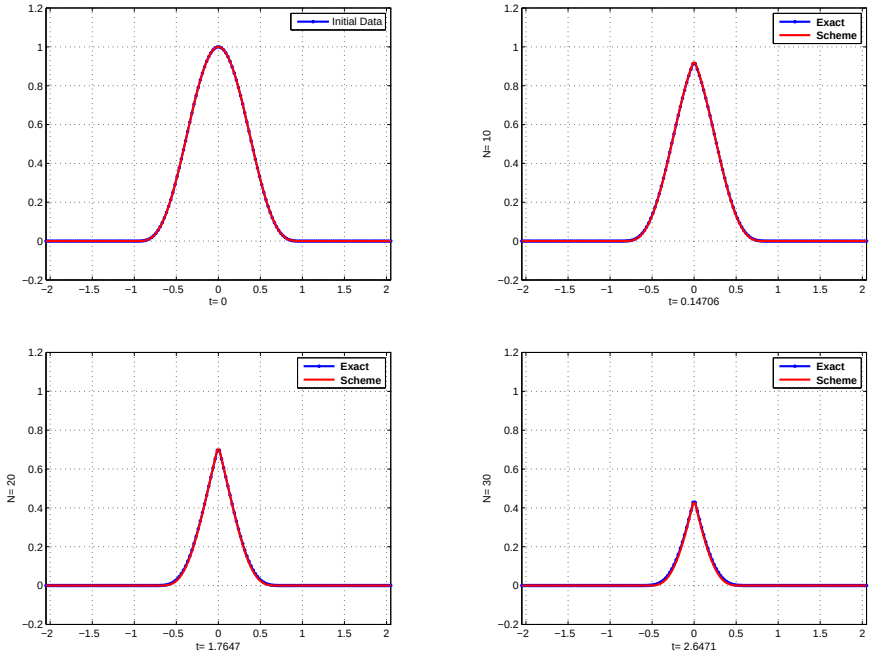

FIGURE 3.10: Example 3.5.3, on the top left is the plot of initial data (3.48) and on right SL-P^1 scheme at $t = 10\Delta t,\ 20\Delta t,\ 30\Delta t$ and $\Delta t = 0.014706$.

Δt	Δx	L^1 Error	L^2 Error	L^∞ Error
0.125000	0.210526	3.11E-002	2.62E-002	2.70E-002
0.055556	0.102564	2.27E-002	2.08E-002	2.52E-002
0.029412	0.050633	1.10E-002	1.01E-002	1.26E-002
0.014706	0.025157	5.96E-003	5.75E-003	7.45E-003
0.007463	0.012539	2.93E-003	2.85E-003	3.72E-003
0.003731	0.006260	1.47E-003	1.44E-003	1.89E-003

TABLE 3.11: (Example 3.5.3), errors for the SL-P^1 scheme with initial condition (3.48) at time $t = 20\Delta t$ and $\Delta t = 0.014706$.

Fig. 3.17 shows that how indicator function works here. In Fig. 3.14, 3.15 and 3.16 are the plots at different time steps for initial data (3.50). Table 3.14, 3.15 and 3.16 are the error tables of SL-P^1, Ultrabee and coupled scheme respectively at time $t = 20\Delta t$ and $\Delta t = 0.014706$.

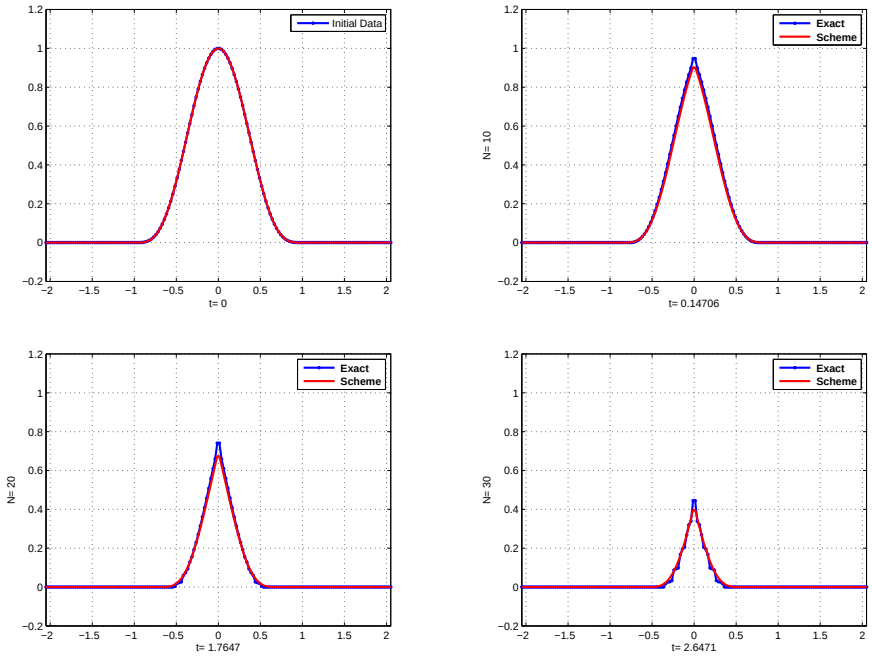

FIGURE 3.11: Example 3.5.3, on the top left is the plot of initial data (3.48) and on right Ultrabee scheme at $t = 10\Delta t,\ 20\Delta t,\ 30\Delta t$ and $\Delta t = 0.014706$.

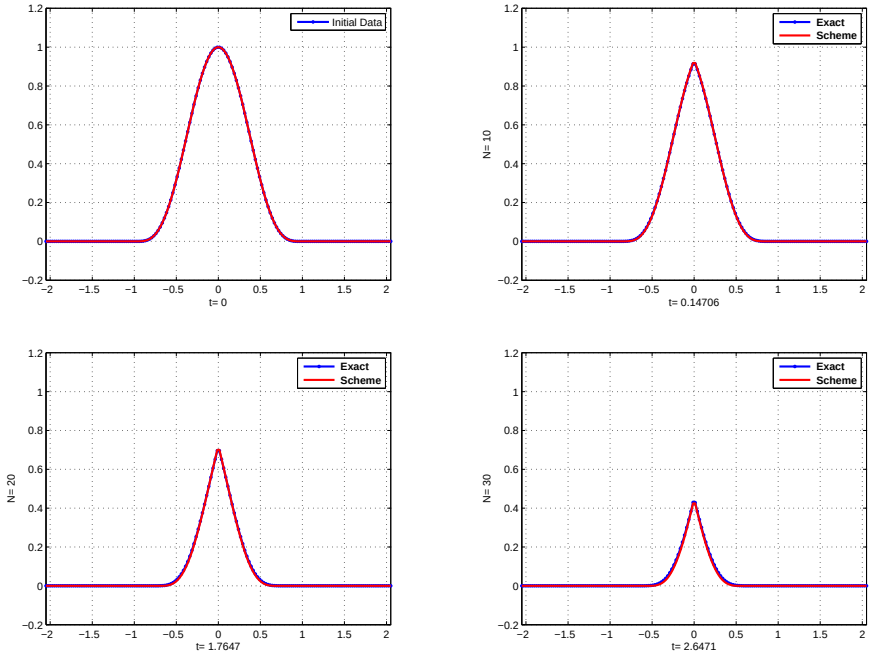

FIGURE 3.12: Example 3.5.3, on the top left is the plot of initial data (3.48) and on right coupled scheme at $t = 10\Delta t, 20\Delta t, 30\Delta t$ and $\Delta t = 0.014706$.

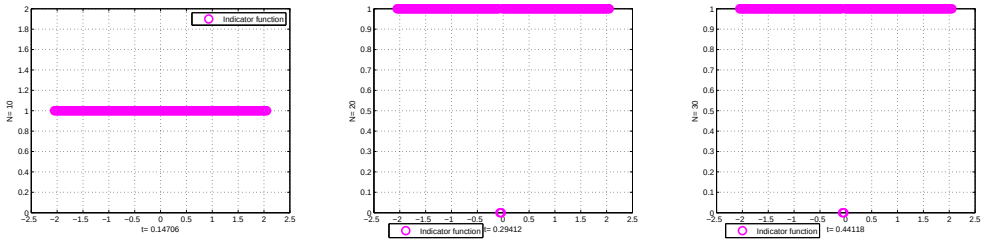

FIGURE 3.13: Example 3.5.2, the plot of the indicator function σ for (3.48) initial data at different time steps $t = 10\Delta t,\ 20\Delta t,\ 30\Delta t$ and $\Delta t = 0.014706$

.

Δt	Δx	L^1 Error	L^2 Error	L^∞ Error
0.125000	0.210526	2.34E-001	2.42E-001	3.28E-001
0.055556	0.102564	8.26E-002	1.27E-001	2.69E-001
0.029412	0.050633	3.86E-002	5.20E-002	1.30E-001
0.014706	0.025157	1.76E-002	2.27E-002	6.69E-002
0.007463	0.012539	8.59E-003	1.04E-002	3.31E-002
0.003731	0.006260	6.80E-003	8.58E-003	2.41E-002

TABLE 3.12: (Example 3.5.3), errors for the Ultrabee scheme with initial condition (3.48) at time $t = 20\Delta t$ and $\Delta t = 0.014706$.

Δt	Δx	L^1 Error	L^2 Error	L^∞ Error
0.125000	0.210526	5.01E-002	4.16E-002	4.27E-002
0.055556	0.102564	2.59E-002	2.35E-002	2.90E-002
0.029412	0.050633	1.16E-002	1.08E-002	1.36E-002
0.007463	0.012539	5.99E-003	5.71E-003	7.34E-003
0.014706	0.025157	2.98E-003	2.90E-003	3.79E-003
0.003731	0.006260	1.49E-003	1.46E-003	1.90E-003

TABLE 3.13: (Example 3.5.3), errors for the coupled SL-P^1 + UB scheme with initial condition (3.48) at time $t = 20\Delta t$ and $\Delta t = 0.014706$.

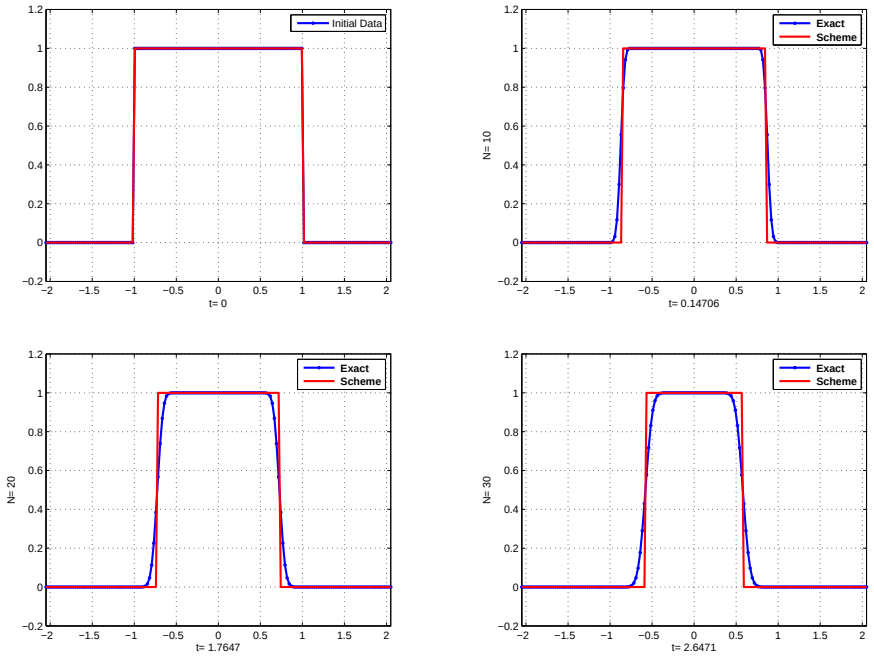

FIGURE 3.14: (Example 3.5.3), on the top on the left is the plot of initial data (3.50) and on right SL-P^1 scheme at $t = 10\Delta t, 20\Delta t, 30\Delta t$ and $\Delta t = 0.014706$.

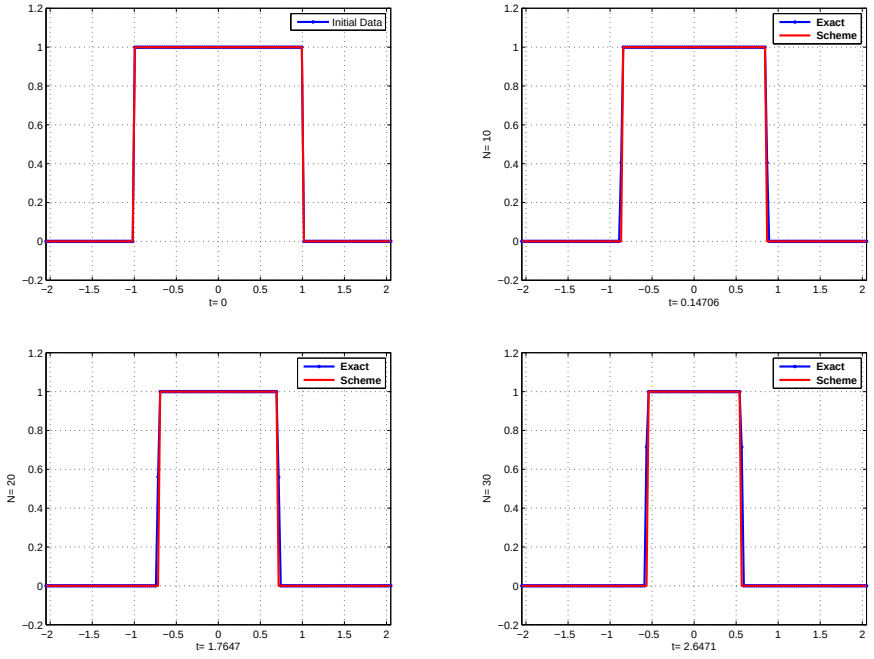

FIGURE 3.15: (Example 3.5.3), on the top on the left is the plot of initial data (3.50) and on right Ultrabee scheme at $t = 10\Delta t, 20\Delta t, 30\Delta t$ and $\Delta t = 0.014706$.

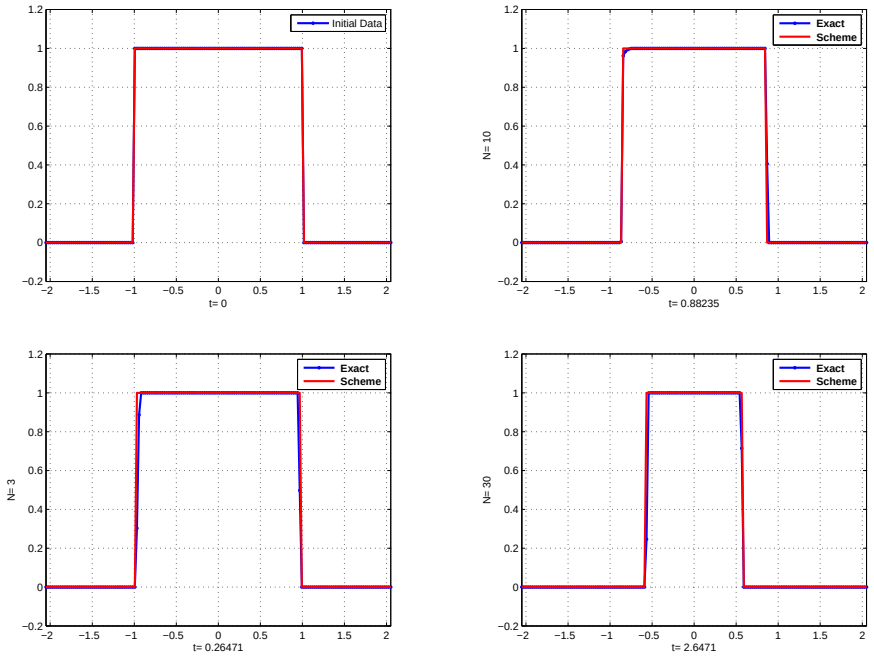

FIGURE 3.16: Example 3.5.3, on the top on the left is the plot of initial data (3.50) and on right coupled scheme at $t = 10\Delta t, 20\Delta t, 30\Delta t$ and $\Delta t = 0.014706$.

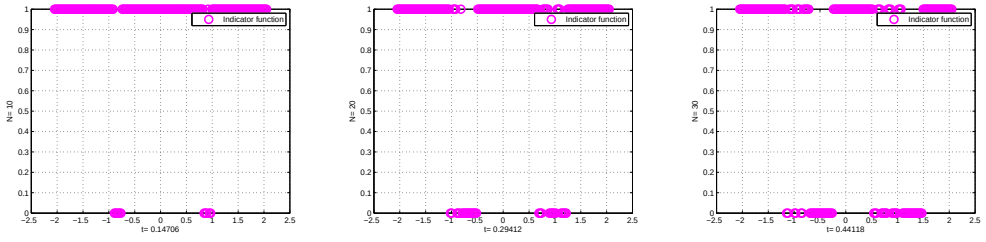

FIGURE 3.17: (Example 3.5.3), the plot of the indicator function σ for (3.50) initial data at different time steps $t = 10\Delta t, 20\Delta t, 30\Delta t$ and $\Delta t = 0.014706$

.

Δt	Δx	L^1 Error	L^2 Error	L^∞ Error
0.125000	0.210526	1.71E-001	2.64E-001	4.06E-001
0.055556	0.102564	1.56E-001	2.10E-001	3.77E-001
0.029412	0.050633	1.12E-001	1.84E-001	4.51E-001
0.014706	0.025157	8.47E-002	1.60E-001	4.90E-001
0.007463	0.012539	6.05E-002	1.34E-001	4.81E-001
0.003731	0.006260	4.29E-002	1.12E-001	4.60E-001

TABLE 3.14: (Example 3.5.3), errors for the SL-P^1 scheme with initial condition (3.50) at time $t = 20\Delta t$ and $\Delta t = 0.014706$.

Δt	Δx	L^1 Error	L^2 Error	L^∞ Error
0.125000	0.210526	3.07E-002	4.73E-002	7.29E-002
0.055556	0.102564	1.03E-001	2.26E-001	5.00E-001
0.029412	0.050633	1.99E-003	6.24E-003	1.96E-002
0.014706	0.025157	7.28E-003	3.24E-002	1.45E-001
0.007463	0.012539	1.28E-003	8.08E-003	5.10E-002
0.003731	0.006260	9.62E-003	8.60E-002	7.68E-001

TABLE 3.15: (Example 3.5.3), errors for the Ultrabee scheme with initial condition (3.50) at time $t = 20\Delta t$ and $\Delta t = 0.014706$.

Δt	Δx	L^1 Error	L^2 Error	L^∞ Error
0.125000	0.210526	7.24E-002	1.02E-001	1.98E-001
0.055556	0.102564	1.39E-001	2.90E-001	7.50E-001
0.029412	0.050633	2.31E-002	8.87E-002	3.93E-001
0.014706	0.025157	1.18E-002	5.54E-002	3.18E-001
0.007463	0.012539	6.14E-003	4.95E-002	4.39E-001
0.003731	0.006260	5.98E-003	6.01E-002	7.24E-001

TABLE 3.16: (Example 3.5.3), errors for the coupled SL-P^1 + UB scheme with initial condition (3.50) at time $t = 20\Delta t$ and $\Delta t = 0.014706$.

Chapter 4

Many-particle limit for traffic flow models on networks

4.1 Introduction

Since many years, traffic problems draw particular attention of the public. Traffic flow can be described at different scales, depending on the level of details one wants to observe. Typically, three scales of observation can be adopted: *microscopic* (single vehicles are tracked), *mesoscopic* (averaged quantities like density and mean velocity are tracked but car-to-car interactions are not lost) and *macroscopic* (only averaged quantities are tracked).

Limiting our attention to differential models, the most famous microscopic models are those of *follow-the-leader* type, also known as *car-following* models. In such a models, the dynamics of each vehicle depend on the preceding vehicles, so that, in the end, the whole traffic flow is determined by the dynamics of the first vehicle (the *leader*) in a cascade fashion. Drawbacks of microscopic model is that they require too many parameters, and high CPU time is needed to run a simulation.

Generally speaking, microscopic models are considered more justifiable because the behavior of every single vehicle can be described with high precision and it is immediately clear which kind of interactions are considered. On the contrary, macroscopic models are based on assumptions which are hardly correct or at least verifiable. As a consequence, it

is often desirable establishing a connection between microscopic and macroscopic models so to justify and validate the latter on the basis of the verifiable modeling assumptions of the former.

Connections between microscopic *follow-the-leader* and macroscopic fluid-dynamics traffic flow models are already well understood in the case of vehicles moving on a *single road*. Analogous connections in the case of *road networks* are instead lacking. This is probably due to the fact that macroscopic traffic models on networks are in general ill-posed, since the conservation of the mass is not sufficient alone to characterize a unique solution at junctions. This ambiguity makes more difficult to find the right limit of the microscopic model, which, in turn, can be defined in different ways near the junctions.

As we also explained in the general introduction of the thesis that we aim to established macroscopic and microscopic connection on the road networks. We propose a very natural extension of a first-order *follow-the-leader* model on road networks and then we prove that its solution tends in the limit to the solution of the LWR-based multi-path model introduced in [22, 23], i.e. as the number of vehicles tends to infinity while their total mass is constant (for more details we refer to see the general introduction).

We would like to point out that for the first-order models on a single unidirectional road, the micro-to-macro limit was already deeply investigated by means of different techniques: the papers [30, 97] use standard techniques coming from the theory of conservation laws. This is the approach we follow in this chapter; the paper [50] instead proves the limit relying on measure theory. The microscopic solution is interpreted as an empirical measure which is proven to converge to the entropy solution of the macroscopic model in the 1-Wesserstein topology. Unlike [30, 97], this approach allows to pass to the limit without shrinking to 0 the mass of the vehicles and without letting the number of vehicles tend to infinity (for more references see general introduction).

To our knowledge, there is no systematic theory about the extension of the follow-the-leader models on networks. It is plain that at the microscopic level one can easily reach a high level of detail, including junctions with spatial extension (non point), multi-lane roads, multi-class vehicles, traffic lights and priorities. Several highly sophisticated simulators are available since many years (free and commercial), see, e.g., [44, 101] and references therein to have an idea of the models and methods commonly used.

Nevertheless, it is unclear which average flux is actually observed at junction by the many-particle limit of any car-following model.

Beside this, let us also mention that the relationship between microscopic and macroscopic models was exploited to create hybrid models, see, e.g., [83]. In such a models the averaged quantities are observed where a detailed description is not needed (e.g., far from the junctions) while a detailed dynamics is considered elsewhere. However, this approach gives no clue about the macroscopic behavior of the microscopic model at junctions.

4.2 Macroscopic model

Macroscopic models are historically inspired from constitutive models for hydrodynamics system, which have similar properties as traffic flow. Traffic flow modeling began in the 1950's with the papers by Lighthill and Whitham [80, 107]. These authors wrote two important paper at that time on kinematics waves, the first on "flood movement in long rivers" and the second on a theory of "traffic flow on long crowded road", drawing similarities between the two types of flow. A similar discussion on traffic flow was published by Richards around the same time [95], independently of Lighthill and Whitham [80, 95, 107]. The common mathematical model is referred to as the LWR model. Its basic principle is the one-dimensional conservation equation.
LWR model relies on the knowledge of an empirically measured flux function, also called the *fundamental diagram* (we will explain in next section) in transportation engineering, for which measurements go back to 1935 with the pioneering work of Greenshields [61]. A number of other flux functions have been proposed in the hope of capturing effects of congestion more accurately, in particular: Greenberg [58], Underwood [106], Newell-Daganzo [37, 85]. The existence and uniqueness of an entropy solution to the Cauchy problem [98] for the class of scalar conservation laws to which the LWR model belongs to the work of Oleinik [87] and Kruzhkov [74] (see also the seminal article of Glimm [57]). Godunov scheme [58, 78] has been developed to solve LWR macroscopic model, which was shown to converge to the entropy solution of the first order hyperbolic PDE.

4.2.1 LWR model on a single road

Let $\rho = \rho(t,x)$ denote the density of vehicles at time t in the point $x \in \mathbb{R}$ and $v = v(t,x)$ their (average) velocity. Given any interval $[a,b] \subset \mathbb{R}$, the total amount of vehicles in it at time t is

$$\int_a^b \rho(t,x)dx$$

and, since it is assumed that vehicles are neither produced nor destroyed in $[a,b]$, the principle of conservation of vehicles states that the time variation of the above quantity is only due to the net flux of vehicles crossing the boundaries $x = a$ and $x = b$:

$$\begin{aligned} \frac{d}{dt}\int_a^b \rho dx &= [\text{flux of vehicles entering at } a] - [\text{flux of vehicles exiting at } b] \\ &= f(t,a) - f(t,b) \end{aligned}$$

where $f := \rho v$ is the traffic flux (i.e. the total number of vehicles crossing the point x per unit time). Therefore

$$\begin{aligned} \frac{d}{dt}\int_a^b \rho(t,x)dx &= \rho(t,a)v(t,a) - \rho(t,b)v(t,b). \\ &= \int_a^b \partial_x(\rho v)dx, \end{aligned} \tag{4.1}$$

Since ρ is bounded and we assume ρ_t exists, we get,

$$\int_a^b \partial_t \rho dx = -\int_a^b \partial_x(\rho v)dx, \tag{4.2}$$

i.e.

$$\int_a^b \left(\partial_t \rho + \partial_x(\rho v)\right) dx = 0.$$

Finally, due to the arbitrariness of the interval $[a,b]$ and assuming formally that the functions ρ and v are smooth, we conclude

$$\partial_t \rho + \partial_x\big(\rho v\big) = 0,$$

which is a first order PDE expressing the conservation of the mass of vehicles. Notice that this is a single equation for two unknowns, therefore it is not sufficient by itself to uniquely determine the distribution of vehicles along the road. However, if an equation of state $v = v(\rho)$ is provided, yielding the velocity v as a known function of the density ρ, then we get an equation for the variable ρ only of the form

$$\partial_t \rho + \partial_x \big(f(\rho)\big) = 0, \;\; f(\rho) = \rho v(\rho). \tag{4.3}$$

The problem is now in principle solvable for ρ. The mapping $\rho \to f(\rho)$ is frequently called the "*fundamental diagram*". Equation (4.3) having the form of a nonlinear hyperbolic conservation law, is referred to as the Lighthill-Whitham-Richards (LWR) model. Various forms of the fundamental diagram are possible (see, e.g., Garavello and Pic-

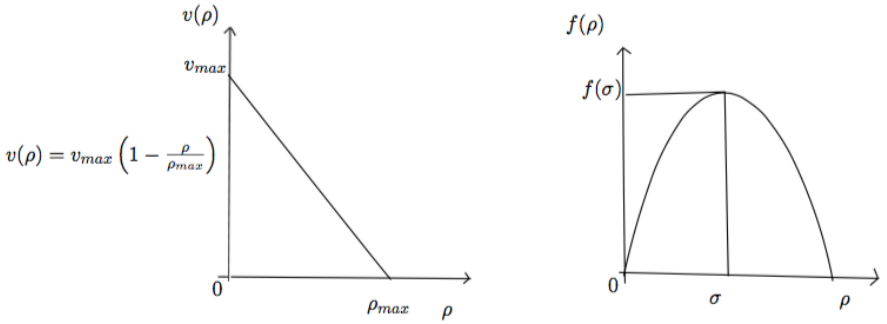

FIGURE 4.1: Speed and flux as a function of the density in the LWR model

coli [54, Chapt. 3]. For example we can consider as prototype the relation (see fig. 4.1, left)

$$v(\rho) = v_{max}\left(1 - \frac{\rho}{\rho_{max}}\right).$$

The macroscopic speed law $\rho \to v(\rho)$ is defined on $[0, \rho_{max}]$ and with values in v_{max} being the maximum speed corresponding to a free highway. v is non-increasing function and $v(0) = v_{max}$, $v(\rho_{max}) = 0$. The choice $v_{max} = \rho_{max} = 1$ gives rise to (see fig. 4.1, right) the traffic flux function

$$f(\rho) = \rho(1 - \rho),$$

a parabolic flux with the following main features:

(i) f is (strictly) concave for $\rho \in [0,1]$;

(ii) f is nonnegative for $\rho \in [0,1]$;

(iii) f has precisely one maximum point at $\rho = \sigma \in [0,1]$, specifically $\sigma = \frac{1}{2}$.

In the sequel we will develop our theory having in mind this function f, however all we will state holds more generally for any flux f complying with the assumptions (i), (ii), (iii) above. In particular, we will be concerned with Cauchy problem

$$\begin{cases} \partial_t \rho + \partial_x \big(f(\rho)\big) = 0, \quad t > 0, \quad x \in \mathbb{R} \\ \rho(x,0) = \rho_0(x) \quad x \in \mathbb{R} \end{cases} \tag{4.4}$$

for a prescribed initial datum $0 \leq \rho_0(x) \leq 1$ representing the initial distribution of vehicles along the road.

4.2.2 LWR model on networks

Macroscopic modeling of the traffic flow on networks is a difficult problem. Many solutions have been proposed in the past, based on heuristic approaches. Macroscopic traffic models on networks were deeply investigated starting from [70]. A complete introduction can be found in the book [54], which discusses several methods to characterize a unique solution at junctions. Let us also mention the source-destination model introduced in [53] (see also [68]) and the buffer models [52, 55, 69]. Recently, a LWR-based multi-path model on networks was introduced in the paper [22], together with a Godunov-based numerical scheme to solve the associated system of conservation laws with discontinuous flux. The relationship between the multi-path model and more standard methods (like, e.g., the one proposed in [29] based on the maximization of the flux at junction) was investigated in [23]. In the following we discuss the approach adapted in [54].

Let $I := [a,b]$ be a generic arc of the graph, i.e. a road. At any time t, the evolution of the vehicle density on the network is computed by a two-step procedure:

- First, a classical conservation law is solved at any internal point of the arcs;
- Second, the densities at endpoints a, b which correspond to a junction are computed. The latter step has not in general a unique admissible solution, so that additional constraints must be added.

Beside the conservation of vehicles at junctions, we assume here that drivers behave in order to maximize the flux at junctions and that incoming roads are regulated by priorities (right of way). The second step is performed by a linear programming method. On each arc, the density $\rho(x,t)$ of all vehicles (no distinction among vehicles is considered here) is given by the entropic solution of

$$\partial_t \rho + \partial_x \big(f(\rho)\big) = 0, \quad t > 0, \quad x \in (a,b) \tag{4.5}$$

$$\rho(x,0) = \rho_0(x) \quad x \in (a,b) \tag{4.6}$$

We consider now a generic junction J, and we denote by $\{I_i := [a_i, b_i]\},\ i = 1, ..., n$ the incoming roads and by $I_j := [a_j, b_j],\ j = n+1, ..., n+m$ the outgoing roads. We assume

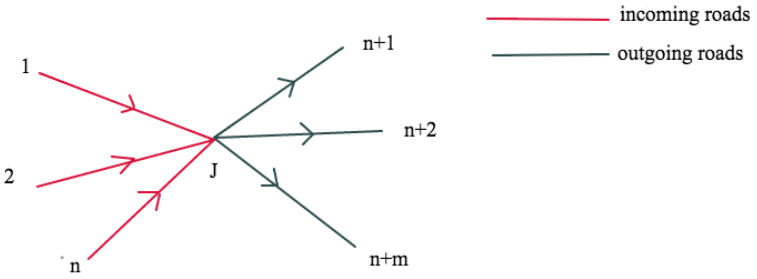

FIGURE 4.2: a junction with n incoming edges and m outgoing edges.

that the choice of the outgoing road is prescribed by a matrix of preferences,

$$A = \begin{bmatrix} \alpha_{n+1,1} & \dots & \alpha_{n+1,1} \\ \dots & \dots & \dots \\ \alpha_{n+m,1} & \dots & \alpha_{n+m,n} \end{bmatrix} \tag{4.7}$$

where $0 \le \alpha_{j,i} \le 1$ for every $i \in \{1, ..., n\}$ and $j \in \{n+1, ..., n+m\}$, and

$$\sum_{j=n+1}^{n+m} \alpha_{j,i} = 1$$

for every $i \in \{1, ..., n\}$. The i-th column of A describes how the traffic from I_i distributes in percentage to the outgoing roads. A basic requirement for a vector $(\rho_1, ..., \rho_{n+m})$ to

be an admissible solution to the problem at J is that

$$\sum_{i=1}^{n} f(\rho_j(b_i-,t)) = \sum_{j=n+1}^{n+1} f(\rho_j(a_j+,t)), \tag{4.8}$$

which translates the fact that the vehicles are conserved at junction. Note that (4.8) can be seen as a generalization of the Rankine-Hugoniot condition at junctions. We define

$$\gamma^i_{max}(\rho(b_i,t)) = \begin{cases} f(\rho(b_i,t)) & \text{if } \rho(b_i,t) \in [0,\sigma],\ i=1,...,n \\ f(\sigma) & \text{if } \rho(b_i,t) \in [\sigma,\rho_{max}],\ i=1,...,n \end{cases} \tag{4.9}$$

and

$$\gamma^j_{max}(\rho(a_j,t)) = \begin{cases} f(\sigma) & \text{if} \quad \rho(a_j,t) \in [0,\sigma],\ j=n+1,...,n+m \\ f(\rho(a_j,t)) & \text{if} \quad \rho(a_j,t) \in [\sigma,\rho_{max}],\ j=n+1,...,n+m \end{cases} \tag{4.10}$$

The quantities $\gamma^i_{max}\rho(b_i,t))$ and $\gamma^j_{max}(\rho(a_j,t))$ represent, respectively, the maximum incoming and the maximum outgoing flux that can be obtained on each road. Then we define

$$\Omega_i := [0, \gamma^i_{max}(\rho(b_i,t))],\ i=1,...,n, \tag{4.11}$$

$$\Omega_j := [0, \gamma^j_{max}(\rho(a_j,t))],\ j=n+1,...,n+m, \tag{4.12}$$

$$\Omega := \left\{(\gamma^1,...,\gamma^n) \in \Omega_1 \times ... \times \Omega_n \mid A(\gamma^1,...,\gamma^n)^T \in \Omega_{n+1} \times ... \times \Omega_{n+m}\right\} \tag{4.13}$$

The sets Ω_i, Ω_j contain all the possible fluxes for the solution at junctions and then the set Ω contains all the possible admissible fluxes at the end of the incoming roads, taking into account the matrix of preferences A. Since we want to maximize the flux at junction, we find the solution(s) of the maximization problem with linear constraints

$$\max_{(\gamma^1,...,\gamma^n)\in\Omega} \sum_{i=1}^{n} \gamma^i. \tag{4.14}$$

Note that the problem (4.14) has not in general a unique solution. To fix this, we assume the additional constraint

$$(\gamma^1,...,\gamma^n) \in \{qs, s \in \mathbb{R}^+\}, \tag{4.15}$$

can be introduced where $q = (q_1, ..., q_n)$ are the so-called priorities (right of way) coefficients such that $q_i \geq 0 \ \forall \ i$ and $\sum_i q_i = 1$. Equation (4.15) translates the fact that some incoming roads have priority with respect to the other roads in assigning their flux to the outgoing roads. The constraint (4.15) guarantees uniqueness of the solution of problem (4.14) (unless a further projection onto Ω is needed, see fig 4.3 left later on). Finally, define $(\gamma_1^*, ..., \gamma_n^*)$ as the unique solution of problem (4.14) (with the additional constraint (4.15) if necessary),

$$(\gamma_1^*, ..., \gamma_n^*) := \arg \max_{(\gamma^1, ..., \gamma^n) \in \Omega} \sum_{i=1}^{n} \gamma^i, \tag{4.16}$$

and consequently,

$$\gamma_j^* := \sum_{i=1}^{n} \alpha_{j,i} \gamma_i^*, \quad j = n+1, ..., n+m \tag{4.17}$$

For example, if $n = 2$ and $m = 1$ (two incoming roads $[a_i, b_i]$, $i = 1, 2$ and one outgoing road $[a_3, b_3]$).

> (**P**) : Assume that not all vehicles can enter the outgoing road. Let C be the amount that can do it. Then rC cars come from first incoming road and $(1 - r)C$ cars from the second road.

We have $A = (1 \ 1)$ and assume that a right of way parameter $r \in (0, 1)$ is given. Then the solution to the Riemann problem $(\rho_{1,0}, \rho_{2,0}, \rho_{3,0})$ is formed by a single wave on each road connecting the initial states to (ρ_1, ρ_2, ρ_3) determined in the following way.

Since we want to maximize going through traffic we set:

$$\gamma^* = \min \left\{ \gamma_{max}(\rho_1, 0) + \gamma_{max}(\rho_2, 0) + \gamma_{max}(\rho_3, 0) \right\}, \tag{4.18}$$

where γ_{max}^i defined in (4.9) and (4.10). Consider the space (γ_1, γ_2) and the line:

$$\gamma_2 = \frac{1 - r}{r} \gamma_1. \tag{4.19}$$

Notice that the line is exactly the locus of points satisfying exactly rule (P) . Define P to be the point of intersection of the line (4.19) with the line $\gamma_1 + \gamma_2 = \gamma_3^*$. Recall that

the final fluxes should belong to the region

$$\Omega = \left\{(\gamma^1, \gamma^2) : 0 \leq \gamma^i_{max}(\rho_i, 0),\ 0 \leq \gamma^1 + \gamma^2 \leq \gamma^*_3\right\}.$$

We distinguish two cases:

a) P belongs to Ω,

b) P is outside Ω.

In the first case we $(\gamma^*_1, \gamma^*_2) = P$, while in the second we set $(\gamma^*_1, \gamma^*_2) = Q$, where Q is the point of the segment $\Omega \cap \left\{(\gamma^1, \gamma^2) : \gamma^1 + \gamma^2 = \gamma^*_3\right\}$ closest to the line (4.19). We show in figure 4.3. Once we have determined γ^*_1 and γ^*_2 (hence also γ^*_3) we can determine

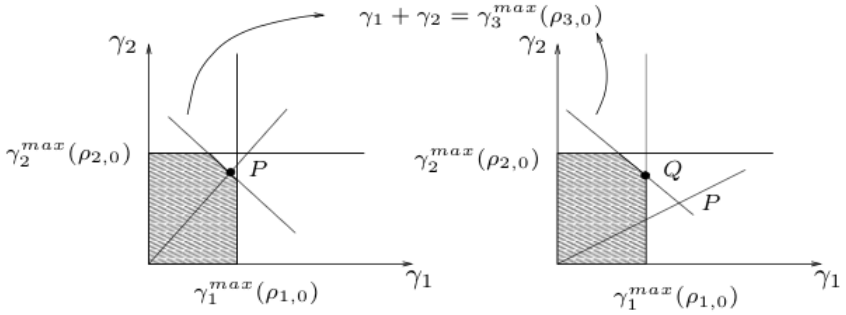

FIGURE 4.3: The cases a) and b) (figures from the book [54]).

in a unique way ρ_i ($i \in \{1, 2, 3\}$). For more details we refer reader to [54]. The idea to consider the LWR model on a network was proposed by Holden and Risebro [70]. Existence of solution to Cauchy problems was proved in the paper by Coclite, Garavello and Piccoli [29].

4.2.3 Numerical approximation by the Godunov scheme

Numerical methods to solve the equation along roads is represented by the Godunov scheme, which is based on the exact solutions to Riemann problems. Our main references are [29, 54]. The idea is the following:

- First the initial datum is approximated by a piecewise constant function.
- Then the corresponding Riemann problems are solved exactly and a global solution is simply obtained by piecing them together

- Finally, one takes the mean and proceeds by induction.

Let us describe briefly the Godunov scheme for solving a conservation law of the form

$$\partial_t \rho + \partial_x \big(f(\rho)\big) = 0, \quad t > 0, \quad x \in [a, b] \tag{4.20}$$

$$\rho(0, x) = \rho_0(x) \quad x \in [a, b], \tag{4.21}$$

on a generic arc $I = [a, b]$ of the network for a time interval $t \in [0, T]$, where T is the final time. We define a numerical grid in $[0, T] \times [a, b]$ with space step Δx and time step Δt, satisfying the CFL condition

$$\Delta t \max_{\rho} |f^{'}(\rho)| \leq \Delta x. \tag{4.22}$$

Let us denote by $(x_k, t_s) := (k\Delta x, s\Delta t),\ k \in \mathbb{Z},\ s \in \mathbb{N}$, the generic grid node and by ρ_k^s the density ρ at (x_k, t_s). Once the initial condition ρ_0 has been projected on the grid, in the internal nodes of the interval $[a, b]$ the density at time t^{s+1} is given by

$$\rho_k^{s+1} = \rho^s - \frac{\Delta t}{\Delta x} \left(G(\rho_k^s, \rho_{k+1}^s) - G(\rho_{k-1}^s, \rho_k^s)\right), \tag{4.23}$$

where the Godunov numerical flux G is defined as

$$G(\rho_\ell, \rho_r) = \begin{cases} \min\{f(\rho_\ell), f(\rho_r)\} & \text{if } \rho_l \leq \rho_r \\ f(\rho_\ell) & \text{if } \rho_l \leq \rho_r \text{ and } \rho_\ell < \sigma \\ f(\sigma) & \text{if } \rho_\ell > \rho_r \text{ and } \rho_\ell > \sigma \geq \rho_r \\ f(\rho_r) & \text{if } \rho_\ell > \rho_r \text{ and } \rho_r > \sigma \end{cases} \tag{4.24}$$

At the boundary nodes we proceed as follows:

- If the node is not linked to any junction, then we assign the desired boundary condition (Dirichlet or Neumann).

- If the node is a right endpoint and corresponds to the i-th incoming road of a junction, we use the maximal flux (14) and set

$$\rho_k^{s+1} = \rho^s - \frac{\Delta t}{\Delta x} \left(\gamma_i^* - G(\rho_{k-1}^s, \rho_k^s)\right), \tag{4.25}$$

- If the node is a left endpoint and corresponds to the j-th outgoing road of a junction, we use the maximal flux (15) and set

$$\rho_k^{s+1} = \rho^s - \frac{\Delta t}{\Delta x}\left(G(\rho_k^s, \rho_{k+1}^s) - \gamma_j^*\right). \tag{4.26}$$

4.2.4 LWR-based multi-path model on networks

In the section 4.2.2 we explained LWR model on networks. In this section we recall LWR-based multi-path model [22, 23] which is an alternative to model in [54]. Main feature of this model is that it selects automatically an admissible solution near junction, hence *ad hoc* external procedure (e.g. maximization of the flux via a linear programming method) is not needed. This model is different from so-called multi-population model or multi-class models [12, 108]. In those cases, the model consist of one equation of a single road (extension to the network is also possible) with different velocity function v_i, one for each class of vehicles. Typically, the populations have different maximal velocities, in order to take into account different types of vehicles or drivers behaviors.
There are similar model presented in [53]. In that case vehicles are divided in different populations on the basis on their source-destination pair. Given total density ω all the vehicles, the density μ^p of p-th population is given by

$$\mu^p(t,x) = \pi^p(t,x,O(p),D(p))\omega(t,x)$$

where $\pi^p(t,x,O,D)$ specifies the percentage of the total density that started from source O, it is moving towards the final destination D, and it is x at time t. Moreover, $O(p)$, $D(p)$ are the origin and the destination associated to the p-th path, respectively. Then, a standard PDE for ω is coupled with a system of PDEs for the coefficients π^p's. We follow the notations and also numerical scheme from the "twin" paper [22] and [23], where they introduced multi-path method for solving macroscopic model on the networks. Let us consider a network, i.e. a directed graph with N_R arcs (roads) and N_J nodes (junctions). Vehicles moving on the network are divided on the basis of their path. Let us assume that the number of possible paths on the graph is N_P and denote those paths by $P^1, ..., P^p, ..., P^{N_P}$. We stress that paths can share some arcs of the network. A point x of the network is characterized by both the path p it belongs to and the distance x from the origin of that path. We denote by $\mu^p(x,t)$ the density

of the vehicles following the p-th path at point x at time $t > 0$, and we assume that $\mu^p(t,x) \in [0, \rho_{max}]$ for some maximal density ρ_{max}. Note that we have, by definition, $\mu^p(t,x) = 0$ if $x \notin P^p$. We also define

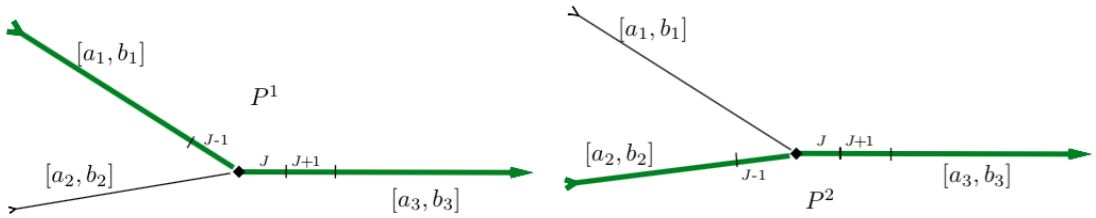

FIGURE 4.4: A network with 3 arcs and 1 junction, representing a merge. Path P^1 (left) and path P^2 (right).

$$\omega^p(t,x) := \sum_{q=1}^{N_p} \mu^q(t,x). \tag{4.27}$$

The function ω is expected to be discontinuous, especially at junctions, and contains all the information about the topology of the network. Note that, for any point x, the densities $\mu^p(x,t)$, $p = 1, ..., N_P$, are admissible if their sum $\omega^p(t,x) \leq \rho_{max}$.

Let us denote by $v(\omega)$ the velocity of vehicles (given as a function of the density) and by $f(\omega) = \omega v(\omega)$ the flux of vehicles. The LWR-based multi-path model is constituted by the following system of N_P conservation laws with space-dependent and discontinuous flux

$$\frac{\partial}{\partial_t}\mu^p(x,t) + \frac{\partial}{\partial_x}\big(\mu^p(x,t)v(\omega^p(x,t))\big)\big) = 0, \quad t > 0, \quad x \in P^p \tag{4.28}$$

Or, equivalently

$$\frac{\partial}{\partial_t}\mu^p(x,t) + \frac{\partial}{\partial_x}\big(\frac{\mu^p(x,t)}{\omega^p(x,t)}f(\omega^p(x,t))\big)\big) = 0, \quad t > 0, \quad x \in P^p \tag{4.29}$$

for $p = 1, ..., N_P$. If $\omega^p = 0$ we have, a fortiori, $\mu^p = 0$ then it is convenient to set $\frac{\mu^p}{\omega^p} = 0$ in (4.29) to avoid singularities. In the following we assume that the flux $f \in C^0([0, \rho_{max}]) \cap C^1((0, \rho_{max}))$ and

$$f(0) = f(\rho_{max}) = 0, \ f \text{ is strictly concave, } f(\sigma) = \max_{\omega \in (0, \rho_{max})} f(\omega) \tag{4.30}$$

Equations of the system (4.28) (or (4.29)) are coupled by means of the velocity v, which depends on the total density ω^p. On the other hand, not all the equations of the system are coupled with each other because paths do not have necessarily arcs in common.

4.2.5 Numerical approximation for the multi-path model

For the numerical discretization of the multi-path equations we employ the Godunov-based scheme introduced in [22]. For the sake of completeness, we briefly recall the scheme in the following. We denote by $\widetilde{\mu}_k^{s,p}$ the approximation of the value $\mu^p(x_k, t_s)$. Along each path p, a space discretization is considered, defining a space step $\Delta x > 0$ and space nodes $x_k := k\Delta x$, $k = 0, \dots, N_x$.

The scheme reads, for any $k = 0, \dots, N_x$ and $s = 0, 1, 2, \dots$,

$$\widetilde{\mu}_k^{s+1,p} = \widetilde{\mu}_k^{s,p} - \frac{\Delta t}{\Delta x}\left(\frac{\widetilde{\mu}_k^{s,p}}{\omega_k^{s,p}}\, g(\omega_k^{s,p}, \omega_{k+1}^{s,p}) - \frac{\widetilde{\mu}_{k-1}^{s,p}}{\omega_{k-1}^{s,p}}\, g(\omega_{k-1}^{s,p}, \omega_k^{s,p})\right) \tag{4.31}$$

with initial conditions $\mu_k^{0,p} = \mu^p(x_k, 0)$, and

$$\omega_k^{s,p} = \sum_{q=1}^{P} \widetilde{\mu}_k^{s,q}.$$

Note that $\omega_k^{s,p}$ is the sum of all densities living at x_k (along path p) at time t_s. The function g is instead the classical Godunov flux (4.24).

To summing up we have seen that the resulting Godunov-based numerical scheme can be implemented in minutes since it requires no additional procedures to manage the solution at junctions. Despite the simplicity of the model and of the numerical discretization, the method shows many interesting properties, some of which do not require ad hoc ingredients necessary in other models. Main features of LWR-based multi-path model are following:

- The model selects automatically a solution at junctions that maximizes the flow from an user point of view: On each single path the density is maximized (user optimum). Therefore, the scheme does not compute in general the maximal flow that could possibly be transferred over the node (global optimum), as it happens in more standard approaches.

- In the challenging case of a merge, proposed numerical scheme is consistent with the Riemann problem. As a consequence, the numerical approximation automatically assigns to the junction a finite spatial dimension and its density evolution is managed by a special flux function. Specifically, the flux function balances the incoming flows and the outgoing flow according to the fact that drivers want to maximize their own flow. It is able to widen temporarily the spaced-junction capacity, allowing the passage of vehicles and making the junction act as a "buffer", we refer reader to see [23] .

- The Model, together with the proposed discretization, fulfills all the 7 requirements for junction models proposed in [104, sect 3.1]. In particular, it is generally applicable irrespectively of the number of incoming and outgoing roads, the traffic never flows backwards and all flows are non-negative, vehicles are conserved, and turning fractions are preserved.

4.3 Microscopic Model

Early microscopic traffic models were proposed by Reuschel (1950) [94] and the physicist Pipes (1953) [91], which was later validated by Chandler [27]. This type of model concentrates on the behavior of each individual vehicle. The driver will adjust his or her velocity and acceleration according to the conditions ahead. Holland [70] describes this approach as providing a natural way to model traffic. In these models each vehicle is influenced directly by the one in front, as often happens in real traffic flow. Thus, vehicle position is treated as a continuous function and each vehicle moves according to an ordinary differential equation normally dependent on its speed and the distance to the next vehicle. The vehicle's progress can be calculated by solving these ordinary differential equations simultaneously. Usually the number of vehicles to be modeled has to be small enough for the approach to be useful. This situation sets traffic modeling apart from other fields, for example fluid mechanics and granular flow, because in these subjects the number of particles to be considered is typically too great for microscopic modeling. We can therefore consider *follow-the-leader* models as an alternative to a continuum approach. There are a number of different assumptions made for the various models of this type about what factors affect drivers decisions to change their behavior, such as the headway, which is defined as the distance in front of a vehicle before the next

vehicle. Gerlough [56] summarized a set of car-following rules in his dissertation about traffic simulation in 1955. These approaches were followed by an avalanche of extensions, such as the non-linear car-following model [36], the optimal velocity model [4], the intelligent driver model [73, 92, 105] and the cellular automaton model [84]. These agent-based models have been tested and applied to many traffic simulation systems, such as CORSIM [31], MITSIM [82], PARAMICS [24] VATSIM [93] and SUMO [103]. Helbing [66] reviewed the history of traffic modeling and broadly classified the modeling approaches into microscopic descriptions and macroscopic descriptions. Here we focus on first order *follow-the-leader model*, where each driver adjusts his velocity to the vehicle directly, and not in front in acceleration.

4.3.1 Follow-the-leader model on a single road

Let us describe the first-order *follow-the-leader* model which we will use as main ingredient in the rest of the chapter. We assume here that vehicles move on a single road with a single lane. Vehicles are initially located one after the other and cannot overtake each other. We denote by n the number of vehicles, by M their total mass, and by $\ell_n > 0$ the length of the vehicles. The parameter ℓ_n is derived by n and M as

$$\ell_n := \frac{M}{n}. \tag{4.32}$$

This assumption is crucial for the micro-to-macro limit since it translates the fact that the total mass does not change when the the number of vehicles tends to infinity, because the cars "shrink" accordingly.

We denote by $y_i(t)$ the position of the i-th car and we assume that at the initial time cars are labeled in order, i.e. $y_1(0) < y_2(0) < \ldots < y_n(0)$. This guarantees that the $(i+1)$-th car is just in front of the i-th one. Moreover, it is assumed that cars do not overlap, i.e. $y_{i+1}(0) - y_i(0) > \ell_n$, $i = 1, \ldots, n-1$. We are now ready to introduce the model, described by the following system of ODEs

$$\begin{cases} \dot{y}_i(t) = w(\delta_i(t)), \quad i = 1, \ldots, n-1 \\ \dot{y}_n(t) = v_{\max}, \end{cases} \tag{4.33}$$

where

$$\delta_i(t) := y_{i+1}(t) - y_i(t)$$

and w is such that

$$w : [\ell_n, +\infty) \to [0, v_{\max}], \qquad w(\delta) := v\left(\frac{\ell_n}{\delta}\right), \tag{4.34}$$

with $v \in \mathrm{Lip}([0,1];[0,v_{\max}])$ any function such that

$$v'(r) \leq 0, \qquad v(0) = v_{\max}, \qquad v(1) = 0. \tag{4.35}$$

The leader is assumed to move at maximal velocity $v_{\max} > 0$. Note that the properties introduced above guarantee that the cars do not overlap at any time $t > 0$, see [50].

The macroscopic limit of the previous model is given by the well known LWR model, which describes the evolution of the average density of vehicles $\rho(t,x) : (\mathbb{R}^+ \times \mathbb{R}) \to [0,1]$ by means of the following conservation law

$$\rho_t + (\rho v(\rho))_x = 0, \qquad t > 0, \quad x \in \mathbb{R}. \tag{4.36}$$

Equation (4.34) makes the link between the two models.

In order to recall precisely the results about the correspondence between the two models, we need to introduce first the natural spaces for the macroscopic density ρ and for the vectors of vehicles' positions $\mathbf{y} = (y_1, \dots, y_n)$, at any fixed time:

$$R := \left\{ r \in L^1(\mathbb{R};[0,1]) \ : \ \int_{\mathbb{R}} r(x)dx = M \text{ and } \mathrm{supp}(\rho) \text{ is compact} \right\}$$

and

$$Y_n := \Big\{ \mathbf{y} \in \mathbb{R}^n \ : \ y_{i+1} - y_i = \delta_i > \ell_n, \quad \forall i = 1, \dots, n-1 \Big\}.$$

We also introduce the operators $E_n : R \to Y_n$ and $C_n : Y_n \to R$, defined respectively as

$$E_n[r(\cdot)] := \mathbf{y} = \begin{cases} y_n = \max(\mathrm{supp}(r)), \\ y_i = \max\left\{ z \in \mathbb{R} \ : \ \displaystyle\int_z^{y_{i+1}} r(x)dx = \ell_n \right\}, \quad i = n-1, \dots, 2, 1 \end{cases} \tag{4.37}$$

and

$$C_n[\mathbf{y}] := r_n = \sum_{i=1}^{n-1} \frac{\ell_n}{\delta_i} \chi_{[y_i, y_{i+1})}. \tag{4.38}$$

The discretization operator E_n acts on a macroscopic density $\rho(t,\cdot)$, providing a vector of positions $\mathbf{y}(t) = E_n[\rho(t,\cdot)]$ whose components partition the support of the density into segments on which ρ has fixed integral ℓ_n. On the contrary, the operator C_n antidiscretizes a microscopic vector of positions $\mathbf{y}$, giving a piecewise constant density $\rho_n(t,\cdot) = C_n[\mathbf{y}(t)]$.

We are now ready to state the main result about the convergence of the microscopic model (4.33) to the macroscopic one (4.36). The proof can be found in [30].

Theorem 4.3.1. *Let (4.34) and (4.35) hold. Fix $T > 0$ and choose $\bar{\rho} = \rho(0,\cdot) \in R \cap BV(\mathbb{R};[0,1])$ and $\bar{\mathbf{y}} = \mathbf{y}(0) = E_n[\bar{\rho}]$. Let $\mathbf{y}(\cdot)$ be the solution of (4.33) with initial condition $\bar{\mathbf{y}}$. Define $\rho_n(t,\cdot) = C_n[\mathbf{y}(t)]$. If there exists $\rho \in L^\infty([0,T];R)$ such that $\lim_{n\to+\infty} \rho_n(t,x) = \rho(t,x)$ a.e., then ρ is a weak solution to (4.36) with initial condition $\bar{\rho}$.*

4.4 Follow-the-leader model on networks

In this section we extend the follow-the-leader model described in section 4.3.1 to a road network. We define a road network as a direct graph with N_{R} arcs (roads) and N_{J} nodes (junctions). We assume that for each junction $j = 1,\dots,N_{\mathrm{J}}$, there exist disjoint subsets $\mathrm{INC}(j)$, $\mathrm{OUT}(j)$, representing, respectively, the incoming roads to j and the outgoing roads from j. Among junctions, we distinguish two particular subsets consisting of origins $\mathcal{O}$, which are the junctions j such that $\mathrm{INC}(j) = \emptyset$, and destinations $\mathcal{D}$, which are the junctions j such that $\mathrm{OUT}(j) = \emptyset$. Finally, we denote by L^{R} the length of the road R for any $\mathrm{R} = 1,\dots,N_{\mathrm{R}}$. At initial time, n vehicles are located anywhere in the network.

4.4.1 A natural extension

A natural extension of the follow-the-leader model is derived as follows. We label the n vehicles by an index $i = 1,\dots,n$ and we denote by $\mathrm{R}(i,t) \in \{1,\dots,N_{\mathrm{R}}\}$ the road that

the vehicle i is traveling at time t. We also denote by $y_i(t)$ the position of the vehicle i at time t, defined as the distance from the origin of the road $\mathrm{R}(i,t)$.

There are three main differences with respect to the model on a single road, which require some modifications in the definition of δ_i and w.

• The concept of "ahead" must be redefined because when a vehicle reaches a junction has, in general, more than one "ahead" to choose. We assume that each vehicle has a sequence of roads (i.e., a path) assigned at the initial time to travel along, so that it is always clear which is the space in front of the vehicle. We also assume that drivers can actually see the space ahead, so that they can always evaluate the distance between them and the car in front, even if the latter is in the next road. Given that, *a vehicle is a leader if it is the first vehicle on its road and there is no other vehicles in the next roads along its path.* It is important to note that now more than one leader can be present on the network at the same time, and vehicles can gain or loose the leadership.

• The vehicle $i+1$ is no longer necessarily in front of vehicle i. This force us to introduce a new notation to refer to the vehicle in front. If a vehicle is not a leader, we denote by $\mathrm{NEXT}(i)$ the label of the car just in front of car i. If it is a leader, we set $\mathrm{NEXT}(i) = \emptyset$.

The distance between a (nonleader) vehicle and the vehicle in front is now computed as

$$\hat{\delta}_i(t) := \begin{cases} y_{\mathrm{NEXT}(i)}(t) - y_i(t), & \text{if } \mathrm{R}(i,t) = \mathrm{R}(\mathrm{NEXT}(i),t) \\ (L^{\mathrm{R}(i,t)} - y_i(t)) + \sum_{\mathrm{S}} L^{\mathrm{S}} + y_{\mathrm{NEXT}(i)}(t), & \text{if } \mathrm{R}(i,t) \neq \mathrm{R}(\mathrm{NEXT}(i),t) \end{cases} \tag{4.39}$$

where the summation with respect to S is done over all the empty roads between $\mathrm{R}(i,t)$ and $\mathrm{R}(\mathrm{NEXT}(i),t)$ (if any) along the sequence of roads followed by vehicle i.

• The non-overlapping condition $\hat{\delta}_i < \ell_n$ is no longer guaranteed, even if it holds at the initial time $t = 0$. To see this, let us consider the simple case of a network with 3 roads and 1 junction, with 2 incoming roads and 1 outgoing road, see Fig. 4.5. Assume that the outgoing road is empty and some cars are traveling along both the incoming roads (Fig. 4.5-left). Assume also that the two leader cars are going to reach the junction nearly or exactly at the same moment (note that both cars are leaders). As soon as one of the two cars goes through the junction, the other one becomes a follower and its distance $\hat{\delta}_i$, defined by (4.39), could be less than ℓ_n or even 0 (Fig. 4.5-right). However, two important observations can be made:

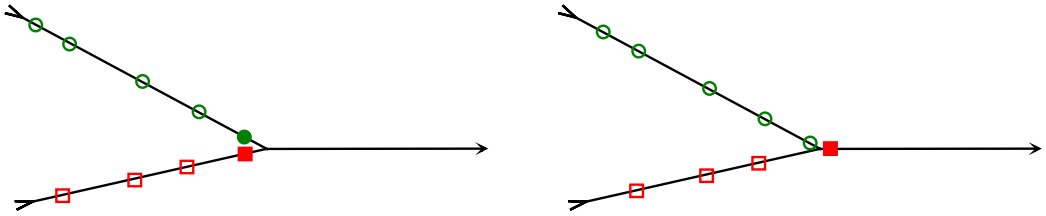

FIGURE 4.5: Overlapping issues across the junction. Leaders are denoted by filled square/circle.

1. The number of overlapping cars at a junction is bounded by the number of incoming roads of that junction. In other words, cars do not stack one over the other, since the newly coming vehicles perceive the presence of the overlapping vehicles in front and behave normally, without getting too close to them. Moreover, the mass of overlapping vehicles will tend to zero as $n \to +\infty$.

2. The space interval in which overlap can occur is $(L^{\mathrm{R}} - \ell_n, L^{\mathrm{R}}]$, which shrinks to $\emptyset$ when $n \to +\infty$.

From now one we allow the above described "mild" overlap to happen and we handle it extending the function w defined in (4.34) by means of a new function w^* defined as follows:

$$w^* : [0, +\infty) \to [0, v_{\max}], \qquad \begin{cases} w^*(\delta) = w(\delta), & \text{if } \delta \geq \ell_n, \\ w^*(\delta) = 0, & \text{if } \delta \leq \ell_n, \end{cases} \tag{4.40}$$

i.e. we assume that (smashed) vehicles with $\hat{\delta}_i < \ell_n$ stops completely until the vehicle in front leaves a space $> \ell_n$, then they re-start moving normally. If more than one vehicle is found to be *exactly* in the same place, the one with the largest label is taken as vehicle "in front" and the others "behind".

We are now ready to introduce the follow-the-leader model on networks. For any $i = 1, \ldots, n$ we write

$$\begin{cases} \dot{y}_i(t) = w^*(\hat{\delta}_i(t)), & \text{if } \textsc{next}(i) \neq \emptyset \\ \dot{y}_i(t) = v_{\max}, & \text{if } \textsc{next}(i) = \emptyset. \end{cases} \tag{4.41}$$

In addition, when $y_i(t) = L^{\mathrm{R}(i,t)}$, the road $\mathrm{R}(i,t)$ must be updated according to the i-th vehicle's path and $y_i(t)$ must be reset to 0 (similarly to a new initial condition).

Remark 4.4.1. *The extension of the follow-the-leader model described above defines implicitly a certain behavior of vehicles at junctions. Since vehicles cannot overtake each other and never stop or slow down at junctions, they basically adopt a FIFO behavior (see [67, Appendix B] for a general discussion in the context of traffic flow). Consider for example the case of a diverge (see Fig. 4.8) and assume that one of the two outgoing roads is fully congested. If the first car on the incoming road wants to go to the congested road, it will stop. After that, all the following cars will stop too, even if they want to turn to the other outgoing road. We will see that the FIFO behavior will be kept in the macroscopic limit.*

4.4.2 The model reformulated

In order to pass to the limit for $n \to +\infty$, it is convenient to reformulate the model introduced in the previous section. Let us consider all the possible paths joining all the origin nodes $\mathcal{O}$ with all the destination nodes $\mathcal{D}$, see Fig. 4.6. Each path is considered as a *single uninterrupted road*, with no junctions. Let us denote by P the total number

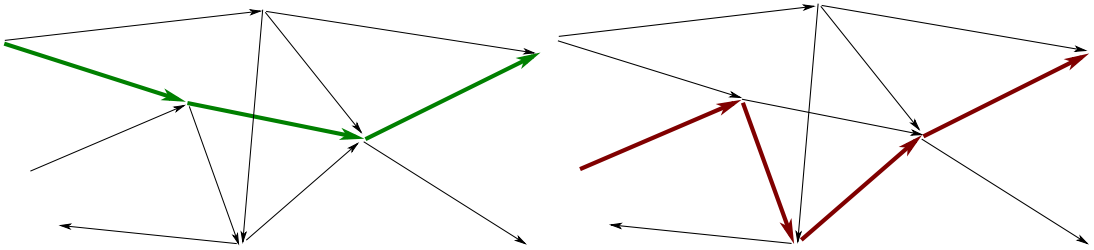

FIGURE 4.6: A generic network. Two possible paths are highlighted. N n arc of the network.

of paths and let us divide the n vehicles in P populations, on the basis of the path they are following.

Let us denote by n_p, $p = 1, \dots, P$, the number of vehicles following the path p and label *univocally* the vehicles by the multi-index (i, p), $i = 1, \dots, n_p$, $p = 1, \dots, P$. Let us also denote by $y_i^p(t)$ the position of the vehicle i of population p at time t, defined as the distance from the origin of the path p (not from the origin of the current road).

Most important, we redefine the concept of distance between two vehicles. First, we define $\text{NEXT}((i,p),q)$ as the nearest vehicle belonging to population q in front of the vehicle (i,p) along the path p (setting it to $\emptyset$ if there is no such a vehicle). Then, we

define the p-distance between a (nonleader) vehicle and the vehicle in front as

$$\delta_i^p(t) := y^p_{\text{NEXT}((i,p),p)}(t) - y_i^p(t).$$

This corresponds to consider only vehicles of population p, neglecting the presence of the others. We also keep considering the distance between two contiguous vehicles regardless the population they belong to, defining, for any nonleader vehicle,

$$\Delta_i^p(t) := y^\bullet_{\text{NEXT}((i,p),\bullet)}(t) - y_i^p(t),$$

where $\text{NEXT}((i,p),\bullet)$ is the vehicle in front of the vehicle (i,p), no matter the population it belongs to and $y^\bullet_{\text{NEXT}((i,p),\bullet)}$ is its position. These two last quantities are defined only if the vehicle (i,p) is not the first on path p, otherwise we set $\text{NEXT}((i,p),\bullet) = \emptyset$.

In the new formulation the model reads, for any $p = 1,\dots,P$ and $i = 1,\dots,n_p$,

$$\begin{cases} \dot{y}_i^p(t) = w^*(\Delta_i^p(t)), & \text{if } \text{NEXT}((i,p),\bullet) \neq \emptyset \\ \dot{y}_i^p(t) = v_{\max}, & \text{if } \text{NEXT}((i,p),\bullet) = \emptyset, \end{cases} \tag{4.42}$$

which is completely equivalent to system (4.41).

It is important to note that the right-hand side of the ODEs (4.42) is in general discontinuous, since cars following paths q's, $q \neq p$, can appear or disappear, thus increasing or reducing abruptly the distance Δ_i^p (or even changing the leader/follower status of car i). To address this issue we will consider the integral form of (4.42) and we assume that there exists a solution in the sense of Carathéodory.traffic

4.5 Micro-to-macro limit

To begin with, we note that condition (4.34) clarifies the relationship between the average density and the distance between vehicles which is valid in the limit $n \to +\infty$ (see Theorem 4.3.1). It states that

$$\rho(t,\cdot) \longleftrightarrow \frac{\ell_n}{\delta(t)}. \tag{4.43}$$

In section 4.4.2 we have introduced p-distances which must be now related to the right average densities. To do that, let us use again the operators E_n and C_n introduced in

section 4.3.1, modifying in a obvious manner the sets R (considering the mass M^p of cars belonging to population p) and Y_n to deal with the new framework. Define, for any p,

$$\mathbf{y}^p := (y_1^p, \dots, y_{n_p}^p), \qquad \mu_n^p(t,\cdot) := C_n[\mathbf{y}^p(t); \delta^p] = \sum_{\substack{\text{followers} \\ \text{of pop. } p}} \frac{\ell_n}{\delta_i^p} \chi_{[y_i^p, y^p_{\text{NEXT}((i,p),p)})}$$

and

$$\mathbf{y} := (\mathbf{y}^1, \dots, \mathbf{y}^P), \qquad \omega_n^p(t,\cdot) := C_n[\mathbf{y}^p(t), \mathbf{y}(t); \Delta^p] = \sum_{\substack{\text{followers} \\ \text{on path } p}} \frac{\ell_n}{\Delta_i^p} \chi_{[y_i^p, y^\bullet_{\text{NEXT}((i,p),\bullet)})}.$$

Both functions $\mu_n^p(t,\cdot)$ and $\omega_n^p(t,\cdot)$ are defined on the whole path p. The functions μ_n^p's correspond to the densities of vehicles following path p, while the function ω_n^p represents the total density along path p, and depends on the positions of all vehicles following path p plus all vehicles following a path q which shares some roads with path p.

Defining the limits (if they exist)

$$\mu^p(t,x) := \lim_{n\to+\infty} \mu_n^p(t,x), \qquad \omega^p(t,x) := \lim_{n\to+\infty} \omega_n^p(t,x),$$

we get, in analogy to (4.43),

$$\mu^p(t,\cdot) \longleftrightarrow \frac{\ell_n}{\delta^p(t)}, \qquad \omega^p(t,\cdot) \longleftrightarrow \frac{\ell_n}{\Delta^p(t)}. \tag{4.44}$$

In order to introduce the macroscopic model we will also need the correspondence between the microscopic and the macroscopic velocity. To this end, we define the function v^* such that

$$v^* : [0,+\infty) \to [0, v_{\max}], \qquad \begin{cases} v^*(r) = v(r), & \text{if } r \le 1, \\ v^*(r) = 0, & \text{if } r \ge 1. \end{cases} \tag{4.45}$$

It is easy to see that the relation in (4.34) still holds, more precisely

$$w^*(\delta) = v^*\left(\frac{\ell_n}{\delta}\right).$$

At this point it is crucial to note that a path, by definition, has no junctions and therefore is indistinguishable from a single road. As a consequence, we can follow in broad terms

the results already proved in [30, 97] for the micro-to-macro limit on a single road.

Using (4.44), and reasoning by analogy with the 1D case, we claim that, for any fixed $p = 1, \dots, P$, the macroscopic equation associated to the model (4.42) is

$$\mu^p_t + \left(\mu^p v^*(\omega^p)\right)_x = 0, \qquad t > 0, \quad x \in \mathbb{R}. \tag{4.46}$$

Note that in equation (4.46) both densities μ^p and ω^p appear. This is due to the fact that equation (4.42) describes the evolution of the population p only, but the velocity is evaluated considering the distance Δ^p, which is indeed related to the *total* density on the path.

To prove the correspondence, let us fictitiously extend each path to $(-\infty, +\infty)$, setting the density to 0 before the first and after the last vehicle. In this way we simplify the problem getting rid of the boundary conditions. Let us denote by $T > 0$ the final time for the simulation and consider a test function $\phi \in C_0^\infty((-\infty, T] \times \mathbb{R}; \mathbb{R})$.

Before entering the proof of the main result, we need to simplify the notations. Fix $p \in \{1, \dots, P\}$ and denote by $i \in \{1, \dots, n_p - 1\}$ the index of a generic (follower) car belonging to the p-th population. Denote the index of the first car ahead of the i-th one, belonging to population p, simply by $i + 1$. Denote by k the index of a generic car belonging to any population, including the p-the one. Denote the index of the car in front of the k-th car by $k + 1$. Finally, denote by k_i the index of the generic car belonging to any population between car i (included) and car $i + 1$ (excluded), see Fig. 4.7(top); and by i_k the index of the first car belonging to population p on the left of the car k ($i_k = k$ if the k-th car belongs to population p), see Fig. 4.7(bottom). Assume for simplicity that the leftmost car belongs to population p so that i_k is well defined.

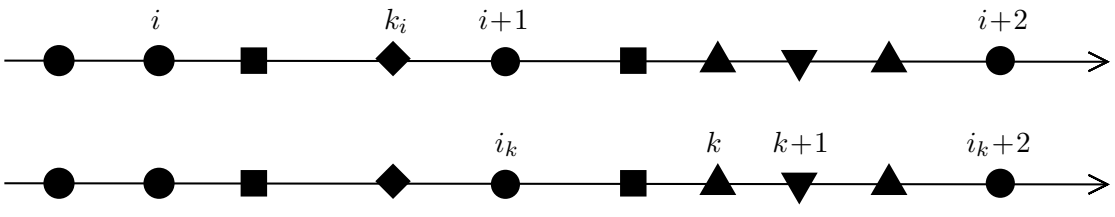

FIGURE 4.7: Path p, definition of k_i (top) and definition of i_k (bottom).

In the following, we drop the superscript p from any symbol. Denote the initial density for the vehicles of population p by $\bar{\mu} = \mu(0,\cdot)$, and define the corresponding initial positions of cars $(\bar{y}_1, \dots, \bar{y}_{n_p}) = E_n[\bar{\mu}]$.

We are now ready to prove the correspondence between the microscopic follow-the-leader model (4.42) and the macroscopic model (4.46) for any fixed $p \in \{1, \dots, P\}$ (we do not consider here the fully coupled problem). As usual [21, Formula (4.5)], we consider the weak (integral) form of the equation (4.46) and we compute

$$I_n := \int_0^T \int_{\mathbb{R}} \big(\mu_n \varphi_t + \mu_n v^*(\omega_n)\varphi_x\big) dx dt + \int_{\mathbb{R}} \bar{\mu}(x)\varphi(0,x)dx = \\ \int_0^T \int_{\mathbb{R}} \mu_n \Big(\varphi_t + v^*(\omega_n)\varphi_x\Big) dx dt + \int_{\mathbb{R}} \bar{\mu}_n(0,x)\varphi(0,x)dx + \int_{\mathbb{R}} \big(\bar{\mu}(x) - \mu_n(0,x)\big)\varphi(0,x)dx.$$

By definitions, the densities μ_n and ω_n are constant in the interval $[y_k(t), y_{k+1}(t)]$ for any t. Therefore we have

$$I_n = \sum_k \int_0^T \frac{\ell_n}{\delta_{i_k}(t)} \int_{y_k(t)}^{y_{k+1}(t)} \left(\varphi_t + \underbrace{v^*\left(\frac{\ell_n}{\Delta_k(t)}\right)}_{=\dot{y}_k(t)} \varphi_x\right) dx dt + \sum_i \frac{\ell_n}{\bar{\delta}_i} \int_{\bar{y}_i}^{\bar{y}_{i+1}} \varphi(0,x)dx + \\ \int_{\mathbb{R}} \big(\bar{\mu}(x) - \mu_n(0,x)\big)\varphi(0,x)dx.$$

Now we note that, for $x \in [y_k(t), y_{k+1}(t)]$,

$$|\varphi_t(t,x) + \dot{y}_k(t)\varphi_x(t,x) - \dot{\varphi}(t, y_k(t))| = \\ |\varphi_t(t,x) + \dot{y}_k(t)\varphi_x(t,x) - \varphi_t(t, y_k(t)) - \dot{y}_k(t)\varphi_x(t, y_k(t))| \le \\ (1 + v_{\max} C_\varphi)|y_{k+1}(t) - y_k(t)|$$

where the quantity $C_\varphi := \|\varphi\|_{C^2}$ uniformly bounds from above the modulus of φ and all its derivatives up to second order. Equivalently, we can write

$$\varphi_t(t,x) + \dot{y}_k(t)\varphi_x(t,x) = \dot{\varphi}(t, y_k(t))) + \mathcal{O}(1)(y_{k+1}(t) - y_k(t)).$$

Using the latter estimate in the expression for I_n above and defining

$$A := \sum_i \frac{\ell_n}{\bar{\delta}_i} \int_{\bar{y}_i}^{\bar{y}_{i+1}} \varphi(0,x)dx, \qquad B := \int_{\mathbb{R}} \big(\bar{\mu}(x) - \mu_n(0,x)\big)\varphi(0,x)dx,$$

we get

$$I_n = \sum_k \int_0^T \frac{\ell_n}{\delta_{i_k}(t)} \int_{y_k(t)}^{y_{k+1}(t)} \dot\varphi(t, y_k(t)))dxdt+ \sum_k \int_0^T \frac{\ell_n}{\delta_{i_k}(t)} \int_{y_k(t)}^{y_{k+1}(t)} \mathcal{O}(1)(y_{k+1}(t) - y_k(t))dxdt + A + B$$

$$=\ell_n \sum_k \int_0^T \dot\varphi(t, y_k(t)) \frac{\Delta_k(t)}{\delta_{i_k}(t)} dt + \mathcal{O}(1)\ell_n \sum_k \int_0^T \underbrace{\frac{\Delta_k(t)}{\delta_{i_k}(t)}}_{\leq 1} \Delta_k(t)dt + A + B$$

$$=\ell_n \sum_i \sum_{k_i} \int_0^T \dot\varphi(t, y_{k_i}(t)) \frac{\Delta_{k_i}(t)}{\delta_i(t)} dt + \mathcal{O}(1)\ell_n \sum_k \int_0^T \Delta_k(t)dt + A + B$$

$$= \ell_n \sum_i \sum_{k_i} \int_0^T \Big(\dot\varphi(t, y_i(t)) + \mathcal{O}(1)(y_{i+1}(t) - y_i(t))\Big) \frac{\Delta_{k_i}(t)}{\delta_i(t)} dt+ \mathcal{O}(1)\ell_n \sum_i \sum_{k_i} \int_0^T \Delta_{k_i}(t)dt + A + B$$

$$= \ell_n \sum_i \int_0^T \Big(\dot\varphi(t, y_i(t)) + \mathcal{O}(1)(y_{i+1}(t) - y_i(t))\Big) \underbrace{\sum_{k_i} \frac{\Delta_{k_i}(t)}{\delta_i(t)}}_{=1} dt+ \mathcal{O}(1)\ell_n \sum_i \int_0^T \sum_{k_i} \Delta_{k_i}(t)dt + A + B$$

$$=\ell_n \sum_i \int_0^T \dot\varphi(t, y_i(t))dt + \mathcal{O}(1)\ell_n \sum_i \int_0^T \delta_i(t)dt + \mathcal{O}(1)\ell_n \sum_i \int_0^T \delta_i(t)dt + A + B$$

$$=\ell_n \sum_i \int_0^T \dot\varphi(t, y_i(t))dt + \mathcal{O}(1)\ell_n \sum_i \int_0^T \delta_i(t)dt + A + B.$$

At this point we got rid of the populations q's, $q \neq p$, and thus we are back to the case of a single road with a single population of vehicles. By the way, we have also resolved the discontinuity issues around the junctions. Therefore, the proof is completed exactly as in [30]:

$$I_n = -\ell_n \sum_i \varphi(0, \bar y_i) + \mathcal{O}(1)\ell_n \int_0^T (y_{n_p}(t) - y_1(t))dt + A + B$$

$$= -\sum_i \frac{\ell_n}{\bar\delta_i}\int_{\bar y_i}^{\bar y_{i+1}} \varphi(0,\bar y_i)dx + \mathcal{O}(1)\ell_n\int_0^T (y_{n_p}(t)-y_1(t))dt+$$

$$= \sum_i \frac{\ell_n}{\bar\delta_i}\int_{\bar y_i}^{\bar y_{i+1}} \varphi(0,x)dx + B$$

$$\sum_i \frac{\ell_n}{\bar\delta_i}\int_{\bar y_i}^{\bar y_{i+1}} \Big(\varphi(0,x)-\varphi(0,\bar y_i)\Big)dx + \mathcal{O}(1)\ell_n\int_0^T (y_{n_p}(t)-y_1(t))dt + B.$$

To proceed further, let us define $\Lambda := \bar y_{n_p+1} - \bar y_1$. We have

$$I_n = \sum_i \frac{\ell_n}{\bar\delta_i}\mathcal{O}(1)\int_{\bar y_i}^{\bar y_{i+1}} \bar\delta_i dx + \mathcal{O}(1)\ell_n(\Lambda + v_{\max}T)T+$$

$$\int_{\mathbb{R}} \big(\bar\mu(x)-\mu_n(0,x)\big)\varphi(0,x)dx$$

$$= \mathcal{O}(1)\ell_n\Lambda + \mathcal{O}(1)\ell_n(\Lambda+v_{\max}T)T + \int_{\mathbb{R}} \big(\bar\mu(x)-\mu_n(0,x)\big)\varphi(0,x)dx.$$

Since $\mu_n(0,\cdot)\to\bar\mu$ (see [30]) and $\ell_n\to 0$, all the terms in the latter quantity vanish as $n\to+\infty$. In conclusion, we have proved the following

Theorem 4.5.1. *Let (4.34) and (4.35) hold, and consider the extensions (4.40) and (4.45). Fix $T>0$, $p\in\{1,\dots,P\}$, and choose $\bar\mu^p = \mu^p(0,\cdot)\in R^p \cap BV(\mathbb{R};[0,1])$ and $\bar{\mathbf{y}}^p = E_n[\bar\mu^p]$. Let $\mathbf{y}^p(\cdot)$ be the solution of (4.42) with initial condition $\bar{\mathbf{y}}^p$ (assuming the other solutions $\mathbf{y}^q(\cdot)$, $q\neq p$ are given). Define $\mu_n^p(t,\cdot) = C_n[\mathbf{y}^p]$. If there exists $\mu^p\in L^\infty([0,T];R)$ such that $\lim_{n\to+\infty}\mu_n^p(t,x) = \mu^p(t,x)$ a.e., then μ^p is a weak solution to (4.46) (assuming the other solutions μ^q, $q\neq p$ are given) with initial condition $\bar\mu^p$.*

Now we note that the system of PDEs (4.46) is nothing else that the multi-path model studied in [22, 23].

$$\mu_t^p + (\mu^p v(\omega^p))_x = 0, \qquad p=1,\dots,P, \quad t>0, \quad x\in \text{path } p \tag{4.47}$$

where $\omega^p(t,x)$ is the sum of all densities $\mu^q(t,x)$, $q=1,\dots,P$, living at time t at the point x along path p. It is a system of P conservation laws with discontinuous flux which provides an alternative method to deal with traffic flow on networks. It consists in a system of conservation laws with discontinuous flux which provides an alternative method to deal with traffic flow on networks. It is characterized by the fact that junctions are embedded in the equations themselves, so that the dynamics at junctions have not to be resolved separately by *ad hoc* procedures, like, e.g., the maximization of the flux. It appears that the model maximizes the flux but under the additional constraints of

equidistribution of the fluxes from the incoming roads (i.e. the incoming roads have assigned the same priority).

4.6 Numerical approximation

In this section we give some details about the discretization of the micro- and macroscopic equations.

4.6.1 The follow-the-leader model

For numerical purposes, it is convenient to discretize the follow-the-leader model as it is described in section 4.4.1, rather than its equivalent formulation on paths.

First we set $v_{\max} = 1$ and

$$v(\rho) = 1 - \rho, \qquad w(\delta) = 1 - \frac{\ell_n}{\delta}. \tag{4.48}$$

Then, we introduce a time step $\Delta t > 0$ and we denote by $\widetilde{y}_i^s$, $s = 1, 2, \dots$ the approximate position of the vehicle i at time $t_s = s\Delta t$. The discretization is obtained by a classical explicit Euler scheme of the form

$$\widetilde{y}_i^{s+1} = \widetilde{y}_i^s + \Delta t \; w^*(\hat{\delta}_i(t_s)), \qquad s = 0, 1, 2, \dots \tag{4.49}$$

with admissible initial conditions $y_i^0 = \bar{y}_i$.

When a vehicle goes beyond the junction, let say $\widetilde{y}_i(t_s) = L^{\mathrm{R}(i,t_s)} + \epsilon$, it is assigned to the next road on the basis of its preference, and its position is updated as $\widetilde{y}_i(t_s) = \epsilon$.

At the discrete level, a CFL-like condition is needed to ensure that vehicles do not bump into the one in front, i.e. to guarantee that $\delta_i > \ell_n$. Far from the junction, this condition is given by

$$\Delta t \; w(\delta_i) < \delta_i \qquad \forall i. \tag{4.50}$$

Substituting (4.48) in (4.50) we get

$$\Delta t = \Delta t(n) < \min_i \frac{\delta_i^2}{\delta_i - \ell_n}. \tag{4.51}$$

Unfortunately, this condition does not prevent vehicle overlapping near the junction, as already discussed in section 4.4.1. In a discrete setting, the overlapping can happen also *after* the junction, more precisely in the space interval

$$(L^{\mathrm{R}_1} - \ell_n, L^{\mathrm{R}_1}] \cup [L^{\mathrm{R}_2}, \Delta t\ v_{\max}],$$

where R_1 and R_2 are two consecutive roads and $\Delta t\ v_{\max}$ is the maximal distance one vehicle can travel in one time step. It can be seen that in the discrete setting the overlapping zone shrinks to $\emptyset$ for $n \to +\infty$ and $\Delta t \to 0$, and not only for $n \to +\infty$. However, the overlapping is still "mild", in the sense that the number of bumped vehicles is bounded by the number of incoming roads, see section 4.4.1.

Remark 4.6.1. *The multi-path model, at least at the discrete level, does not allow the total density to be larger than 1 [23, Sect. 3.2]. This seems in contradiction with the possibility of overlapping in the microscopic model. Actually this is not, because the overlapping is "mild", i.e. it concerns at most a finite number of cars, and then it is invisible at macroscopic level. However, a counterpart of the overlapping features at macroscopic level exists: the cells after the junctions act as a sort of* buffer *[23, Sect. 5.2], which is able to gather a flux of vehicles larger than maximal one, i.e.* $\max_\rho f(\rho)$*, with* $f(\rho) := \rho v(\rho)$*. The actual maximal flux is instead* $N_{\mathrm{inc}} \max_\rho f(\rho)$*, where* N_{inc} *is the number of incoming roads.*

4.7 Numerical tests

In this section we confirm the theoretical findings of the previous sections by means of some numerical tests. We consider the case of a simple network with 1 junction and (i) a merge, (ii) a diverge, and (iii) 2 incoming roads and 2 outgoing roads, see Fig. 4.8. In the cases (ii) and (iii), additional parameters are needed to describe the behavior of the vehicles at the junction. They are usually referred to as *distribution coefficients* and specify the percentage of vehicles which wish to turn to the left and to the right.

Since we are considering here simple networks with only 1 junction, specifying for each car the turning conduct at junction is equivalent to define a path on the network. In the case of more complex networks with more than 1 junction, we should instead assign the whole sequence of decisions each car makes at junctions. If we stick with per-junction

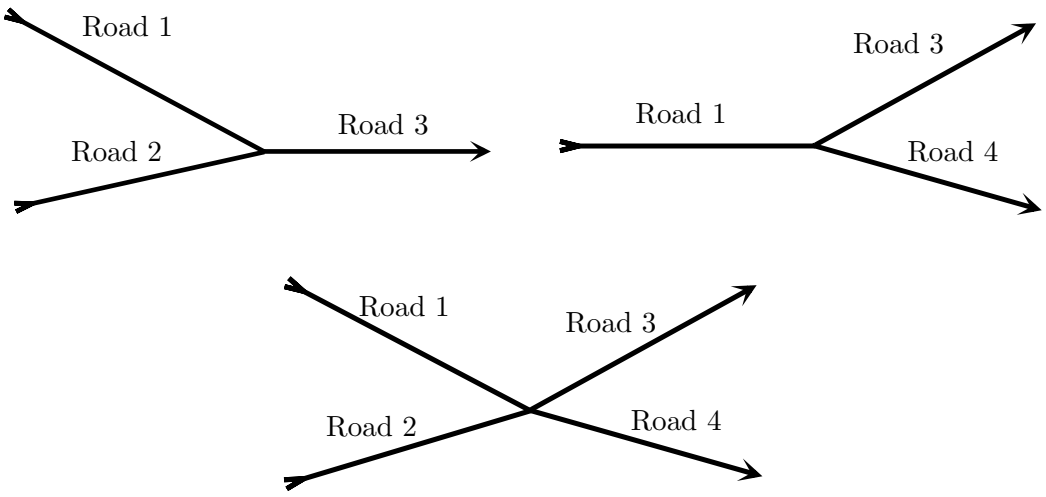

FIGURE 4.8: A merge (top, left), a diverge (top, right), and a junction with 2 incoming and 2 outgoing roads (bottom).

coefficients, thus losing the global behavior of drivers, we expect convergence, in the limit, to the hybrid version of the multi-path model described in [23, Remark 1].

Let us denote the distribution coefficients by $\mathcal{P}_{a\to b}$, where a is the index of the incoming road and b is the index of the outgoing road. Clearly it is required that

$$\sum_b \mathcal{P}_{a\to b} = 1 \qquad \forall a.$$

In the follow-the-leader model, each vehicle traveling along road a is assigned to the road b with probability $\mathcal{P}_{a\to b}$. In the multi-path model, these coefficients are used to define properly the partial densities μ^p's at the initial time given the initial condition for the total density.

To improve readability and ease the comparison, we show the total density ω^p brought back on the roads, rather than on the paths (where they are originally defined). We assume that all roads have the same length $L^{\mathrm{R}} = 4 \times 10^3$, and we divide them in $N_x^{\mathrm{R}} = 100$ space nodes. We employ Dirichlet-0 boundary conditions at the beginning of the incoming roads and the end of the outgoing roads.

Comparison with the solution of the multi-path scheme is obtained by computing the average density of the microscopic vehicles, defined for each space node k and time step

s as

$$\Psi_k^s[\widetilde{\mathbf{y}}^s] := \frac{1}{\Delta x} \sum_{\{i \,:\, \widetilde{y}_i^s \in [x_k, x_{k+1})\}} \ell_n, \tag{4.52}$$

which corresponds to sum the total mass found in each space cell and divide it by the length of the cell. This average density seems to be more stable than $C_n[\mathbf{y}]$ as defined in (4.38), especially around junctions and when n is very large.

4.7.1 Merge

In this section we consider a network with three arcs and one junction, with two incoming roads and one outgoing road. We denote by ρ^1, ρ^2 and ρ^3 the density on the first incoming road, the second incoming road and the outgoing road, respectively (Fig. 4.8). Initial conditions are

$$\rho^1(0,x) = 0.5, \qquad \rho^2(0,x) = 0.3, \qquad \rho^3(0,x) = 0 \qquad \forall x.$$

We run the simulation until the final time $T_f = 3 \times 10^3$. Fig. 4.9 shows the density computed by the multi-path model and the follow-the-leader model for two different choices of ℓ_n and Δt. Since we compare two numerically approximate densities, we

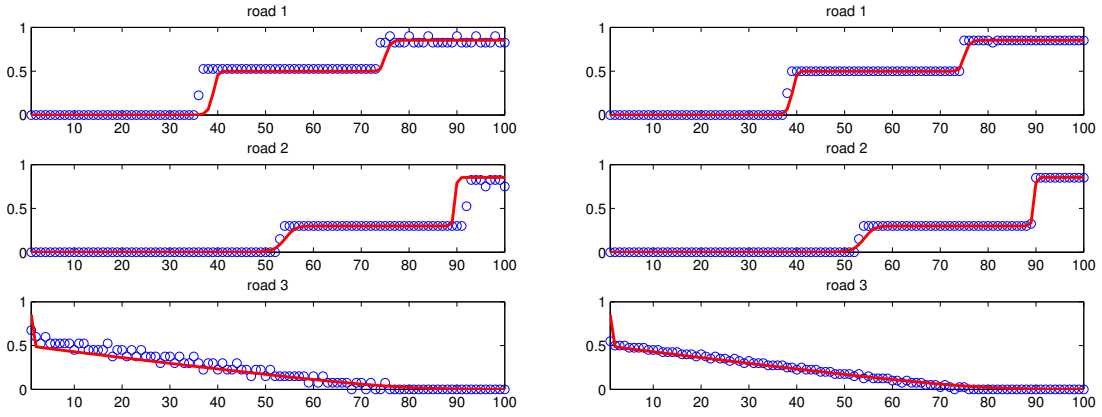

FIGURE 4.9: Merge, results of the simulation at final time. Total density ω^p redefined on roads (red line) and density of microscopic vehicles Ψ (blu circles). Left: $\ell_n = 3$ (max number of cars per cell $= 13.\bar{3}$), $\Delta t = 3$. Right: $\ell_n = 1$ (max number of cars per cell $= 40$), $\Delta t = 0.2$.

expect a perfect match only for $n \to +\infty$ and $\Delta t, \Delta x \to 0$. That said, numerical evidence confirms the convergence results, and also shows that the microscopic scheme

is not diffusive as instead it is the macroscopic scheme. This is perfectly visible across the discontinuities.

4.7.2 Diverge

In this section we consider a network with three arcs and one junction, with two incoming roads and one outgoing road. We denote by ρ^1, ρ^3 and ρ^4 the density on the incoming road, the first outgoing road and the second outgoing road, respectively (Fig. 4.8). Initial conditions are

$$\rho^1(0,x) = 0.5, \qquad \rho^3(0,x) = 0, \qquad \rho^4(0,x) = 0 \qquad \forall x,$$

and distribution coefficients are

$$\mathcal{P}_{1\to 3} = 0.8, \qquad \mathcal{P}_{1\to 4} = 0.2.$$

We run the simulation until the final time $T_f = 3\times 10^3$. Fig. 4.10 shows the density computed by the multi-path model and the follow-the-leader model for two different choices of ℓ_n and Δt. Again, numerical evidence confirms the convergence results, however, the

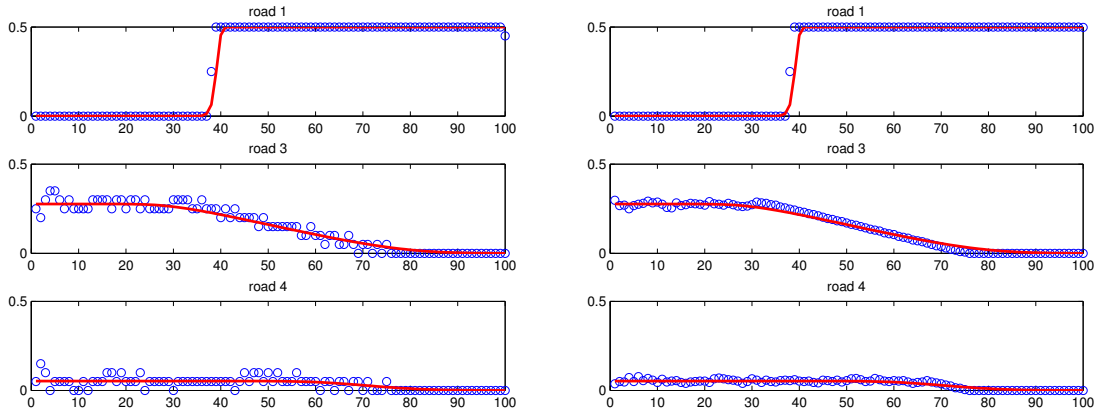

FIGURE 4.10: Diverge, results of the simulation at final time. Total density ω^p redefined on roads (red line) and density of microscopic vehicles Ψ (blu circles). Left: $\ell_n = 2$ (max number of cars per cell = 20), $\Delta t = 4$. Right: $\ell_n = 0.1$ (max number of cars per cell = 400), $\Delta t = 0.25$.

convergence is much slower than the previous case. This is probably due to the presence of the distribution coefficients $\mathcal{P}$ which introduce stochasticity in the system.

4.7.3 Junction with two incoming and two outgoing roads

In this section we consider a network with four arcs and one junction, with two incoming roads and two outgoing roads. We denote by ρ^1, ρ^2, ρ^3 and ρ^4 the density on the first incoming road, the second incoming road, the first outgoing road, and the second outgoing road, respectively (Fig. 4.8). Initial conditions are

$$\rho^1(0,x) = 0.4, \qquad \rho^2(0,x) = 0.5, \qquad \rho^3(0,x) = 0, \qquad \rho^3(0,x) = 0 \qquad \forall x,$$

and distribution coefficients are

$$\mathcal{P}_{1\to3} = 0.7, \qquad \mathcal{P}_{1\to4} = 0.3, \qquad \mathcal{P}_{2\to3} = 0.6, \qquad \mathcal{P}_{2\to4} = 0.4.$$

We run the simulation until the final time $T_f = 4 \times 10^3$. Fig. 4.11 shows the density computed by the multi-path model and the follow-the-leader model. Again, numerical

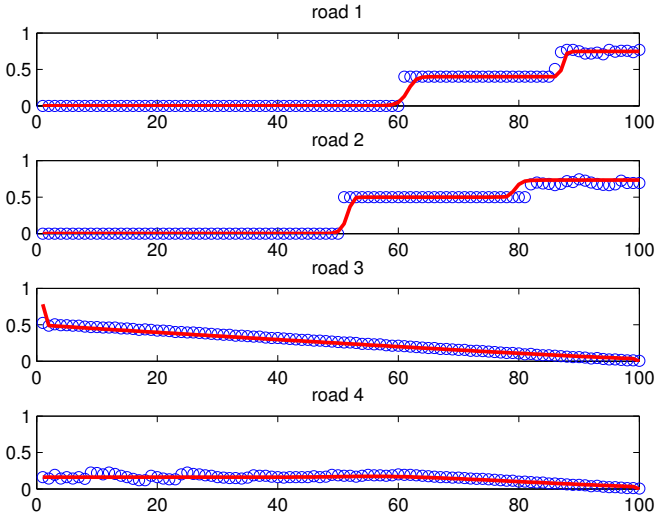

FIGURE 4.11: Diverge, results of the simulation at final time. Total density ω^p redefined on roads (red line) and density of microscopic vehicles Ψ (blu circles). $\ell_n = 0.25$ (max number of cars per cell = 160), $\Delta t = 0.1$.

evidence confirms the convergence results, however, the convergence is even slower than the previous case.

Appendix A

An essentially non-oscillatory (ENO) scheme of second order

We recall here a simple ENO method of order two based on the work of Osher and Shu [71] for Hamilton Jacobi equation (the ENO method was designed by Harten et al. [65] for the approximation solution of non-linear conservation law). Let m be the minmod function defined by

$$m(a,b) = \begin{cases} a & \text{if } |a| \leq |b|,\ ab > 0 \\ b & \text{if } |b| < |b|,\ ab > 0 \\ 0 & \text{if } ab \leq 0 \end{cases} \tag{A.1}$$

(other functions can be considered such as $m(a,b) = a$ if $|a| \leq |b|$ and $m(a,b) = b$ otherwise). Let $D^{\pm}u_j = \pm(u_{j\pm1} - u_j)/\Delta x$ and

$$D^2 u_j := \frac{u_{j+1} - 2u_j + u_{j-1}}{\Delta x^2}.$$

Then the right and left ENO approximation of the derivative can be defined by

$$\bar{D}^{\pm}u_j = D^{\pm}u_j \mp \frac{1}{2}\Delta x\ m(D^2 u_j, D^2 u_{j\pm1})$$

and the ENO (Euler forward) scheme by

$$S_0(u)_j := u_j - \tau h^M(x_j,\ \bar{D}^- u_j,\ \bar{D}^+ u_j).$$

The corresponding RK2 scheme can then be defined by $S(u) = \frac{1}{2}(u + S_0(S_0(u)))$.

Appendix B

Overview of results of Hamilton-Jacobi equations

Appendix B: *O*verview of results of Hamilton-Jacobi equations

Here we recall some basic definitions and theoretical results about HJ equations. We first introduce the notion of viscosity solution of the HJ equation

$$H(x, v(x), \nabla v(x)) = 0 \quad x \in \Omega, \tag{B.1}$$

where Ω is an open domain of $\mathbb{R}^d$ and Hamiltonain $H = H(x, r, p)$ is a continuous real valued function on $\Omega \times \mathbb{R} \times \mathbb{R}^d$. This notion allows us to obtain important existence and uniqueness results for some equations of the form (B.1). It is well known that HJ equation is in general not well-posed. It is possible to show several examples in which any classical (that is of class C^1) solution exists or infinite weak (that is a.e. differentiable) solutions exist.

Definition 11. *A continuous function v is a viscosity solution of the equation (B.1) if the following conditions are satisfied:*

(*i*) *Viscosiy subsolution test i.e. for any test function $\phi \in C^1(\Omega)$, if $x_0 \in \Omega$ is a local maximum point for $v - \phi$, then*

$$H(x_0, v(x_0), \nabla\phi(x_0)) \leq 0$$

((*ii*) *viscosiy supersolution test for any test function* $\phi \in C^1(\Omega)$*, if* $x_0 \in \Omega$ *is a local minima point for* $v - \phi$*, then*

$$H(x_0, v(x_0), \nabla\phi(x_0)) \geq 0$$

The importance of "viscosity solutions" is that it can recovered as the limit function $v = \lim_{\epsilon \to 0+} v^\epsilon$ where $v^\epsilon \in C^2(\Omega)$ is the classical solution of the regularized problem

$$-\epsilon\Delta v^\epsilon + H(x, \nabla v^\epsilon) = 0, \quad x \times \Omega \tag{B.2}$$

in the case v^ϵ exists and converges locally uniformly to some continuous function v. This method is named vanishing viscosity, and it is the original idea behind this notion of solution. It was presented by Crandall and Lions [34]. Our main focus is on time dependent first order Hamilton-Jacobi equation

$$\begin{cases} \partial_t v + H(x, \nabla v) = 0, \quad (t, x) \in [0, T] \times \Omega \\ v(0, x) = v_0(x), \quad x \in \Omega. \end{cases} \tag{B.3}$$

where Ω is an open domain of $\mathbb{R}^d$ and the Hamiltonian H is continuous and real valued function on $\Omega \times \mathbb{R} \times \mathbb{R}^d$. For details we refer the books [6, 9].

Definition 12. $v \in BUC(\Omega \times T)$ *is a viscosity solution in* $\Omega \times (0, T)$ *of the equation* (B.3) *if and only if, for any* $\phi \in C^1(\Omega \times (0, T))$*, the following conditions holds:*

(*i*) *at every point* $(t_0, x_0) \in \Omega \times (0, T)$*, local maximum of* $v - \phi$*,*

$$\phi_t(t_0, x_0) + H(x_0, t_0, v(x_0, t_0), D\phi(t_0, x_0)) \leq 0 \tag{B.4}$$

(i.e. v is a viscosity subsolution.)

(*ii*) *at every point* $(t_0, x_0) \in \Omega \times (0, T)$*, local minimum of* $v - \phi$*,*

$$\phi_t(t_0, x_0) + H(x_0, t_0, v(x_0, t_0), D\phi(t_0, x_0)) \geq 0 \tag{B.5}$$

(i.e. v is a viscosity supersolution.)

In the following we present some comparison results between viscosity sub- and super solution which gives the uniqueness for the particular case $H(x,t,v,Dv) = H(t,Dv)$.

Theorem B.0.1. *Assume $H \in C((0,T)\times\mathbb{R}^d)$. Let $v_1, v_2 \in (0,T)\times\mathbb{R}^d$ be, respectively viscosity sub- and supersolution in $(0,T)\times\mathbb{R}^d$ of the equation*

$$\partial_t v + H(x, Dv) = 0. \tag{B.6}$$

Then,

$$\sup_{([0,T]\times\mathbb{R}^d))} (v_1 - v_2) \leq \sup_{([0,T]\times\mathbb{R}^d)} (v_1(0,.) - v_2(0,.)). \tag{B.7}$$

Proof. The proof can be found in [6], p. 56. Notice that more general comparison results for more general Hamiltonians can be found in [5]. □

Representation formulae and Legendre transform:

In some cases it is possible to derive representation formula for the viscosity solution. This formula has a great importance from both the analytical and the numerical points of view. Concerning HJ equations, the representation formula is known as Hopf-Lax formula. It is typically related to the problem

$$\partial_t v + H(Dv) = 0, \quad (t,x) \in [0,T]\times\Omega \tag{B.8}$$

$$v(0,x) = v_0(x), \quad x \in \Omega. \tag{B.9}$$

where $H : \mathbb{R}^d \to \mathbb{R}$ is convex and satisfies the coercivity condition:

$$\min_{|p|\to+\infty} \frac{H(p)}{|p|} = +\infty. \tag{B.10}$$

Definition 13. *Let (B.10) satisfied. We define Legendre-Fenchel conjugate (Legendre-Fenchel transform) of H for $q \in R^d$ as:*

$$H^*(q) = \sup_{p\in\mathbb{R}^d} \{p.q - H(p)\}. \tag{B.11}$$

Note that the convexity assumption on H implies that H is continuous, and being also coercive in the sense of (B.10), the sup in (B.11) is in fact a maximum. In general, Legendre-Fenchel transform may not allow for an explicit computation.

Theorem B.0.2. *The function v defined by the following Hopf-Lax formula*

$$v(x,t) = \inf_{y \in R^d} \left[v_0(y) + tH^* \left(\frac{x-y}{t} \right) \right] \tag{B.12}$$

is Lipschitz continuous, differentiable almost everywhere in $(0,+\infty) \times \mathbb{R}^d$ and solves a.e. the initial value problem (B.8).

Proof. The proof can be found in [39], p. 126. □

Theorem B.0.3. *The unique viscosity solution of (B.8) is give by the* Hopf-Lax *representation formula.*

Proof. The proof can be found in [39], p. 561. □

Conclusion and perspectives

In chapter 1 we have seen that proposed "filtered" scheme which behaves as a high order scheme when the solution is smooth and as a first order monotone scheme otherwise. It has a simple presentation that is easy to implement. Rigorous error bounds hold, of the same order as the Crandall-Lions estimates in $\sqrt{\Delta x}$ where Δx is the mesh size. In the case the solution is smooth a high-order consistency error estimate also holds. We show on several numerical examples the capability of the scheme to stabilize an otherwise unstable scheme, and also we observe a precision close to a second order ENO scheme on basic linear and non linear examples. In chapter 2, we used the idea of filtered scheme for the approximation of Hamilton-Jacobi equations in a general convergent setting. We consider in particular a simple coupling between a monotone first order scheme and a second order centered scheme, applied to front propagation problems in 2D and 3D. It could be interesting to use filter scheme on DG discretization. Filtering technique is rather general to be applied to many different situations and problems. Another future development possibility to solve second order HJB equation by filtered schemes.

In chapter 3, We have seen in the above examples coupling of anti-diffusive scheme and semi-Lagrangian scheme is working very well for discontinuous viscosity solutions. Hence when we have some discontinuity or jump then scheme switches to anti-diffusive scheme and in this way the iterative scheme is not diffusive. We presented a coupling between Ultra-bee and Semi-Lagrangian scheme but the coupling idea can be applied to other schemes and can be even simpler when coupling schemes which work on the same grid and the same type of approximate values. As we have seen that the scheme is working well on our 1-dimensional tests problems, so the next step would be to develop the analysis of coupled scheme to HJ equations and to extend the coupling technique to 2D problems.

Finally, in chapter 4 we have investigated the many-particle limit for a quite natural extension of the follow-the-leader model on networks. Numerical tests have shown a slow convergence to the limit solution. This requires a large number of particles (and computational time) to get a reasonable precision comparable with that of the associate macroscopic model. On the other hand, our results justify any multiscale approaches where the micro and the macro scale live together and exchange information. The

convergence result proven in in chapter 4 is only one of the possible micro-to-macro limits which can be investigated in the framework of traffic flow models on networks. Although the proposed follow-the-leader model is likely the most natural extension to networks that one can imagine, other models can be also considered. First of all, one could define the proper follow-the-leader model which corresponds, in the limit, to the LWR model with maximization of flux at junctions. This requires a nontrivial management of the junctions, in which an authority is able to decide who passes the junction and when. At the discrete level, the authority has to choose among all vehicles which reach the junction in one time step.

Second, one can consider analogous techniques for second-order models. In this case the problem is completely open because a second-order multi-path does not yet exist and then it can be difficult to find the right limit model.

Finally, it could be interesting the investigation of the many-particle limit for meso-to-macro models. To this end, useful references could be the papers [46], which deals with kinetic models on networks, and [45] about fundamental diagrams for kinetic equations.

Bibliography

[1] R. Abgrall. Numerical discretization of the first-order hamilton-jacobi equation on triangular meshes. *Communications on Pure and Applied Mathematics*, 49: 1339–1373, 1998.

[2] R. Abgrall. Construction of simple, stable and convergent high order scheme for steady first order Hamilton-Jacobi equation. *SIAM J. Sci. Comput.*, 31:2419–2446, 2009.

[3] A. Aw, A. Klar, M. Materne, and M. Rascle. Derivation of continuum flow traffic models from microscopic follow-the-leader models. *SIAM J. Appl. Math.*, 63:259–278, 2002.

[4] M. Bando, K. Hasebe, A. Nakayama, A. Shibata, and Y. Sugiyama. Dynamic model of traffic congestion and numerical simulation. *Physical Review E*, 51(2): 1035–1042, 1995.

[5] M. Bardi. A boundary value problem for the minimum time function. *SIAM J. Control Optim.*, 27:776–785, 1998.

[6] M. Bardi and I. Capuzzo Dolcetta. *Optimal control and viscosity solutions of Hamilton-Jacobi-Bellman equations. Systems and Control.* Foundations and Applications. Birkhauser, Boston, 1997.

[7] M. Bardi and M. Falcone. An approximation scheme for the minimum time function. *SIAM J. Control Optim.*, 28:950–965, 1990.

[8] M. Bardi and M. Falcone. Discrete approximation of the minimal time function for systems with regular optimal trajectories in A. Bensoussan, J.L. Lions (eds.) Analysis and optimization of systems (antibes). *Lecture Notes in Control and Inform. Sci., vol. 144, Springer*, 144:103–112, 1990.

[9] G. Barles. *Solution de viscositè des èquations de Hamilton-Jacobi.* Mathematiques et applications, Springer, Paris, 1994.

[10] G. Barles and P.E. Souganidis. Convergence of approximation schemes for fully nonlinear second order equations. *Asymptot. Anal.*, 4:271–283, 1991.

[11] N. Bellomo and C. Dogbe. On the modeling of traffic and crowds: A survey of models, speculations, and perspectives. *SIAM Rev.*, 53:409–463, 2011.

[12] S. Benzoni-Gavage and R. M. Colombo. An n-population model for traffic flow. *European J. Appl. Math.*, 14:587–612, 2003.

[13] O. Bokanowski and H. Zidani. Anti-dissipative schemes for advection and application to HJB equations. *J. Scient. Comput.*, 30(1):1–33, 2007.

[14] O. Bokanowski, E. Cristiani, and H. Zidani. An efficient data structure and accurate scheme to solve front propagation problems. *J. Sci. Comput.*, 42 (2):251–273, 2010.

[15] O. Bokanowski, N. Forcadel, and H. Zidani. l^1-error estimates for numerical approximation of Hamilton-Jacobi-Bellman equation in dimension 1,. *Math. Comp.*, 79:1395–1426, 2010.

[16] O. Bokanowski, N. Megdich, and H. Zidani. Convergence of a non-monotone scheme for HJB equations with discontinuous initial data. *Numerische Math.*, 115 (1):1–44, 2010.

[17] O. Bokanowski, Y. Cheng, and C.-W. Shu. A discontinuous galerkin scheme for front propagation with obstacle. *Numer. Math.*, 126(2):1–31, 2013.

[18] O. Bokanowski, J. Garcke, and I. Griebel, M.and Klompmaker. An adaptive sparse grid semi-Lagrangian scheme for first order Hamilton-Jacobi-Bellmanequations. *J. Sci. Comput.*, 55 (3):575–605, 2013.

[19] O. Bokanowski, F. Falcone, and S. Sahu. An efficient filtered scheme for some first order Hamilton-Jacobi-Bellman equations. *Submitted*, 2014.

[20] O. Bokanowski, M. Falcone, R. Ferretti, L. Grüne, D. Kalise, and H. Zidani. Value iteration convergence of ϵ-monotone schemes for stationary Hamilton-Jacobi equations. *Discrete Contin. Dyn, Syst. Se. A*, 35:4041–4070, 2015.

[21] A. Bressan. *Hyperbolic Systems of Conservation Laws. The One-Dimensional Cauchy Problem*. Oxford Lecture Series in Mathematics Vol. 20, Oxford University Press, New York,, 2000.

[22] M. Bretti, G. Briani and E. Cristiani. An easy-to-use algorithm for simulating traffic flow on networks: numerical experiments. *Discrete Contin. Dyn. Syst. S*, 7: 379–394, 2014.

[23] M. Briani and E. Cristiani. An easy-to-use algorithm for simulating traffic flow on networks: Theoretical study. *Netw. Heterog Media.*, 9:519–552, 2014.

[24] G. Cameron, B. Wylie, and D. McArthur. *Moving vehicles on the connection machine*. 1994.

[25] E. Carlini, M. Falcone, and R. Ferretti. An efficient algorithm for Hamilton-Jacobi equations in high dimension. *Comput. Vis. Sci.*, 7(1):15–29, 2004.

[26] E. Carlini, R. Ferretti, and G. Russo. A weighted essentially nonoscillatory, large time-step scheme for Hamilton-Jacobi equations. *SIAM J. Sci. Comput.*, 27(3): 1071–1091, 2005.

[27] P.E. Chandler, R. Herman, and E. Montroll. Traffic dynamics: studies in car following. *Operations Research*, 6(2):165–184, 1958.

[28] B. Cockburn and C.-W. Shu. TVB Runge-Kutta local projection discontinuous Galerkin finite element method for conservation laws iii: One-dimensional systems,. *Journal of Computational Physics*, 84:90–113, 1989.

[29] G. M. Coclite, M. Garavello, and B. Piccoli. Traffic flow on a road networks. *SIAM J. Math. Anal.*, 36:1862–1886, 2005.

[30] R. M. Colombo and E. Rossi. On the micro-macro limit traffic flow. *Rend. Sem. Mat. Uni. Padova*, 131:217–235, 2014.

[31] CORSIM. Corridor simulation (corsim/ tsis). URL http://ops.fhwa.dot.gov/trafficanalysistools/corsim.htm.

[32] G. Costeseque. *Analyse et modelisation du trafic routier: Passage du microscopique au macroscopique*. Master, thesis, Ecole des Ponts Paris-Tech,, 2011.

[33] R. Courant, E. Isaacson, and M. Rees. On the solution of nonlinear hyperbolic differential equations by finite differences. *Comm. Pure Appl. Math.*, 5:243–255, 1952.

[34] M. G. Crandall and P. L. Lions. Two approximations of solutions of Hamilton-Jacobi equations. *Comput. Methods Appl. Mech. Engrg.*, 195:1344–1386, 1984.

[35] M.G. Crandall and P-L. Lions. Viscosity solutions of hamilton-jacobi equations. *Transactions of the American Mathematical Society*, 277(1):1–42, 1983.

[36] R. Herman D. Gazis and R. Rothery. Nonlinear follow-the-leader models of traffic flow. *Oper. Res.*, 9:545–567, 1961.

[37] C. Daganzo. The cell transmission model: a dynamic representation of highway traffic consistent with the hydrodynamic theory. *Transportation Research Part B*, 28(4):269–287, 1994.

[38] B. Desprè and F. Lagoutière. Contact discontinuity capturing schemes for linear advection and compressible gas dynamics. *J. Sci. Comput*, 16:479–524, 1999.

[39] L. C. Evans. *Partial Differential Equations, Graduate Studies in Mathematics.* American Mathematical Society (AIMS), Princeton, 2010.

[40] M. Falcone. *The minimum time problem and its applications to front propagation in A. Visintin e G. Buttazzo (eds), Motion by mean curvature and related topics.* 1994.

[41] M. Falcone and R. Ferretti. Discrete time high-order scheme for viscosity solutions of Hamilton-Jacobi equation. *Numer. Math.*, 67:315–344, 1994.

[42] M. Falcone and R. Ferretti. *Semi-Lagrangian Approximation Schemes for Linear and Hamilton-Jacobi Equations.* SIAM-Society for Industrial and Applied Mathematics, Philadelphia, 2014.

[43] M. Falcone, T. Giorgi, and P. Loreti. Level set of viscosity solutions: some applications to front and rendez-vous problem. *SIAM J. Appl. Math.*, 54(5):1335–1354, 1994.

[44] M. Fellendorf and P. Vortisch. Microscopic traffic flow simulator vissim. *In: J. Barceló (Ed.), Fundamentals of traffic simulation, Series in operation research & management science*, 145:63–93, 2010.

[45] L. Fermo and A. Tosin. Fundamental diagrams for kinetic equations of traffic flow. *Discrete Contin. Dyn. Syst. Ser. S*, 7:449–462, 2014.

[46] L. Fermo and A. Tosin. A fully-discrete-state kinetic theory approach to traffic flow on road networks. *Math. Models Methods Appl. Sci.*, 25:423–461, 2015.

[47] R. Ferretti. Convergence of semi-Lagrangian approximations to convex Hamilton-Jacobi equations under (very) large Courant numbers. *SIAM J. Numer. Anal.*, 40 (6):2240–2253, 2002.

[48] U. S. Fjordholm. *High-order accurate entropy stable numerical schemes for hyperbolic conservation laws*. PhD thesis, ETH Zurich Switzerland, 2013.

[49] U. S. Fjordholm, S. Mishra, and E. Tadmor. Arbitrarily high order accurate entropy stable essentially non-oscillatory schemes for systems of conservation laws. *SIAM J. Numer. Anal.*, 50:423–444, 2012.

[50] M. Di Francesco and M.D. Rosini. Regourus derivation of the Lighthill-Whitham-Richards model from the follow-the-leader model as many particle limit. *Archive for Rational Mechanics and Analysis*, pages 1–41, 2015.

[51] B. D. Froese and A. M. Oberman. Convergent filtered schemes for the monge-ampre partial differential equation. *SIAM J. Numer. Anal.*, 51:423–444, 2013.

[52] M. Garavello and P. Goatin. The cauchy problem at a node with buffer. *Discrete Contin. Dyn, Syst. Ser. A*, 32:1915–1938, 2012.

[53] M. Garavello and B. Piccoli. Source-destination flow on a road network. *Comm. Math. Sci.*, 3:261–283, 2005.

[54] M. Garavello and B. Piccoli. *Traffic Flow on Networks. AIMS series on Applied Mathematics*, volume 1. 2006.

[55] M. Garavello and B. Piccoli. A multi buffer model for LWR road networks. *Advances in Dynamic Network Modeling in Complex Transportation Systems, Complex Networks and Dynamic Systems.*, 2:143–161, 2013.

[56] D. L. Gerlough. *Simulation of freeway traffic on a general-purpose discrete variable computer*. 1955.

[57] J. Glimm. Solutions in the large for nonlinear hyperbolic systems of equations. *Communication on Pure and Applied Mathematics,*, 10(2):697–715, 1965.

[58] S. Godunov. A difference method for numerical calculation of discontinuous solutions of the equations of hydrodynamics. *Matematicheskii Sbornik*, 89(3):271–306, 1959.

[59] S. Gottlieb and C.-W. Shu. Total variation diminishing Runge-Kutta schemes. *Math. Comp.*, 67(221):73–85, 1998.

[60] J. M. Greenberg. Extensions and amplifications of a traffic model of aw and rascle. *SIAM J. Appl. Math.*, 62:729–745, 2001.

[61] B. Greenshields. A study of traffic capacity. *Proceedings of the Highway Research Board*, 14:448–477, 1935.

[62] R. Habermas. *Mathematical Models: Mechanical Vibrations, Population Dynamics and Traffic Flow*. Prentice-Hall, Inc, Englewood Cliffs, New Jersey, USA., 1997.

[63] A. Harten. High resolution schemes for hyperbolic conservation laws. *J. Comput. phys.*, 49:357–393, 1983.

[64] A. Harten. On a class of high resolution total-variation finite difference schemes. *SIAM J. Numer. Anal.*, 21:1–23, 1984.

[65] A. Harten, B. Engquist, S. Osher, and S.R. Chakravarty. Uniformly high order essentially non-oscillatory schemes. *J. Comput. phys.*, 4:231–303, 1987.

[66] D. Helbing. Traffic and related self-driven many-particle systems. *Review of Morden Physics*, 73(4):1067–1141, 2001.

[67] M. Herty and Klar. Modeling, simulation, and optimization of traffic flow networks. *SIAM J. Sci. Comput.*, 25:1066–1087, 2003.

[68] M. Herty, C. Kirchner, S. Moutari, and M. Rascle. Multicommodity flows on road networks. *Comm. Math. Sci.*, 6:171–187, 2008.

[69] M. Herty, J.-P. Lebacque, and S. Moutari. A novel model for intersections of vehicular traffic flow. *Netw. Heterog. Media*, 4:813–826, 2009.

[70] H. Holden and N. H. Risebro. mathematical model of traffic flow on a network of unidirectional roads,. *SIAM J. Math. Anal.*, 26:999–1017, 1995.

[71] C. Hu and C.-W. Shu. A discontinuous Galerkin finite element method for Hamilton-Jacobi equations. *SIAM J. Sci. Comput. Anal.*, 21:666–690, 1999.

[72] H. Ishii. Uniqueness of unbounded viscosity solution of Hamilton-Jacobi equations. *Indiana Univ. Math. Journal*, 33(5):721–748, 1984.

[73] M. Helbing D. Kesting, A. Treiber. Enhanced intelligent driver model to access the impact of driving strategies on traffic. *Philosophical Transactions of the Royal Society A*, 368 (1928):4585–4605, 2010.

[74] S. Kruzhkov. First order quasilinear equations in several independent variables. *Mathematics of the USSR-Sbornik*, 10(2):217–243, 1970.

[75] A. Kurganov and E. Tadmor. New high-resolution semi-discrete central schemes for Hamilton-Jacobi equations. *Journal of Computational Physics*, 160:720–742, 2000.

[76] Culbert B. Laney. *Computational Gasdynamics*. Cambridge University press, New York, 1998.

[77] O. Lepsky, C. Hu, and C.-W. Shu. Analysis of the discontinuous Galerkin method for Hamilton-Jacobi equations. *Applied Numerical Mathematics*, 33:423–434, 2000.

[78] R. J. LeVeque. *Finite volume methods for hyperbolic problems.* Cambridge University Press, Cambridge, 2002.

[79] F. Li and C.-W. Shu. Reinterpretation and simplified implementation of a discontinuous Galerkin method for Hamilton-Jacobi equations. *SIAM J. Sci. Comput. Anal.*, 18(11):1204–1209, 2005.

[80] M.J. Lighthill and G. B. Whitham. On kinetics waves. ii theory of traffic flows on long crowded roads. *Proc. Roy Soc. Lond. A.*, 2999:317–345, 1955.

[81] P.-L. Lions and P. E. Souganidis. Convergence of MUSCL and filtered schemes for scalar conservation laws and Hamilton-Jacobi equations. *Numer. Math.*, 69(4): 441–470, 1995.

[82] MITSIM. Mitsimlab open source (open source version). URL `http://mit.edu/its/mitsimlab.html`.

[83] S. Moutari and M. Rascle. A hybrid Lagrangian model based on the Aw-Rascle traffic flow model. *SIAM J. Appl. Math.*, 68:413–436, 2007.

[84] K. Nagel and M. Schreckenberg. A cellular automaton model for freeway. *Journal de Physique*, 12 (12):2221–2229, 1992.

[85] G. Newell. A simplified theory of kinematic waves in highway traffic, part ii: queueing at freeway bottlenecks. *Transportation Research Part B*, 27(4):289–303, 1993.

[86] A.M. Oberman and T. Salvador. Filtered schemes for hamilton-jacobi equations:a simple construction of convergent accurate difference schemes. *Journal of Computational Physics.*, 284:367–388, 2015.

[87] O. Oleinik. Discontinuous solutions of non-linear differential equations. *Uspekhi Matematicheskikh Nauk*, 12(3):3–73, 1957.

[88] S. Osher and F. Ronald. *Level set method and dynamic implicit surfaces*, volume 153. Applied Mathematical Sciences, Springer, 2003.

[89] S. Osher and J. A. Sethian. Fronts propagation with curvature dependent speed: algorithms based on Hamilton-Jacobi formulations. *J. Comput. Phys.*, 79:12–49, 1988.

[90] S. Osher and C.-W. Shu. High order essentially non-oscillatory schemes for Hamilton-Jacobi equations. *SIAM J. Numer. Anal.*, 4:907–922, 1991.

[91] L. A. Pipes. *J. App. phys.*, 24:209, 1953.

[92] I. Prigogine and R. Herman. *Kinetic Theory of Vehicular Traffic.* Elsevier, 1971.

[93] K.A. Redmill and U. Vatsim Ozguner. A vehicle and traffic simulator. *IEEE 2nd International Conference on Intelligent Transportation Systems, Intelligent Transportation Systems*, pages 656–661, 2001.

[94] A. Reuschel. *Osterr. Ing. Archiv*, 4:193, 1950.

[95] P. I. Richards. Shock waves on the highway. *Operation Research*, 4:42–51, 1956.

[96] P. L. Roe. Some contributions to the modeling of discontinuous flows. lectures. *App. Math*, 22:163–193, 1985.

[97] E. Rossi. A justification of a lwr model based on a follow the leader description,. *Discrete Contin. Dyn, Syst. Ser. A*, 7:579–591, 2014.

[98] D. Serve. *Systems of conservation laws*. Diderot, Paris, 1996.

[99] J. Sethian. Curvature and evolution of fronts. *Comm. in Math. Phys.*, 101:487–499, 1985.

[100] J.A. Sethian. *Level set method evolving in geometry, fluid mechanics, computer vision, and materials science*, volume 3. Cambridge Monographs on applied and Computational Mathematics, Cambridge University press, 1996.

[101] J. Shen and X. Jin. Detailed traffic animation for urban road networks. *Graphical Models*, 74:165–282, 2012.

[102] P. Soravia. Estimates of convergence of fully discrete schemes for the Isaacs equation of pursuit-evasion differential games via maximum principle. *SIAM J. Control Optim.*, 36(1):1–11 (electronic), 1998.

[103] SUMO. *Simulation of urban mobility (open source version)*. URL http://sumo.sourceforge.net/.

[104] C.M.J. Tampère, R. Corthout, and L.H. Cattrysse, D. Immers. A generic class of first order node models for dynamic macroscopic simulation of traffic flows. *Transportation research Part B*, 5:289–309, 2011.

[105] M. Treiber and D. Helbing. Micro simulations of freeway traffic including control measures. *Automatisierungstechnik*, 49:478–484, 2001.

[106] H. Underwoofd. Speed, volume, and density relationships: Quality and theory of traffic flow. *Yale Bureau of Highway Traffic*, 4:141–188, 1961.

[107] G. B. Whitham. *Linear and non linear waves*. Wiley, New York,, 1974.

[108] G. C. Wong and S. C. Wong. A multi-class traffic flow model- an extension of LWR model with heterogeneous drivers. *Transportation Research Part A*, 36:827–841, 2002.